ENGINEERING METAL PARALLEL PLATE WAVEGUIDES AS A 2-D PLANE FOR HIGH RESOLUTION THz TIME DOMAIN SPECTROSCOPY

By

SREE HARSHA SRIKANTAIAH

Bachelor of Science in Physics
Sri Sathya Sai Institute of Higher Learning
Prashanthi Nilayam, Andhra Pradesh, India
2001

Master of Science in Physics (Photonics)
Sri Sathya Sai Institute of Higher Learning
Prashanthi Nilayam, Andhra Pradesh, India
2003

Submitted to the Faculty of the
Graduate College of the
Oklahoma State University
in partial fulfillment of
the requirements for
the Degree of
DOCTOR OF PHILOSOPHY
July, 2011

ENGINEERING METAL PARALLEL PLATE

WAVEGUIDES AS A 2-D PLANE

FOR HIGH RESOLUTION

THz TIME DOMAIN SPECTROSCOPY

Dissertation Approved:

Dr. Daniel R. Grischkowsky

Dissertation Adviser

Dr. Weili Zhang

Committee Member

Dr. Alan Cheville

Committee Member

Dr. Aihua Xie

Outside Committee Member

Dr. Mark E. Payton

Dean of the Graduate College

Acknowledgements

I thank Dr. Daniel Grischkowsky my advisor for allowing to me be a part of his research group and setting me on a path for achieving scientific excellence. His immense knowledge, wisdom and the extremely high standards set by him for laboratory performance has inspired me to achieve great things. I am really proud of what we have accomplished together in the past five years. Sir Issac Newton once said and I quote *"If I have seen further it is by standing on the shoulders of giants".* This quotation is very dear to my heart and it summarizes my feeling today when I look back at the past few years here at OSU, as a part of the THz research group…I really was standing on shoulders of giants…the basis on which this work was built on was in part greatly based on all the scholarly accomplishments of Dr. Grischkowsky and earlier members of his research team and the eminent researchers that were drawn to work in this group. I have grown to be a good researcher being in the company of such good people

I thank Dr. Norman Laman from whom I have learnt the nuts and bolts of working in a THz lab. I owe a lot to you Norman; it was great having a postdoc like you in the lab. It was easy for me to learn new things, knowing that after every Dr. G meeting I could always come back to you and discuss and understand stuff which flew over my head. We have spent some interesting time in the lab, in particular the days we spent fixing the Ti: sapphire laser (which I must confess, I broke…I still don't understand how the prism fell of its base….) will never be forgotten. I also thank Dr. Joseph Melinger from Naval research labs, who has been a part of the waveguide THz -TDS team from the very beginning and whose visits I always looked forward to. Each of your visits were action packed with interesting discoveries and I learnt great many things from you. I am happy to have been able to work with you.

I will be ungrateful if I don't acknowledge the help and support I received from my friends back in India from the Laser lab at HCU. Srinivas and Prem, from whom I

picked up the important skills of working on the optics bench, without the encouragement from you both and support from Bhaktha, Chaitanya and Ravikanth, I would have never come to the United States and achieved my dream of obtaining my Ph.D. I really miss those days we spent at HCU.

I thank my team mates here at UTOL with whom I have shared great many good times. Ranjan, Matt, Mufei, Adam, Yuguang, Xinchao, Chen, Yihong and Mahboubeh, I extend my appreciation and gratitude. I would like to specially thank Michael and Alisha who joined the group towards the latter part of my stay here. Michael I must say I picked up some neat skills from you and that we did some good work together and I miss all that long conversations we had in the lab. In your words…you are "not too bad"….. Alisha thanks for being a great minion…just kidding… it was nice having you here at NRC and I think we have shared some great time working in the lab and a special thanks for introducing me to your wonderful husband Max and all your nice friends. I have spent some wonderful time with you guys in Stillwater.

I also thank Vasantha and Pavan, the friends whom I brought with me from India. They have been with me from the very beginning, here at OSU and have been a part of my many ups and downs. I have shared a great many good times with you guys and Mansi and will always remember the good days we spent together. I also thank Subbu, Sailesh, Haripriya, Venkat, Praveen and Kishan…you guys received me here at Stillwater when I first arrived and during the great "Sree tore his knee episode", you guys took me in and looked after me like family. I will never forget your help and am very grateful to you guys.

Last but not the least I extend my heartfelt gratitude to my parents and sister especially to my mother …who did not quite understand why I had to spend so many years at school to get a Ph.D. They have been a great pillar of support to me and I thank you for your patience.

TABLE OF CONTENTS

Chapter Page

LIST OF TABLES

LIST OF FIGURES

Chapter 1
Introduction

*"…everything that living things do can be understood in terms of the jiggling and wiggling of atoms …" R. P. Feynman**

1.1 Terahertz time domain spectroscopy

The past decade has seen tremendous growth and innovation in the field of terahertz (THz) technologies. The development of new sources and detectors based on photoconductive switches [1, 2], optical rectification and electro optic effects [3, 4] has inspired research in new forms which was until now limited because of lack of efficient means of generation and detection of THz radiation. The THz frequency band is sandwiched between the microwave and infrared bands of the electromagnetic (EM) spectrum and hence is known to exhibit properties and phenomena observed in both the regions of the EM spectrum. This implies that, techniques and methods efficiently employed in both the regions of the spectrum can be applied at THz frequencies with interesting outcomes.

---

[*] *Feynman, R. P., "Six easy pieces: Essentials of physics by its most brilliant teacher", page 59, Reading, Mass.: Helix Books, 1995*

One application which is seen being applied prominently is the technique of THz time domain spectroscopy (THz-TDS) and has been used as a tool to study material properties at these frequencies i.e. from 0.1 – 10 THz (3 mm-30 μm, 3.33-333 cm^{-1}). TheTHz band has been shown to contain wealth of information regarding low frequency vibrational modes of molecules both inter- and intra-molecular. This frequency band has photon energies in the range of milli electronvolt (meV) range and is known to strongly interact with systems that possess characteristic lifetimes in the picosecond range and molecular transitions in the meV energy domain. Examples of such systems include weakly bonded molecular crystals, hydrated biological matter and relaxation dynamics in aqueous liquids, etc. The study of the vibrational modes in such systems, yield valuable insight into the crystalline nature of the molecular solid. To date a wide variety of materials including semiconductors [5-7], gases [8], illicit drugs [8], explosives [-651950840,11] and other chemical compounds have been characterized using THz-TDS.

Prior to the development of THz-TDS, Fourier transform infrared spectrometers were employed to extract the same vibrational information. But this technique was plagued by relatively poor performance of the infrared sources and detectors in the THz region. The development of the femtosecond laser enabled the development of a completely new optoelectronic technique of generation and detection of THz radiation based on optical excitation of photoconductive switches. The THz-TDS spectrometer constructed using these photoconductive switches has been shown to exhibit a very high signal to noise ratio (S/N) (as high as 10,000:1) in the same frequency spectrum [12].

An important aspect which often influences the nature of the spectroscopic data obtained is the state of the sample. Gases exhibit very sharp and numerous spectral

features associated vibrational and rotational modes. Liquids on the other hand often exhibit broadband absorption behavior and do not usually possess any narrow absorption resonances. Non-polar liquids usually weakly absorb in the THz and far infra red region while polar liquids exhibit broadband absorption throughout the entire THz spectrum. Water in particular is nearly opaque to THz radiation with an absorption dominated by intermolecular interactions of induced and permanent dipole moments, in the hydrogen bonded network of water molecules. ($\alpha \approx 200$ cm^{-1} at 1 THz). Coming to the samples in solid state the absorption response is dependent on the crystallinity of the sample. More crystalline the sample is the sharper are the absorption features. Amorphous samples often show broadband absorption like liquids with no distinct spectral features showing up. This property is helpful in industrial quality control where sample quality can be controlled by monitoring the vibrational spectral features associated with the samples. In fact, there many commercial THz devices already in production exploiting this feature.

All the work presented in this thesis is on the characterization of vibrational responses of polycrystalline solid samples of molecules. The standard way of characterizing solid samples is either by using a single crystals (wafers for semiconductors) or by making a diluted pellet of the crystalline material mixed with a transparent host like polyethylene (1cm diameter, 2mm thick). Single crystals are the best samples for obtaining good spectroscopic data but more often than not they are hard to grow (for proteins and nucleic acids) and, even if possible to be grown, they cannot be thick samples due to the increased absorption in the THz range. Hence these samples have to be thin, which in turn puts a measurement limitation, wherein long temporal scans needed to resolve sharp spectral features are impregnated with Fresnel reflection

from the sample faces. These reflections introduce oscillations in the spectrum and thereby limit the maximum scan length. The same is true with pellets but pellets come along with a host of other problems which again affect spectroscopic measurement. The process of making a pellet has an inherent drawback in the sense a significant amount of inhomogeneous broadening of the vibrational modes is induced during the process of making the pellet. Pellet making involves grinding the molecular sample to fine powder and exposure to high pressure, which leads to fractures and defects in the microcrystals comprising the pellet. In addition these microcrystals are randomly oriented within the pellet with respect to the polarization of the incident THz radiation which adds to the inhomogeneous broadening. Also these pellets are made of a poor thermal conductor as the binding and diluting material, which implies that the low temperature studies often do not take place at the desired temperature and there is a radial temperature gradient across the pellet. Hence disorder and poor thermal conductivity limit the resolution of the vibrational modes that can be determined.

These experimentally determined vibrational modes often guide theoretical molecular modeling used to study THz properties of solid-state materials is often accomplished using computational techniques based on density functional theory or molecular dynamics (like GAUSSIAN, CHARMM, Dmol^3, Crystal, CPMD) [13]. However, in the solid state where intermolecular coupling can be strong due to hydrogen bonding, calculation of the low-frequency modes requires more sophisticated modeling and has been accomplished only recently [14]. Often it is observed that, it is hard to achieve a precise match between theoretical predictions and actual experimental observations. This is sometime due to experimental limitations of the existing techniques

in resolving the vibrational resonances of the molecular solids. Precise, high resolution, experimental measurements of low frequency modes of molecules in the solid state will lead to better modeling and hence better understanding of dynamics of these molecules. In addition, more precise measurements can lead to the establishment of a more detailed spectral database, and can assist in accurate identification of a test material. Hence, there is a need to develop a new high resolution technique of determining the THz vibrational modes of molecules in the solid state efficiently and accurately at the same time being applicable to a wide variety of materials.

1.2 Guided Wave spectroscopy of molecules

A complimentary approach to the standard freely propagating THz time domain spectroscopy has been that of using guided waves. Guided waves offer better sample detection sensitivity due to confinement of THz radiation within sub-wavelength gaps over a long interaction length. Increased detection sensitivity translates to sub milligram sample quantity required for characterization. There have been many earlier demonstrations of application of waveguides for performing sensitive spectroscopy at THz frequencies. There have been several examples where waveguides have been employed with subpicosecond THz pulses to measure absorption resonances in materials. An early demonstration was made by Sprik et al. [15], who used THz pulses propagating along coplanar transmission lines to measure magnetic resonances of an inorganic powder deposited along the transmission lines. More recently, Walther et al. [16] have coupled free space THz pulses onto metal wires and, through THz-TDS, detected

vibrational resonances of small quantities of lactose powder deposited along the wire. A third example was demonstrated recently by Byrne et al. [17], who used the evanescent wave above a micro-strip waveguide to measure the 0.53 THz vibrational absorption line for a sub-milligram quantity of polycrystalline lactose that spatially overlapped with the evanescent wave. These examples demonstrated the capability of the guided wave technique to characterize very small quantities of analyte sample. But, in each of these demonstrations, the bandwidth of the measurement was restricted to frequencies up to about 1 THz. For vibrational spectroscopy, it is generally desirable to have a broader spectral bandwidth to detect vibrational absorption resonances that occur at frequencies higher than 1 THz.

In all these earlier demonstrations the limiting factors for the performance of the techniques, were the bad performance of the waveguides chosen. All these waveguides were lossy, dispersive and did not support good bandwidth. So, in order to increase the efficiency of the waveguide based spectroscopy technique, it is important to find a waveguide which has better performance characteristics in terms of bandwidth, dispersion and coupling.

1.3 Metal parallel plate waveguides for THz-TDS

The development in THz technology has also resulted in growing interest in the development of wave guiding structures. Over the past decade, several attempts have been made to engineer efficient waveguides which support single mode and low loss propagation at THz frequencies. Engineering ideas from optical as well as microwave

frequencies have been invoked to come up with the "*ideal waveguide*" at THz frequencies. Several investigations have been carried out with dielectric as well as metal waveguides with various geometries (circular, rectangular and parallel plate) [18-20]. Of all these above waveguides, metal parallel plate waveguides (PPWG) [21] have so far been the only waveguides to exhibit single mode propagation with relatively low loss and no modal dispersion. The transverse electromagnetic mode (TEM) of the PPWG can be very efficiently coupled into and out of the waveguide with high spatial confinement of the THz wave within the gap. Moreover metal PPWGs can be easily fabricated at any machine shop with very great ease in comparison to other THz waveguides. Mendis et.al. [21] were the first to demonstrate the versatility of this waveguide in the year 2001. Since then, this capability to efficiently confine and propagate THz waves within the PPWG has been exploited to study various structures and interconnects, ranging from photonic crystal structures [22-23] to 2D interconnect structures [24] incorporated within the 2D plane of the PPWG.

Recently, Zhang et.al. [25] used these metal PPWGs to demonstrate there applicability for sensitive spectroscopy by detecting "*nanometer thick water layers"* within the waveguide. This demonstration was a first big step towards the applicability of metal PPWGs for waveguide THz-TDS.

Keeping this background in mind, we (Dr. Daniel Grischkowsky, Dr. Joseph Melinger (Naval Research Labs, Washington), Dr. Norman Laman and I) have attempted to demonstrate the applicability of these PPWGs for performing sensitive spectroscopy of polycrystalline films of molecular solids. Our initial effort was to demonstrate the sensitivity of the PPWG in detection of chemical samples similar to the water film

measurement. During this quest we not only demonstrated the sensitivity of the PPWG for these chemical films (microgram sample detection) but also discovered a *"surprising and desirable effect"* of the PPWG in facilitating the measurement of substantially *"narrow absorption line features"* in comparison to the standard THz-TDS techniques using pellets and comparable to the data obtained with single crystals. This discovery has opened up a totally new way for performing THz spectroscopy of molecules in solid state and has turned out to be an important THz spectroscopic tool, which when applied along with the standard THz-TDS and FTIR techniques can be used to completely characterize molecular solids at THz frequencies.

In this thesis, I summarize the work done at Ultrafast Terahertz Research Laboratory (UTOL) at Oklahoma State University on exploiting this line narrowing effect and developing the metal PPWG as a new spectroscopic tool for obtaining high resolution THz absorption spectra of polycrystalline molecular solids. This is the first demonstration of this spectroscopic technique, which uses the distortion free single TEM mode propagation of THz radiation within the PPWG for analyzing microgram sample quantities and obtaining high resolution spectral finger prints, with performance rivaling that of single crystal spectroscopy. The versatility of this technique has been demonstrated by characterizing a broad spectrum of chemicals covering most of the materials measured by THz spectroscopy so far, thereby establishing waveguide THz-TDS as a new spectroscopic technique at THz frequencies.

Yet another dimension of the PPWG for application in sensitive spectroscopy was investigated using Bragg structures within the PPWG. These weak Bragg gratings

(micron deep) within the PPWG give rise to very high Q resonances and these can be used for very sensitive detection of chemicals and thin films.

1.4 Outline

The outline of the thesis is as follows. **Chapter 2** describes the background and motivation in choosing metal parallel plate waveguides for waveguide THz-TDS. It will also include review of the design and performance characteristics of the PPWG and introduce the technique of high resolution waveguide THz-TDS using an organic molecule tetracyanoquinodimethane (TCNQ) as an example.

Chapter 3 discusses the technique of waveguide THz-TDS in detail and elaborates on the different performance aspects, sensitivity and other experimental details in applying metal PPWGs for high resolution THz spectroscopy.

In **Chapter 4,** examples of the application of waveguide THz-TDS in obtaining the high resolution vibrational modes of different kinds of molecules is presented.

Chapter 5 focuses on another dimension of applicability of metal PPWG for spectroscopy, i.e. thin film sensing. This chapter focuses on incorporation of high Q Bragg resonant structures on to the 2D plane of the PPWG. Application towards sub micron thin film detection is discussed.

Chapter 6 focuses on the coupling techniques used to couple THz radiation into and out of the PPWG. Experiments carried out on improving the coupling and

performance of the PPWG by applying the microwave technique of horn antennas is described and then compared to the existing quasi optic coupling using Si lenses.

Chapter 7 summarizes the work done and also provides information on future plans and applications using the PPWGs.

Chapter 2

Metal parallel plate waveguides: Adapting them to perform Waveguide THz-TDS

2.1 Terahertz time domain spectroscopy

THz time domain spectroscopy (THz-TDS) is an experimental techniques used to study material properties using sub picoseconds THz pulses having a frequency content between 0.1 THz - 10 THz. A standard THz-TDS system is as shown in Fig 2.1. THz radiation is generated and detected using photoconductive switches driven by 10 mW optical pulse trains from an 800 nm, 80 fs, 100 MHz mode locked Ti: sapphire femtosecond laser. The emitted THz radiation is collimated using a high resistivity Si lens attached to the back of the source chip and an off axis paraboloidal mirror. The source chip (Fig 2.1 (b)) consists of a simple coplanar transmission line structure of the chip consists of two 10 μm wide metal lines separated by 80 μm, fabricated on high resistivity GaAs. Irradiating the metal - semiconductor interface (edge) of the positively biased line with focused ultrafast laser pulses produces synchronous bursts of THz radiation. This occurs because each laser pulse creates a spot of photocarriers in a region of extremely high electric field. The consequent acceleration of the carriers generates the burst of radiation. The major fraction of the THz radiation is emitted into the GaAs

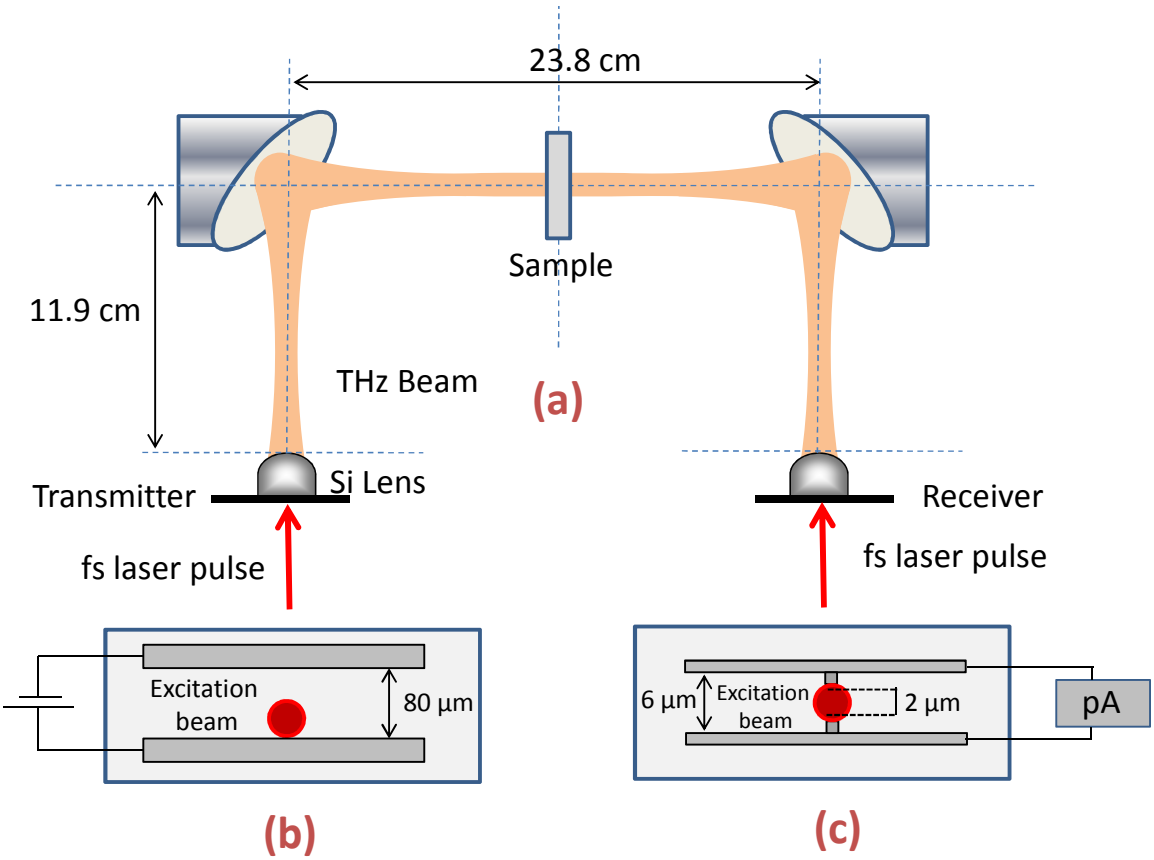

Fig 2.1 (a) Layout of Standard THz-TDS system, **(b)** THz emitter and **(c)** THz receiver

substrate in a cone normal to the interface and is then collected and collimated by a crystalline high resistivity silicon lens attached to the back side of the chip.

The THz radiation detector is an ion-implanted SOS detection chip with the antenna geometry shown in Fig. 2.1(c). The 4 μm wide antenna structure is embedded in a coplanar transmission line consisting of two parallel 2 μm wide aluminum lines separated from each other by 6 μm. The electric field of the focused incoming THz radiation induces a transient bias voltage across the 2 μm gap of this receiving antenna, connected to a low noise current amplifier. The amplitude and time dependence of this transient voltage is obtained by measuring the collected charge (average current) versus the time delay between the THz pulses and the Ti: sapphire detection pulses. These pulses in the 10 mW laser detection beam synchronously gate the receiver by driving the photoconductive switch. In other words, the switch is closed by the photocarriers created by the 80 fs laser pulse; the switch then reopens in approximately 600 fs due to the short carrier lifetime in ion-implanted SOS. The transmitter and receiver chip are incorporated in a confocal optical system (4f geometry) consisting of two off-axis parabolic mirrors with a focal length of 11.9 cm. This confocal system as shown in Fig 2.1 (a) produces a collimated THz beam at the focus of the 2 parabolic mirrors, with a frequency dependent beam waist. Due to the broad bandwidth of the system, the beam waist at the center of the system ranges from approximately 9 mm at 0.5 THz to 1 mm at 4 THz.

The generated THz pulse is shown by the single-scan measurement in Fig. 2.2 (a). The pulse shown has a S/N of 5000:1. The corresponding amplitude spectrum of this pulse is shown in Fig.2.2 (b). The S/N ratio of the amplitude spectrum is shown in the logarithmic plot of Fig. 2.2 (c). Here, the dynamic range or S/N is displayed as 700:1.

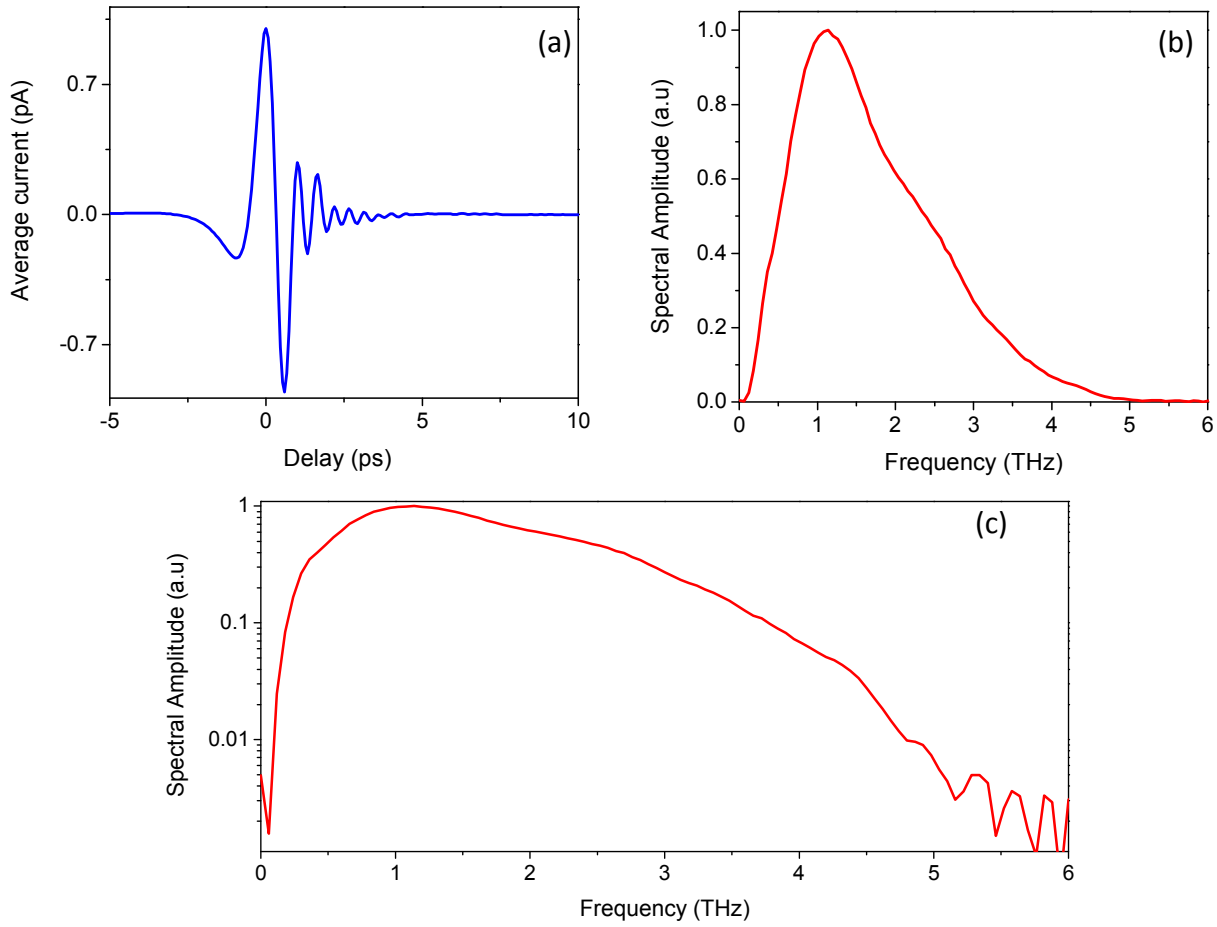

Fig 2.2 (a) Normalized Typical free-space THz pulse and corresponding amplitude spectrum with both **(b)** linear and **(c)** logarithmic vertical scales.

The conventional technique for performing THz spectroscopy using this system is by forming a pellet that contains a small amount of the molecule to be studied dispersed in a much larger quantity of a low absorbance host material like polyethylene. The pellet is placed in the collimated THz beam between the transmitter and receiver as shown in fig 2.1 (a). The corresponding amplitude spectra are obtained by taking the numerical Fourier transform of the measured time domain THz pulse. By noting the difference in transmission between the reference pulse and the sample pulse one can obtain information about the absorption and dispersive characteristics of the sample.

2.2 Metal parallel plate waveguide: Sub wavelength confinement of THz radiation

Though efficient and broadband coupling of THz pulses has been achieved for a wide array of waveguides like circular and rectangular metal waveguides [18-19], single crystal sapphire fibers [20], and plastic ribbon waveguides [26], they all suffer from a common problem which make them unsuitable for sub ps pulse propagation and hence for spectroscopy. Despite achieving single mode coupling and propagation, they all suffer from group velocity dispersion (GVD). It has been shown that excessive pulse broadening owing to GVD will not occur for the TEM mode of a two-wire coplanar line, co-axial line or a parallel plate waveguide, which does not have cut off frequency. The group velocity and dispersion of the TEM mode are influenced solely by the surrounding dielectric.

Of the three waveguides quasi optic coupling of the freely propagating THz radiation to the complex field patterns of the TEM mode of the coaxial line and the twin line are found to be not effective. However it can be used to spatially confine THz radiation by efficiently coupling freely propagating THz pulses into metal PPWG. The first PPWG demonstration [21] showed low-loss; single TEM-mode propagation with virtually no group velocity dispersion. Undistorted, propagation of the incoming THz pulse was observed within the bandwidth from 0.1 to 4 THz for a PPWG length of 24.4 mm.

2.2.1 Metal parallel plate waveguide – Theory

The fundamental equation governing the input and output relationship of the system, assuming single-mode propagation, can be written in the frequency domain as:

$$E_{out}(\omega) = E_{ref}(\omega) T C^2 \exp(-j(\beta_z - \beta_0)L) \exp(-\alpha L) \qquad (2.1)$$

where $E_{out}(\omega)$ and $E_{ref}(\omega)$ are the complex spectral components at angular frequency ω of the output and reference electric fields, respectively; T is the total transmission coefficient, which takes into account the reflections at the entrance and exit faces; and C is the amplitude coupling coefficient, the same for both the entrance and the exit faces, analyzed generally in terms of the standard overlap-integral method [19], which takes into account the similarity of the excitation beam to the guided-mode profiles. L is the distance of propagation, a is the amplitude absorption constant, β_z is the phase constant, and $\beta_0 = 2\pi/\lambda_0$, where λ_0 is the free-space wavelength. The phase term in Eq 2.1 illustrates the experimental condition in which the spatial distance between the transmitter and receiver is fixed.

Using the well-known two-dimensional analysis, [27-28] for an input electric field that is linearly polarized in a direction normal to the plane of the waveguide plates (y), only (transverse magnetic) TM modes can exist in the waveguide. Assuming a loss-less case for the propagation in the z – directed, the non vanishing terms of the field components can be written as:

$$H_x = A_m \cos\left[\frac{m\pi}{b}y\right] e^{-j\beta_z z} \tag{2.2}$$

$$E_y = \frac{A_m \beta_z}{\omega_0 \varepsilon} \cos\left[\frac{m\pi}{b}y\right] e^{-j\beta_z z} \tag{2.3}$$

$$E_z = \frac{A_m \beta_z}{j\omega_0 \varepsilon} \left[\frac{m\pi}{b}\right] \sin\left[\frac{m\pi}{b}y\right] e^{-j\beta_z z} \tag{2.4}$$

where,

$$\beta_z^2 + \left[\frac{m\pi}{b}\right]^2 = \beta_0^2 = \omega_0^2 \mu\varepsilon \tag{2.5}$$

where m = 0, 1, 2,… and $0 \leq y \leq b$. Here ω, μ, β, ε have their usual meanings, b is the plate separation , A_m is a constant dependent on the excitation of the waveguide, and subscript "o" stands for free space quantities.

The cutoff frequencies are given by:

$$f_{cm} = \frac{mc}{2bn_d} \tag{2.6}$$

where n_d is the refractive index of the dielectric medium between the plates. The lowest order TM_0 mode is in fact the TEM mode and has no cutoff. And also for perfectly

conducting plates the TEM mode has no GVD with both the group and phase velocities being equal to *c*. The wave impedance is equal to the intrinsic impedance of free-space η_0, for the air filled case.

2.3 Design and adaptation of the parallel plate waveguide for spectroscopy

The PPWG consists of 2 polished metal plates (Cu/Al/Au coated Cu or Al) separated by a gap (50 -100μm) formed by two spacers placed at the four corners, between the plates which are then bolted together. The dimensions of the waveguide plates are 28 mm (width) x 30 mm (length) x 10 mm (thickness). Two plano-cylindrical high resistivity lenses are used at the input and exit faces to couple the THz radiation in and out of the PPWG. The lenses are 15 mm x 10 mm x 6.56 mm with a 5 mm radius of curvature (see Fig 2.3). The input Si lens focuses the incoming terahertz pulse to an elliptical spot with the minor axis of 150 μm, perpendicular to the waveguide plates, and the linearly wavelength-dependent major axis is 9 mm at 1 THz, parallel to the waveguide plate. This coupling of a freely propagating THz beam into the PPWG located at the beam waist of a confocal THz system has been shown to be efficient over the entire bandwidth.

The insertion of the two required cylindrical lenses separated by their focal lengths reduces the amplitude of the transmitted THz pulse by the multiplicative factor 0.4 = 0.8 x 0.5 , where 0.5 is the Fresnel transmission through the uncoated high-resistivity Si lenses (due to the reflective losses of 4 surfaces). The factor 0.8 is the quasi-optical amplitude coupling (transmission) through the two confocal lenses. For a 30 mm

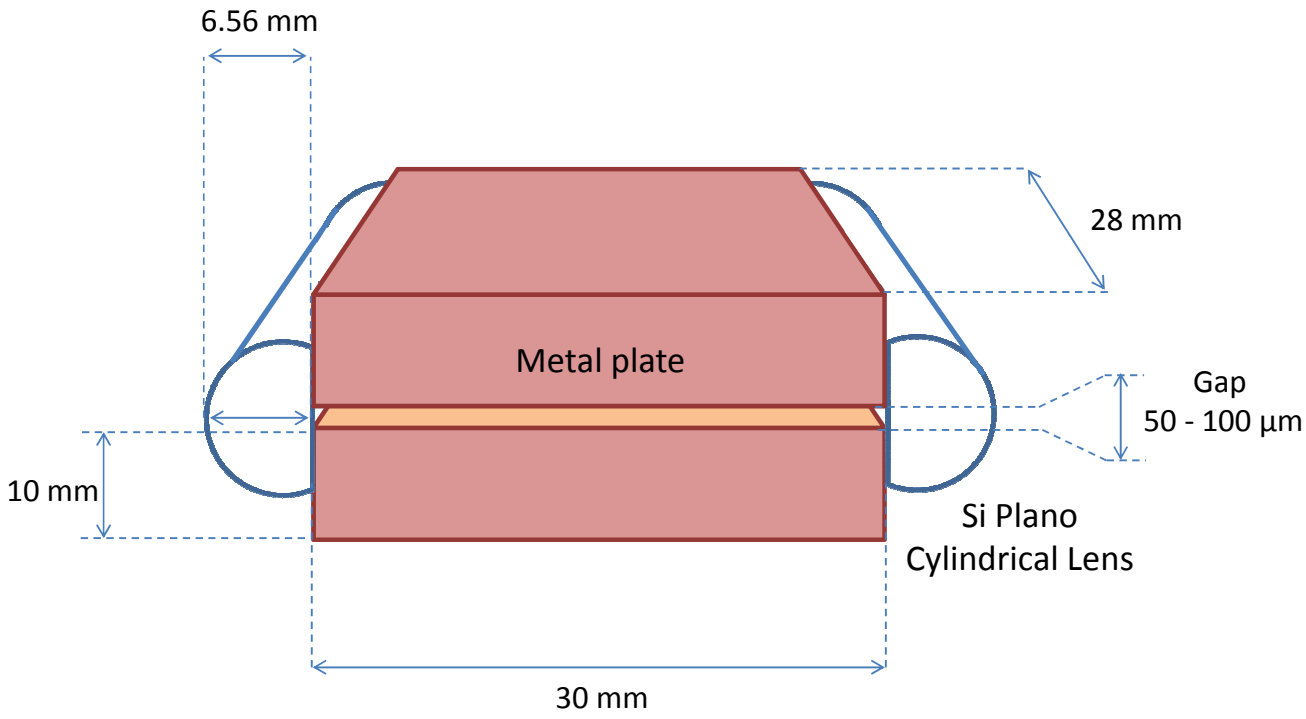

Fig 2.3 Metal parallel plate waveguide

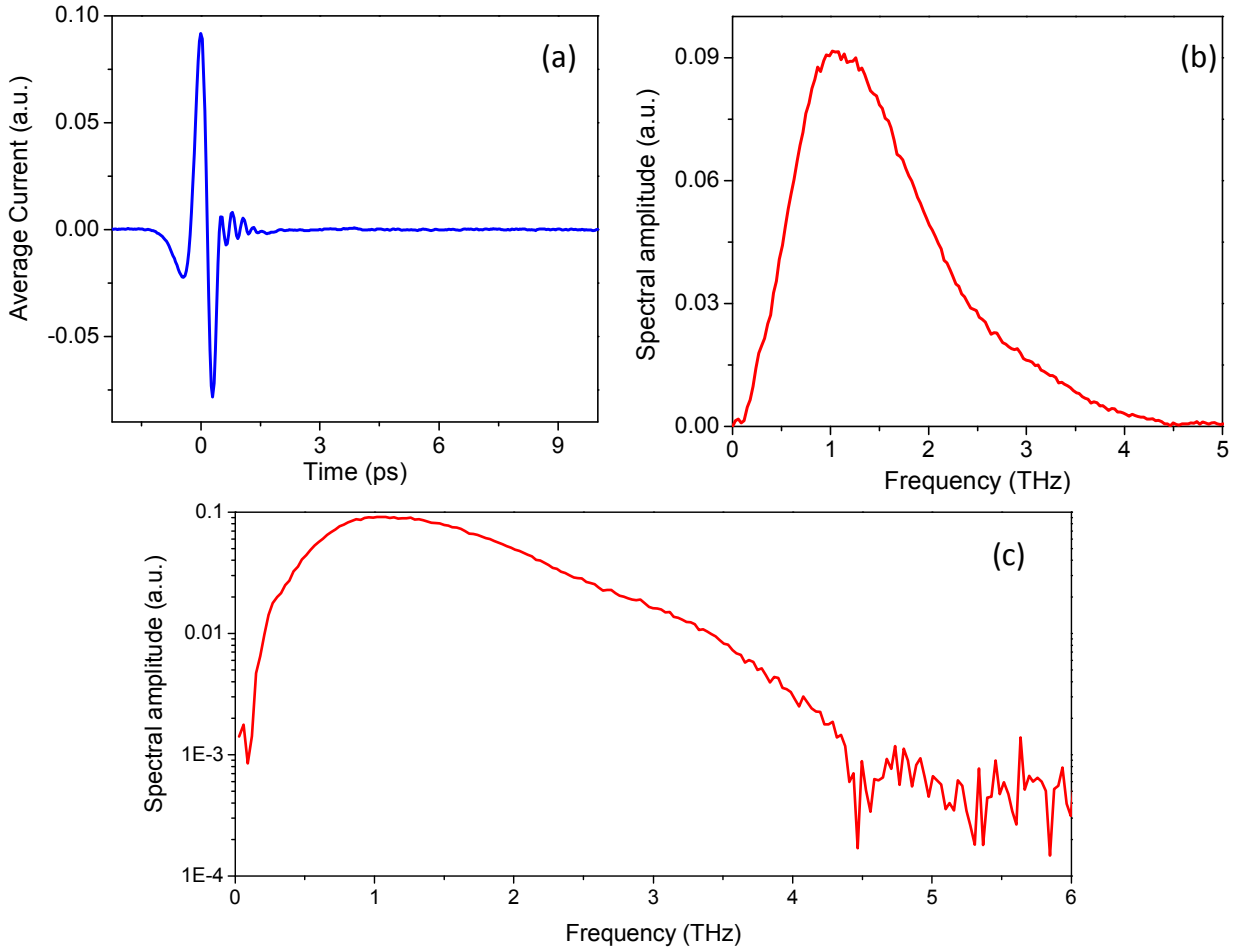

Fig. 2.4 (a) THz pulse transmitted through 30 mm long Cu waveguide with 50 μm gap normalized to free-space signal in Fig. 2.2(a) and corresponding amplitude spectrum normalized to free-space spectrum with both **(b)** linear and **(c)** logarithmic vertical scales

long, 50 μm air spaced Cu parallel plate waveguide, with the foci of the lenses separated by the waveguide, the amplitude transmission was reduced to 0.18 = 0.45 x 0.8 x 0.5, similar to the situation for the experiments to be described later. The additional factor of 0.45 is mainly due to the waveguide coupling loss, with a smaller loss due to waveguide absorption. The single scan measured THz pulse transmitted through an empty waveguide is shown in Fig. 2.4 (a). Here the pulse amplitude is normalized to the free space THz pulse of Fig. 2.2 (a) and shows a reduced amplitude transmission of 0.09, which includes the additional factor of 0.5 due to the strong reflections from the Si windows on the vacuum chamber (part of the cryogenic setup described later) [P5]. The corresponding amplitude spectrum shown in Fig. 2.4 (b) has been normalized to the free space spectrum of Fig. 2.2 (b). The waveguide-transmitted spectrum is shown logarithmically in Fig. 2.2 (c).

2.3.1 Absorption losses of the PPWG due to metal conductivity

The theoretical absorption coefficient (Ohmic loss) [27-29] for an air spaced parallel plate waveguide is determined by:

$$\alpha_0 = \frac{R}{\eta_0 b} \tag{2.7}$$

where,

$$R = 10.88\, X\, 10^{-3}\, [10^7/(\sigma_R \lambda_0)]^{0.5} \tag{2.8}$$

$$\eta_0 = (\mu_0/\varepsilon_0)^{0.5} \approx \quad 377\Omega \tag{2.9}$$

b is the gap between the waveguide plates, σ_R is the real part of the conductivity and λ_0 is the free space wavelength. The frequency dependent metal conductivity can be modeled by the Drude theory:

$$\sigma = \sigma_R + i\sigma_i = \sigma_{DC} i\Gamma/(\omega + i\Gamma) = i\varepsilon_0\omega_p^2/(\omega + i\Gamma) \tag{2.10}$$

Where ε_0 is the free-space permittivity, ω is the angular frequency, ω_p is the angular plasma frequency and Γ is the electron scattering rate. The expression for conductivity can be rewritten in the form:

$$\sigma = \varepsilon_0\omega_p^2/[\Gamma(1 + \omega^2/\Gamma^2)] + i\varepsilon_0\omega_p^2\omega/[\Gamma^2(1 + \omega^2/\Gamma^2)\,] \tag{2.11}$$

At THz frequencies $\omega << \Gamma$ and we can make a good approximation that:

$$\sigma_R \approx \varepsilon_0\omega_p^2/\Gamma \tag{2.12}$$

For bulk aluminum, $\Gamma/2\pi$ = 19.4 THz at 295 K [30]. According to Matthiessen's rule, $\Gamma = \Gamma_p + \Gamma_D$ is the sum of the temperature dependent term Γ_p, generally dominated by phonons at experimental temperatures and a temperature independent term Γ_D, generally dominated by lattice defects. [29].

Hence, the measured performance of the THz single mode metal waveguides and the THz TEM mode metal parallel plate waveguides in particular is limited by the metal conductivity. One way to improve performance would be to increase the metal conductivity. A simple and effective method to increase conductivity has been to cool metals to liquid nitrogen temperatures [31, 32]. Experiments performed by Laman et.al [29] demonstrated that the increase in conductivity was modest and hence the increase in waveguide transmission was not as high as expected (expected to increase by 8 times when cooled to 77K) when metal PPWGs were cooled to 77K. They observed moderate

increase in transmission throughput upon cooling to 77 K. Figure 2.5 shows the transmitted THz pulse and spectrum through an Al air filled parallel plate waveguide at 295 K and at 77 K. Cooling to 77 K increases the waveguide transmission by about 30 %. This moderate increase in performance of the metal PPWG is still desirable, since when these waveguides are adapted for spectroscopy, one always cools the waveguides to cryogenic temperatures to overcome the thermal broadening mechanisms which obscure the absorption modes of samples. Increase in transmission at cryogenic temperatures in turn results better signal to noise which is greatly desirable.

From Fig 2.5 (a) it is clear that the THz pulse arrives earlier in time when cooled to 77 K. This is attributed to the temperature dependent refractive index of silicon (dn/dT $=1.3 \times 10^{-4}$/ K) [97], with which the cylindrical lenses used for THz coupling, are made of. This shift in pulse position in time with decrease in temperature can be also used as a tool to monitor waveguide temperature. The relative change between 295 K and 77 K in the refractive index ($\Delta n/n = -8.5 \times 10^{-3}$) is the dominant effect since it is much larger than the corresponding change in the length of the silicon ($\Delta L/L = -0.23 \times 10^{-3}$) due to the linear thermal expansion coefficient [98].

2.4 Guided wave THz time domain spectroscopy

Single mode and dispersion free propagation of THz pulses in a metal PPWG opens up the possibility of carrying out novel spectroscopic investigations within the sub-wavelength gap of the PPWG. Waveguide THz-TDS utilizes THz spatial confinement to sub-wavelength dimensions together with long propagation lengths to dramatically improve the sample filling factor and consequently the sensitivity. For the TEM mode of

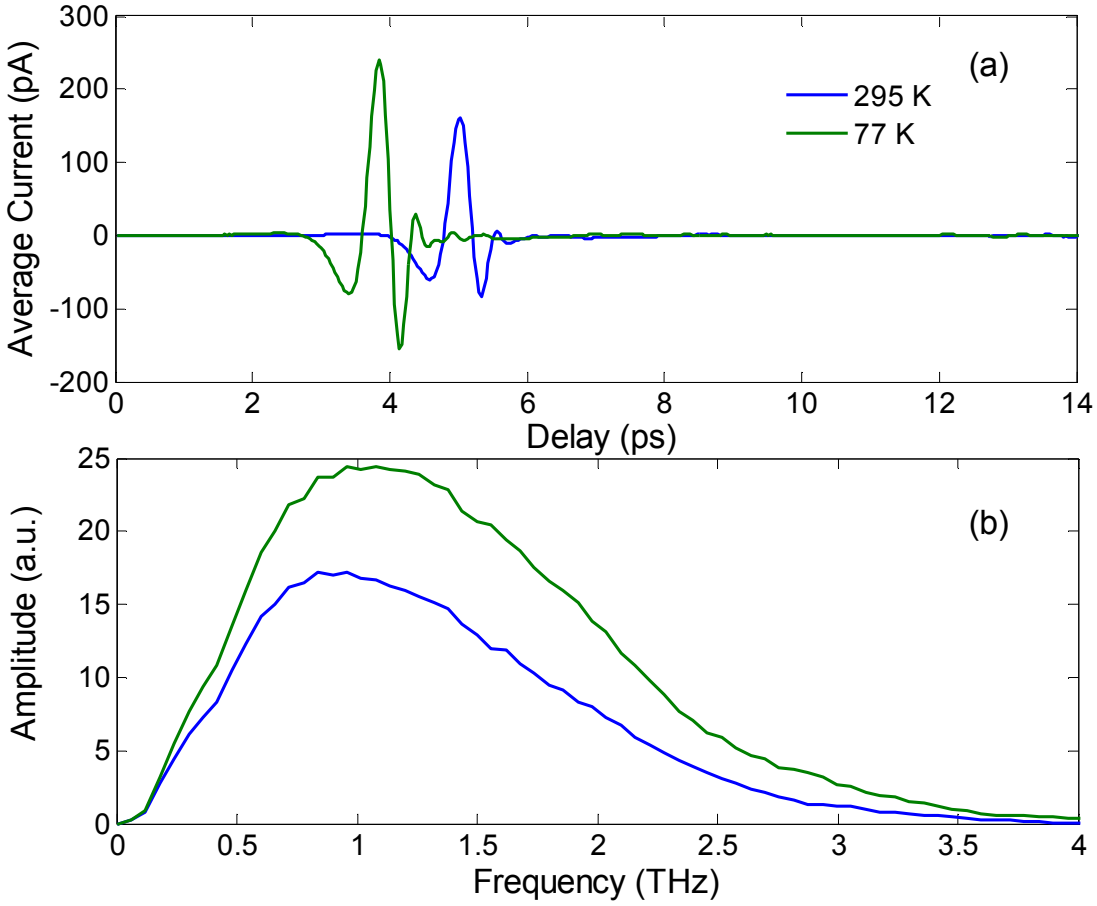

Fig 2.5 Transmitted THz pulses (a) and corresponding spectrum (b) through an air filled Al parallel plate waveguide at 295 K and at 77 K.

parallel plate metal waveguides, the spatial confinement, determined by the separation b between the plates, can be easily $b = \lambda/10$. By comparing the signal from the empty waveguide with that from the waveguide containing the sample layer, one can extract the changes in both amplitude and phase caused by the addition of the layer. Knowing the layer thickness, one can then obtain the absorption and the index of refraction of the layer material. The high sensitivity of this measurement technique is proportional to the ratio between the length and the plate separation of the waveguide. For a PPWG with a gap b and length L, with a film of refractive index n_l the predicted sensitivity enhancement (Γ) is given by [19]:

$$\Gamma = \frac{L}{n_l^3 b} \tag{2.13}$$

This high sensitivity of the PPWG in detecting thin dielectric layers was demonstrated by Zhang.et al in 2004 by detecting nm thick water layers within the metal PPWG [25].This demonstration established the sensitivity of the THz waves confined to the sub wavelength gaps of the PPWG.

This sensitivity enhancement achieved in the PPWG was the inspiration to apply these waveguide to perform spectroscopy of polycrystalline thin films of molecules. As discussed earlier, the PPWG assembly used for this study consists of two metal plates with identical dimensions of 28 mm (width) x 30 mm (length) x 10 mm (thickness). Typically the gap separation is maintained at 50 μm and is achieved by two 50 μm thick brass metal spacers. Thin polycrystalline films of the samples are cast on the bottom plate and then swabbed to form a sample area typically 15mm (wide) x 25 mm (long) as illustrated in Fig 2.6.

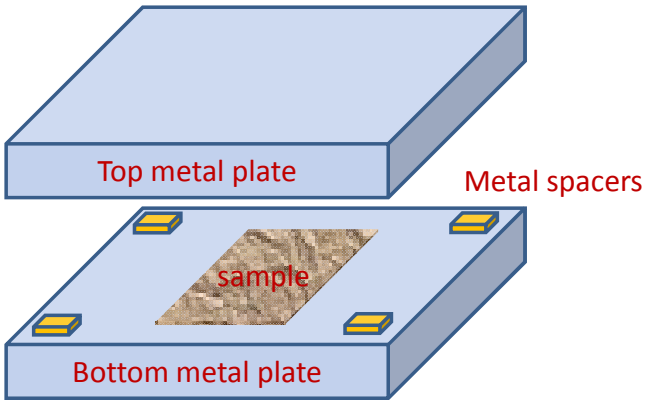

Fig 2.6 Exploded view of PPWG with polycrystalline film used for waveguide THz-TDS

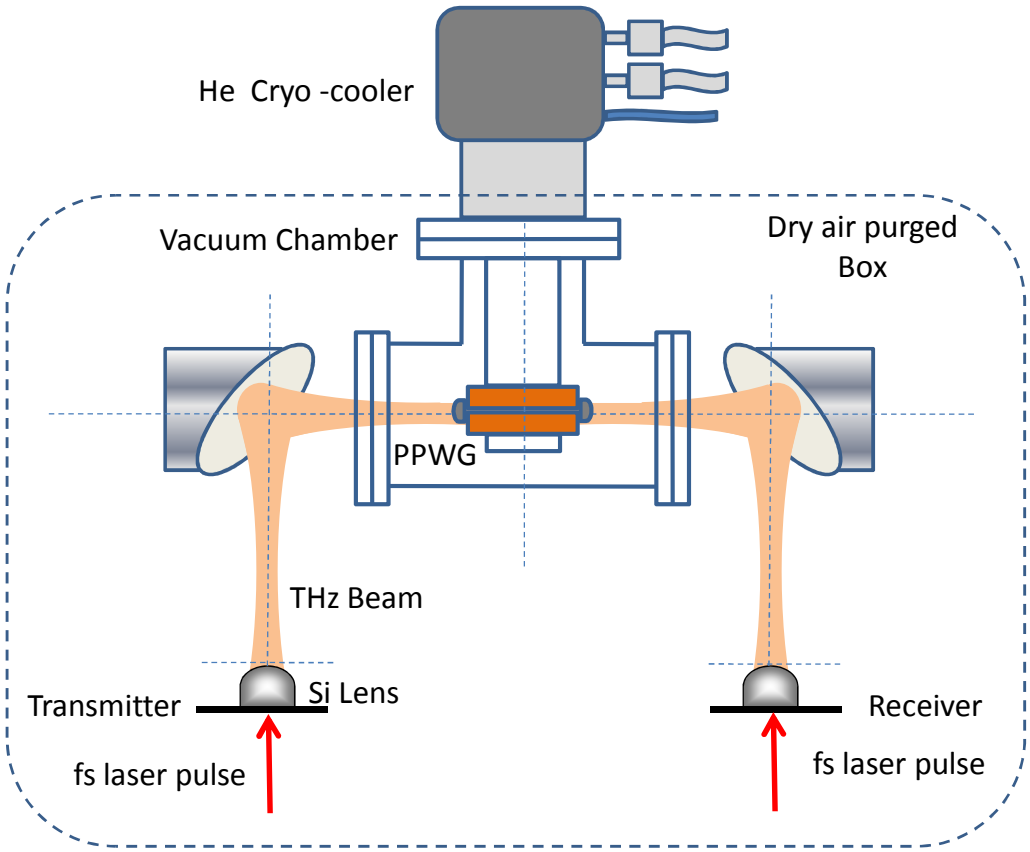

Fig 2.7 Waveguide THz-TDS setup with cryogenic capability

A free-space THz beam is coupled into and out of the waveguide using two identical plano cylindrical high resistivity Si lenses attached to the input and exit faces of the PPWG using custom built lens holders. This PPWG assembly is introduced into a standard THz-TDS system illustrated earlier in Fig 2.1. For experiments at low temperature, the PPWG assembly is placed inside a vacuum chamber with straight-through optical access (2 cm thick Si windows) and is mechanically attached to the cold finger of a two-stage mechanical He cryocooler (or a liquid N2 cold finger), as shown in Fig 2.7. The sample temperature is measured by a Si diode temperature sensor attached to the waveguide. The variation of the absorption spectra with temperature is tracked by taking data at various intermediate temperatures.

2.4.1 Data collection

Typically data (electric field amplitude) is measured in the time domain by varying the delay of the optical pump beam at the receiver chip with respect to the in coming THz pulse. The amplitude spectrum A_{spec} corresponding to each transmitted THz pulse through waveguide is obtained by taking numerical fast Fourier transform of the measured time domain pulse. The spectral resolution of each measurement is directly dependent on the length of the time domain pulse measured. The instrumental spectral resolution is determined by this maximum temporal scan length, limited by Fresnel reflections from the 6.56 mm thick plano-cylindrical Si coupling lenses of the PPWG or the internal reflections of the 2 mm pellet for pellet measurements. For the pellet measurements, typical scan lengths of 33 ps are used. Scan lengths of 150 ps were used for the waveguide measurements, corresponding to a limiting resolution of 6.67 GHz. The time constant on the lock-in amplifier was set at 100 ms with a 400 ms delay for each

data point collected in the time domain. The total time taken for each temporal scan consisting of 2000 data points was 20 min. An average of 6 - 12 such scans was used to improve the S/N. All scans are zero padded by approximately 5 - 10 times before taking the fast Fourier transform to obtain the spectral amplitude.

2.4.2 Zeropadding

Zero padding is often used in THz-TDS, whereby extending the time domain data with zeros causes the subsequent Fourier transform to perform an interpolation in frequency domain between the linearly independent real data points, separated from each other by 6.67 GHz, for a 150 ps scan length. Zeropadding only interpolates between the existing data points and does not increase the frequency resolution of the measurement.

An important measurement consideration one has to bear in mind while doing high resolution measurements is that, a too early truncation of the time domain pulse and starting the zero padding before the pulse has damped out, results in a broadened line shape accompanied by small spectral shifts. However, when a time pulse signal has disappeared into the noise as in our experiments, subsequent zero padding should not affect the line shape and not produce observable frequency shifts. This is illustrated in fig 2.8. In the top frame of Fig 2.8, a long temporal scan of 133ps is shown which corresponds to a spectral resolution of 7.5 GHz. The bottom frame illustrates the effect of truncation of temporal pulse prematurely. A truncated pulse of 33.3 ps scan length (30 GHz resolution) despite being zero padded to the same temporal length as the long scan never fully recovers the complete spectral data, the actual linewidth nor the actual line center.

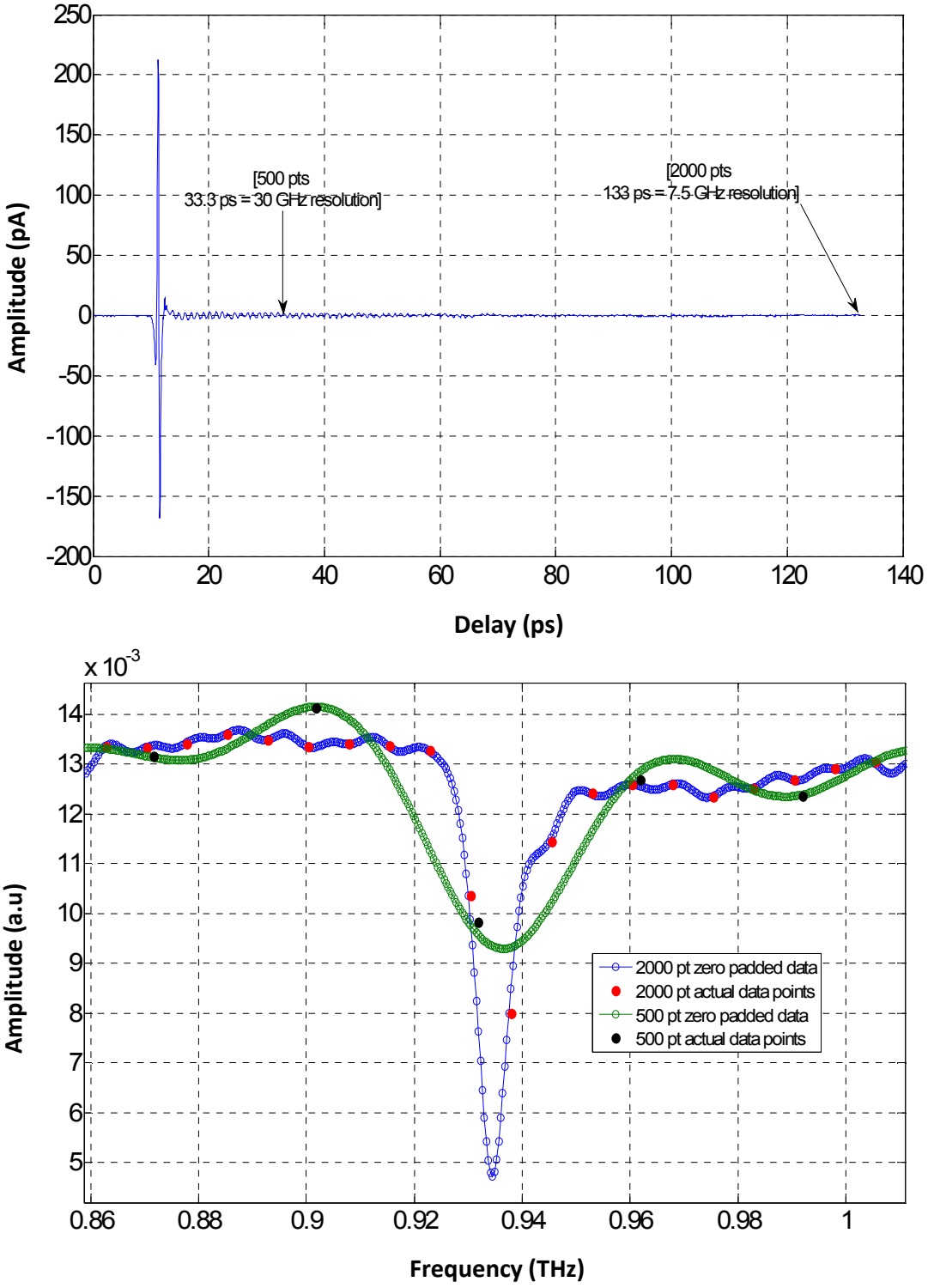

Fig 2.8 Illustration of the effects of early truncation on determination spectral linewidths and line centers

2.4.3 Extraction of the absorbance spectrum

The recovery of accurate absorbance spectra is more challenging for waveguide THz-TDS because of slight changes in the frequency-dependent THz transmissions that occur when the PPWG is reassembled. For some films, accurate absorbance spectra at room temperature can be recovered without disturbing the waveguide by first measuring the THz transmission of the PPWG containing the film and then removing the film by rinsing with an appropriate solvent through the open access on the side of the assembly. An example of an absorbance spectrum for a sample film (7, 7, 8, 8-tetracyanoquinodimethane -TCNQ) determined in this manner is shown in Fig 2.9 (a) and (b). The recovery of absorbance spectra at 77 K is more challenging as the PPWG with the sample is enclosed within the vacuum chamber and the cold temperature of the waveguide does not allow rinsing the sample through the open edges as an option.

Hence for majority of the samples studied using waveguide THz-TDS, we use an approximate method to determine absorbance spectra for the waveguide films. The reference transmission spectrum (A_{ref}) is estimated from the film transmission spectrum (A_{spec}) by first choosing points along the transmission profile that lie outside the absorption lines and then fitting the points with a smooth function (spline) to obtain a reference profile, which includes any broadband absorption and is illustrated for a TCNQ film at 77 K in Fig 2.8 (c) and (d). While this method yields only approximate line intensities, and not the broadband absorption, it is possible to extract accurate line frequencies and line widths. The amplitude absorbance was then calculated via the expression:

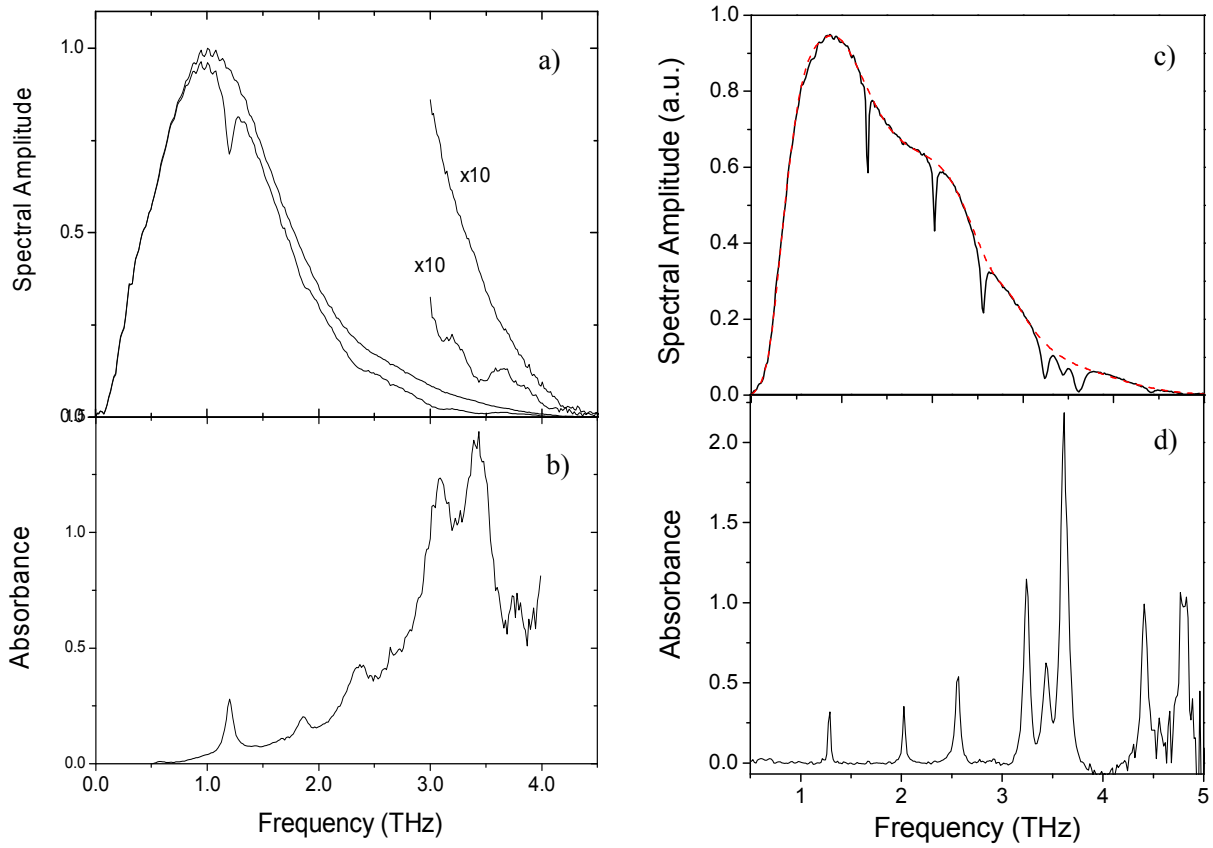

Fig 2.9 (a) Amplitude spectrum at 295 K for a TCNQ waveguide film in a Cu PPWG **(bottom curve),** and for the empty PPWG after washing away film **(top curve)**, **(b)** the resulting absorbance spectrum for the TCNQ film, **(c)** amplitude spectrum for the same film at 77 K and the spline reference fit to the spectrum, and **(d)** the resulting absorbance for the TCNQ film. [publication P2]

$$Absorbance = -\ln\left[\frac{A_{spec}}{A_{ref}}\right] \tag{2.14}$$

The measurement of the actual absorption coefficient and index of refraction of the crystals comprising the microcrystalline layer is not experimentally feasible because of the inhomogeneity of the sample layer and the lack of knowledge of the thickness of the sample layer. In the earlier waveguide THz-TDS measurement of a 20 nm homogeneous water layer, it was possible to obtain an in situ reference pulse. There, the 20 nm layer thickness was obtained by fitting the measured index to that of bulk water [25].

2.4.4 Determination of absolute absorption coefficient of sample films

The polycrystalline films cast on the metal films are often discontinuous and have microcrystals scattered across the metal surface. This makes the estimation of film thickness difficult and hence determining the absolute absorption coefficient is also difficult. But in cases where one can cast a uniform film (polymer films for example) determination of film thickness is easy and an absolute value for the sample film can be calculated using the absorbance relation:

$$A = \alpha f L \tag{2.15}$$

where,

$$f = (t/b)/n^3 \tag{2.16}$$

is the filling factor, L is the length of the film, α is the power absorption coefficient, t is the thickness of the film, b is the gap width of the PPWG, and A is the absorbance. This technique was used by Zhang et.al [25] to determine the absorption coefficient of the nm water layers within the PPWG. For non-uniform polycrystalline films, an equivalent

homogeneous layer can be approximated and the approximate thickness of the film can be used to estimate the absorption coefficient.

2.4.5 Sample preparation: casting the polycrystalline thin film

The key requirement for the success of waveguide THz-TDS is the ability to cast a thin polycrystalline film of the molecule on the metal plates. Failure to obtain a good polycrystalline film has produced featureless THz spectrum in many molecules we have investigated and defeats the purpose of the technique. Most of the polycrystalline films are prepared by dropcasting solutions onto Al or Cu plates while some required sublimation. One of the challenges of this work is to find an appropriate method to obtain an ordered polycrystalline film. Initially, we prepare a film by dropcasting a solution of the molecule onto an optically polished, plasma cleaned copper waveguide plates. Dropcasting involves taking a known amount of the solution of the desired material in an appropriate solvent and then spreading it across the metal waveguide plate with a syringe/dropper and then allowing the solvent to dry out. This process results in a polycrystalline film which is considerably uniform. If this process does not yield a visibly crystalline film, then attempts are made with different solvents and substrates like Al plates, etched Al or Cu Plates, Au coated Al plates, and brushed Al or Cu plates. Failing this, a film is deposited via sublimation. Sublimation involves placing a known quantity of the sample solid in a closed glass container. The waveguide plate is attached to a cold finger which acts as a lid for the container. The container is then evacuated and the sample heated. Under low pressure and heating the sample sublimes and coats the cold waveguide plate to form a thin layer of polycrystalline film of the sample.

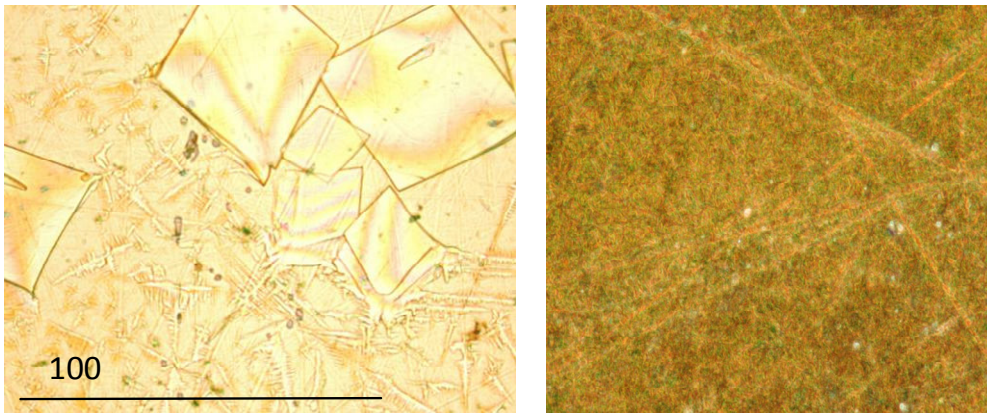

Fig 2.10 Optical micrographs of TCNQ planar crystals on the Cu plate **(a)** Acetone drop-cast film **(b)** Sublimed film. [publication P2]

We have also observed that the formation of crystalline films of many of the biological molecules like nucleosides, deoxynucleosides which are often soluble in water, are very sensitive to humidity and temperature. The formation of crystalline film happened over a period of few days after the dropcast or sublimation. This can be attributed to the fact that these materials slowly reach the complex hydrogen bonded network of the crystalline state over a long period. Many of the organic compounds and amino acids we have investigated form crystalline films easily, some appearing in a few minutes to a few hours depending on the solvent used. Typical appearance of a planar crystalline film obtained from drop-casting and sublimation of TCNQ is shown in Fig 2.10 (a) and (b) respectively.

Sometimes dropcasting may not yield a good crystalline film and sublimation may not be a feasible option due to the melting point of the sample being very high or the sample may degrade on heating. For such molecules, we have used suspension/colloids of the sample in an immiscible solvent and then dropcast this suspension on the metal plate. This method may not result in recrystallization on the metal surface but allows us to cast an uniform film suitable for waveguide THz-TDS.

Once we have a planar polycrystalline film we remove the relatively thick edges of the film with a solvent soaked swab, to leave a visibly uniform film on the surface of the waveguide plate. The mass of the film on the waveguide plate can be estimated by dissolving a similarly prepared film with a solvent and comparing the UV-Vis absorption spectrum to that of a solution of known concentration. These films are then incorporated within a PPWG and then used for waveguide THz-TDS.

Chapter 3

Waveguide THz-TDS: Demonstration of High Sensitivity and Line-narrowing

3.1 Introduction

In this chapter the application of PPWGs for waveguide THz-TDS is discussed and the observed spectroscopic results are discussed in detail. By presenting waveguide measurement data for specially chosen molecules is presented to highlight the capabilities of the new technique. Using these examples the new techniques abilities and drawbacks are presented. As discussed in the previous chapter, an important requirement for this technique to work is that one should be able to cast a polycrystalline thin film on the metal waveguide plate. Dropcasting and sublimation techniques have been used to cast films of the samples for our study. Optical microscopic investigation and X-ray diffraction studies have confirmed that small microcrystals of high crystallinity are formed on the metal plates with great degree of planar order.

The technique of waveguide THz-TDS was developed in 3 stages. They are elaborated as follows:

Step 1. Adapt metal PPWGs for sensitive spectroscopy of molecular solids with a goal of detecting minute sample quantities using the sensitivity enhancement of the waveguide. The surprise discovery of the *"effect of line narrowing of THz vibrational modes"* for the polycrystalline films within the PPWG was made. Vibrational modes showed significant reduction in inhomogeneous broadening and linewidths upto 5- 10 times narrower than the pellet samples was observed even at room temperature. [Publications P1 – P10]

Step 2. Cool PPWGs with sample films to 77 K using liquid nitrogen to get rid of thermal broadening mechanisms (homogeneous). Drastic reduction in linewidths of absorption features was observed with cooling. The linewidths measured for some of the samples were the smallest ever. Capability of measuring high resolution THz vibrational modes polycrystalline films of molecular solids was established by demonstrating the technique for a wide sample range. [P1-P10]

Step 3. The third stage was a significant improvement to the technique. Ability to cool the waveguide samples to 10 K was developed using a 2 stage He-cryo cooler. The true power of waveguide THz-TDS technique was realized with this additional cooling capability with demonstration of measurement of linewidths as narrow as 7 GHz (limited by the instrument resolution – due to reflection from the 6.56 mm thick Si coupling lenses). [publication P5]

3.2 Comparison of Waveguide THz-TDS with the standard Pellet THz-TDS: line narrowing and sub-milligram sample requirement

In order to compare the performance of the two techniques namely the pellet and the waveguide, a proper choice of starting sample was necessary. The molecule 1,2-dicyanobenzene (12DCB) was chosen as it is known to have vibrational modes in the THz spectral region [35]. Dicyanobenzene is an organic compound mainly used as a precursor to the synthesis of pthalocyanine pigments (textile dyes, paper industry), fluorescent brighteners and photographic sensitizers. It is a benzene derivative having two cyano groups. The molecule is known to have three isomeric states differing only in the position of the cyano groups and are called 1,2-, 1,3- and 1,4- dicyanobenzenes depending on the position of the cyano groups. They are white to off white colored compounds soluble in toluene, chloroform and acetone. The dicyanobenzenes are known to have strong vibrational lines in the far infra red (THz) region and have been studied by a number of groups. The dicyanobenzene isomers have strongly coupled electro-negative cyano groups connected to the pi bonded benzene ring, which allows partial atomic charges to undergo vibrational dipolar motions and can enhance THz absorption.

12DCB was purchased from Sigma Aldrich and used without further purification. The 12DCB Pellet was made by uniformly mixing fine powders of the sample with polyethylene powder and then pressing them using a Carver hydraulic press into 2 mm thick pellets (~5mg/100mg) with 1 cm diameter. Alternately for the waveguide measurements, thin polycrystalline films of these samples were dropcast on Cu waveguide plates, from 2mg/ml toluene solutions. The optical micrograph of the

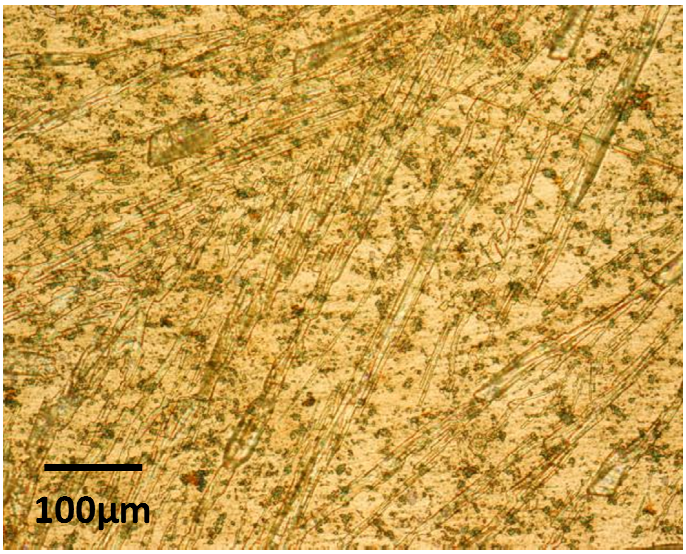

Fig 3.1 Optical micrograph of the polycrystalline film of 1,2 Dicyanobenzene

polycrystalline thin film is shown in Fig 3.1. The amount of sample contained in a typical film was estimated to be around 50-60 μg using UV-Vis spectroscopy. The transmission spectrum for both pellet and waveguide films were measured using a standard THz-TDS setup (discussed in Chapter 2) at room temperature and later cooled to 77 K and then remeasured. The transmission spectrum for both the pellet and the waveguide film is shown in Fig 3.2. The transmission spectrum for 12DCB pellet shows the presence of 3 distinct lines at room temperature at 0.76, 1.58 and 2.29 THz, with FWHM linewidths of 0.06 THz, 0.18 THz and 0.35 THz respectively. These resonances agree with previously observed data from other groups [35].

Spectral resonances at room temperature are often broadened by thermal broadening mechanisms as well as other dynamic relaxation process. Hence, cooling to cryogenic temperature results in quenching of such processes and often results in narrower linewidths and also resolution of otherwise smeared weaker resonances. Upon cooling the 12DCB pellet to 77 K we observed only minimal narrowing of the spectral features accompanied by blue shift of resonances at 1.58 and 2.29 THz as can be seen fig 3.2 and 3.3.

In contrast to the pellet, the waveguide film for 12DCB shows significantly sharper and well resolved vibrational lines even at room temperature. Fig 3.4 shows the transmission spectra for 12DCB film within a Cu PPWG. The waveguide film shows pronounced line narrowing upon cooling to 77 K. At room temperature the 12DCB film reveals 4 distinct spectral lines at 0.65, 1.20, 1.40 and 1.85 THz. Upon cooling to 77 K, the spectral lines in the waveguide film dramatically sharpen, split and shift to higher frequencies. Six lines below 3 THz at 0.77, 1.44, 1.67, 2.10, 2.40 and 2.68 THz are seen.

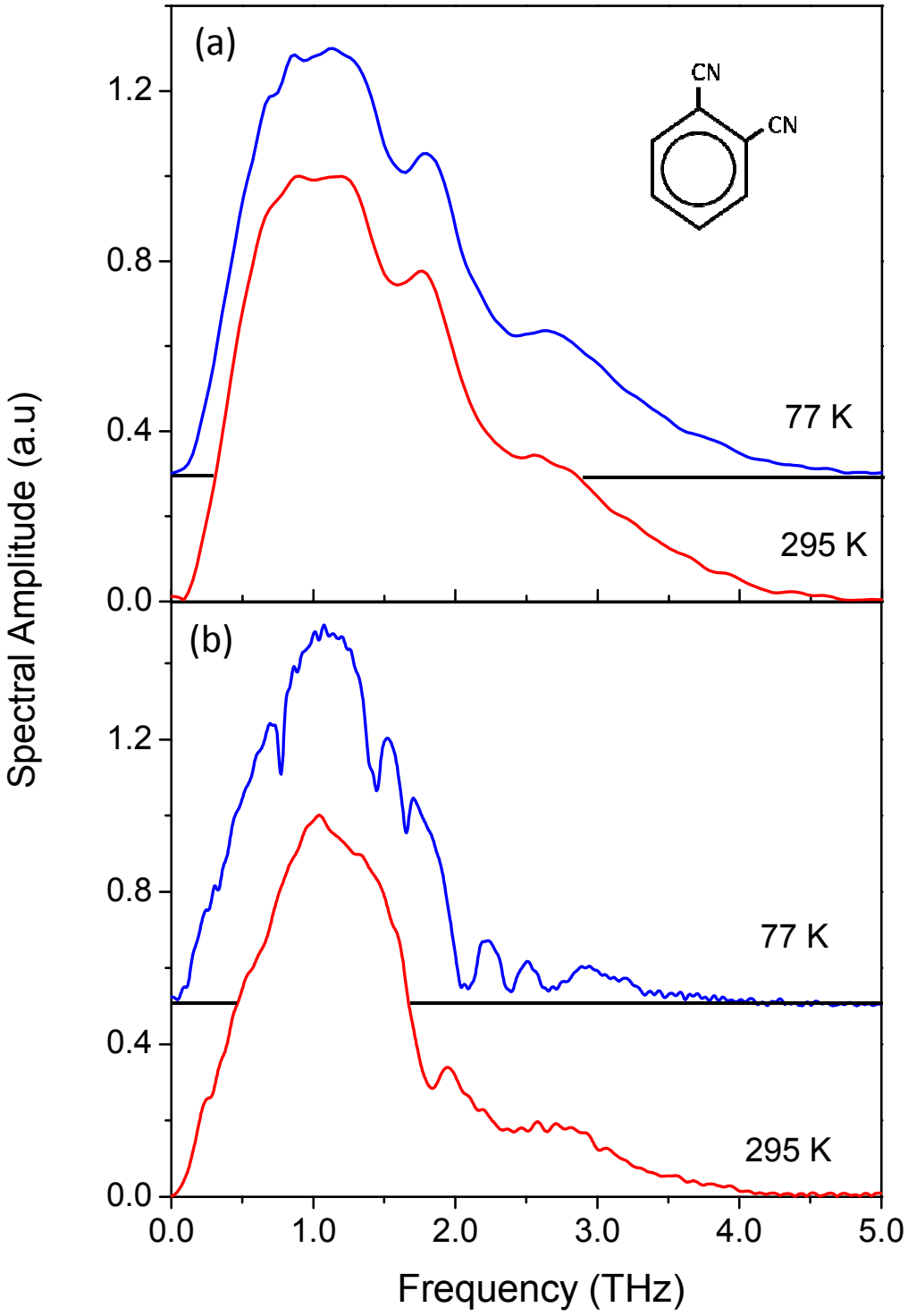

Fig 3.2 (a) Transmitted THz spectrum through a **(a)** 12DCB pellet and **(b)** 12DCB waveguide film at 295 K and 77 K [publication P1]

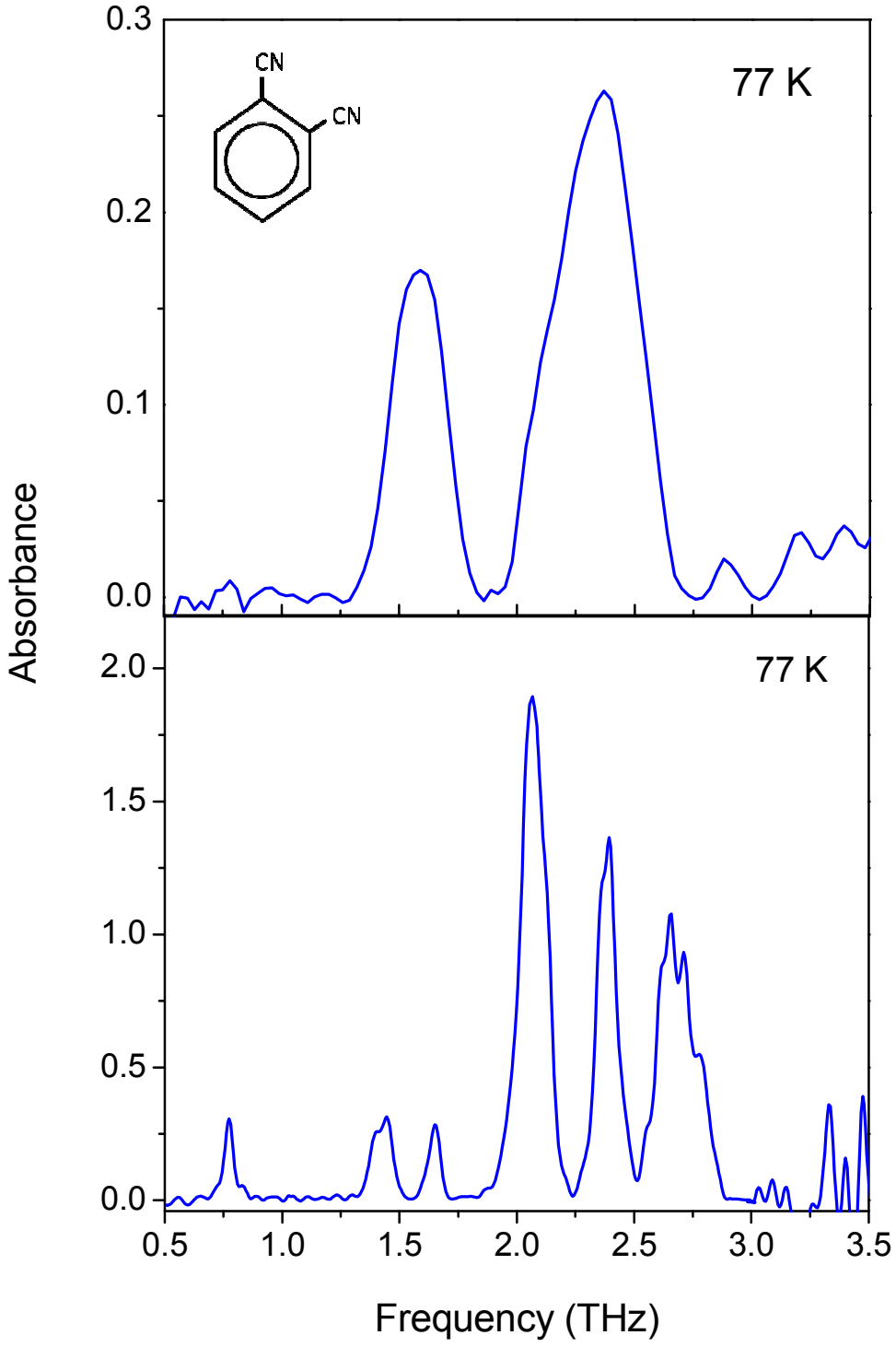

Fig 3.3 Absorbance spectrum of 12DCB **(top)** pellet waveguide film **(bottom)** in Cu PPWG at 77 K. [publication P1]

Modes at 1.67 and 2.10 THz have FWHM linewidths of approximately 0.025 THz and 0.065 THz respectively and are more than a factor of 5 sharper than the corresponding lines in the pellet. Furthermore, the line frequencies at low temperature are substantially blue shifted from their positions at room temperature. For example, the mode at 2.68 THz has shifted by 0.33 THz from its room temperature position. The absorbance spectrum of the pellet and waveguide samples at 77 K is illustrated in Fig 2.3. The Line narrowing effect can be clearly seen from these absorbance spectra. The increased resolution and line narrowing results in a more informative vibrational spectrum with observation of 6 resonances in comparison to just two with the pellet.

Also the sample quantity used for the waveguide measurement used is much lesser than that used for the pellet measurement and is about 100 times lesser. As discussed in chapter 2 substantial sensitivity enhancement is predicted for waveguide measurement of a thin film relative to the traditional single pass through the film of same thickness. For a PPWG of length *L (2.5cm)* and a plate separation *b (50μm),* the sensitivity enhancement is given by $\Gamma = L/n^3b$. If we consider the refractive index of the polycrystalline film to be $n = 1.7$ consistent with values for other organic solids at THz frequencies [36], we get a value for $\Gamma = 102$. This sensitivity enhancement is clearly confirmed experimentally by the *"100 times"* less sample required for waveguide THz-TDS (5 mg in the pellet compared to 50 μg in the waveguide film).

3.3 Physical reasons for line narrowing for waveguide films

The linewidths of THz vibrational modes in solids are known to be a convolution of various line broadening mechanisms which can be broadly classified into homogeneous and inhomogeneous. The observed lineshape of the resonance is hence a superposition of the individual contributions arising from each of these broadening mechanisms. Homogeneous broadening is known to be a dynamic effect often resulting from thermal collisions and is strongly dependent on the thermal state of the sample under characterization. For the case of homogeneous broadening all the mechanisms responsible for the resonance line give contributions which have the same peak center frequency and width. The most obvious case occurs when the linewidth is caused by the finite lifetime of the states between which the transitions occur (see Fig 3.3). [37] These temperature dependent broadening mechanisms however can be quenched by lowering the temperature of the sample. Inhomogeneous broadening on the other hand arises from a wide variety of causes often associated with the environment and state the solid sample is in like random strains, electric fields, and other perturbations from defects in the lattice containing the molecule whose line transitions are studied and can be classified as highly structure dependent. Such broadening often is very insensitive to temperature and cannot be got rid of by lowering the temperature of the sample. One more thing to note is that for the case of inhomogeneous broadening the centers have a wide variety of peak frequencies (see Fig 3.4). Their widths are usually similar but are appreciably less than the width of the distribution of the peak frequencies. Examples of such broadening mechanisms are strain broadening (due to dislocations and point defects in the host lattice containing the molecules), broadening due to the random electric fields and charge

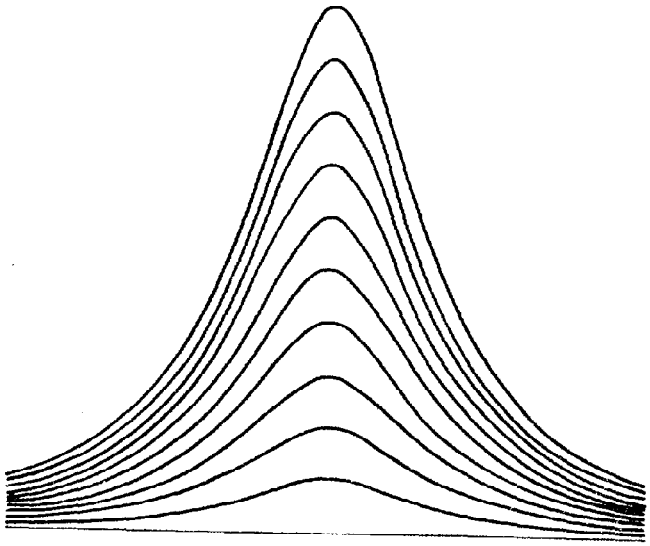

(a)

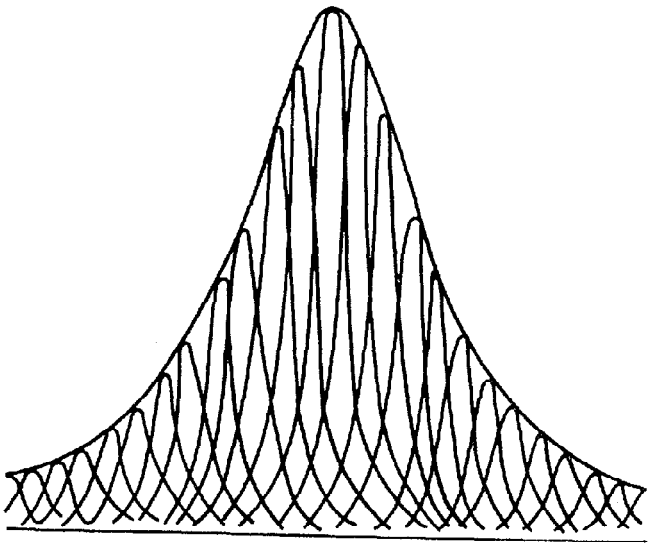

(b)

Fig 3.4 A schematic illustrating the cases for the two main types of broadening mechanisms, **(a)** Homogeneous and **(b)** Inhomogeneous broadening [37].

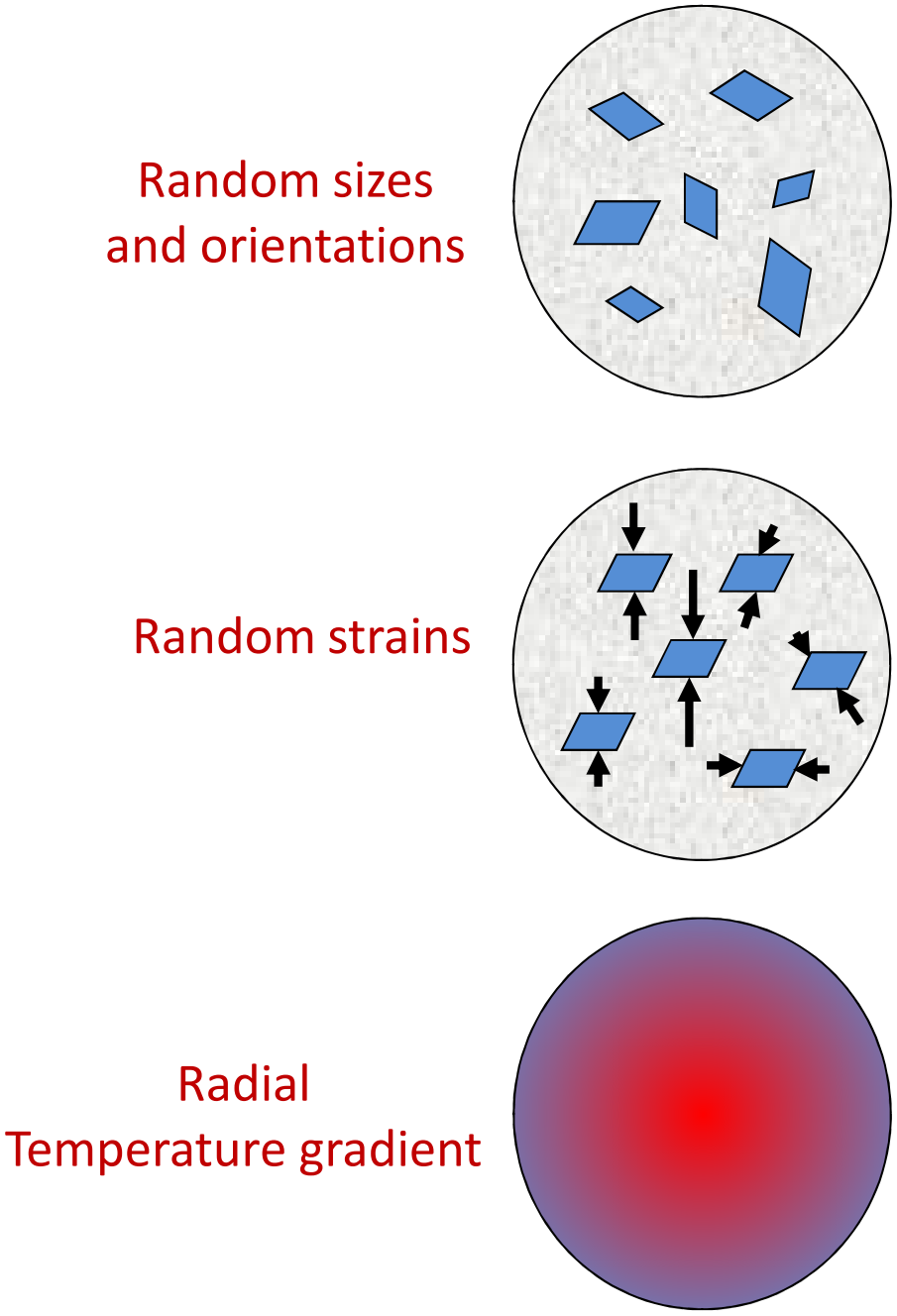

Fig 3.5 Illustration of line broadening mechanisms in a pellet sample.

gradients of charged defects, and the hyperfine interaction of the wave function of the molecule with nuclei of neighboring ions. [37]

Coming to the situation we have, wherein we are comparing the narrow linewidths associated with waveguide films, we can understand is it as follows. The pellets consist of a random distribution of micro crystals of different shapes and sizes in the polyethylene matrix and might have also undergone structural damages due to the application of high pressure during the preparation of the pellet. As a result of this random distribution and strained microcrystals we expect that the THz vibrational line shapes to be greatly dominated by inhomogeneous broadening. This is confirmed by the fact that the features in the pellet spectrum do not narrow or sharpen much upon cooling (and as we discussed earlier inhomogeneous broadening mechanisms are temperature independent). One another thing that also needs to be considered is the fact that the host material in the pellet is a dielectric (polyethylene), the bad thermal conductivity of the host material keeps different parts of the pellet (radially) at different temperatures when cooled and never reaches the desired low temp. These effects are illustrated in fig 3.5.

On the other hand the waveguide films exhibit significant line narrowing and sharpening upon cooling, suggesting that the lines of the waveguide film are dominated by homogeneous broadening mechanisms. A microscopic investigation of the dropcast polycrystalline film reveals that the film is composed a large number of micro crystals that are randomly distributed on the copper waveguide surface but with a great deal of planar orientation (Fig 3.6). The waveguide films exhibit a significant of planar order with respect to the metal surface. This orientation eliminates the effect of inhomogeneous broadening mechanisms. The planar ordering of micro crystals together with the

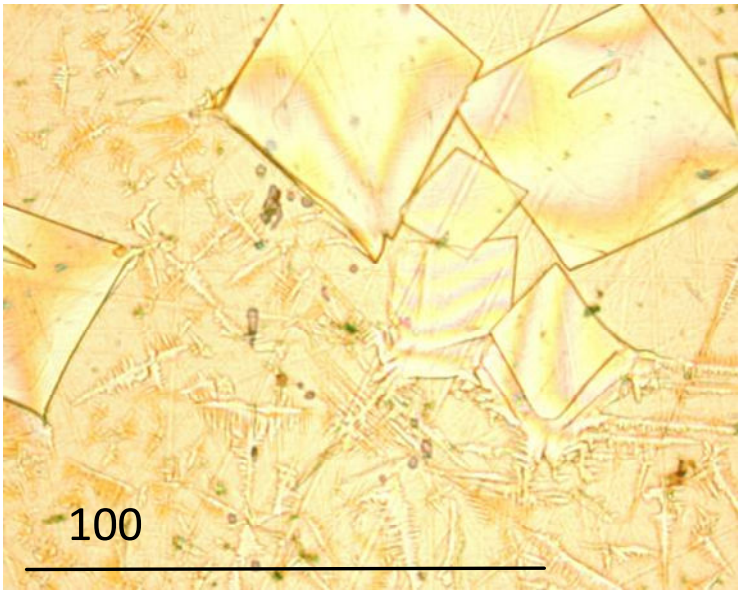

Fig 3.6 Optical micrograph of the polycrystalline thin film of TCNQ on Cu surface.

[publication P2]

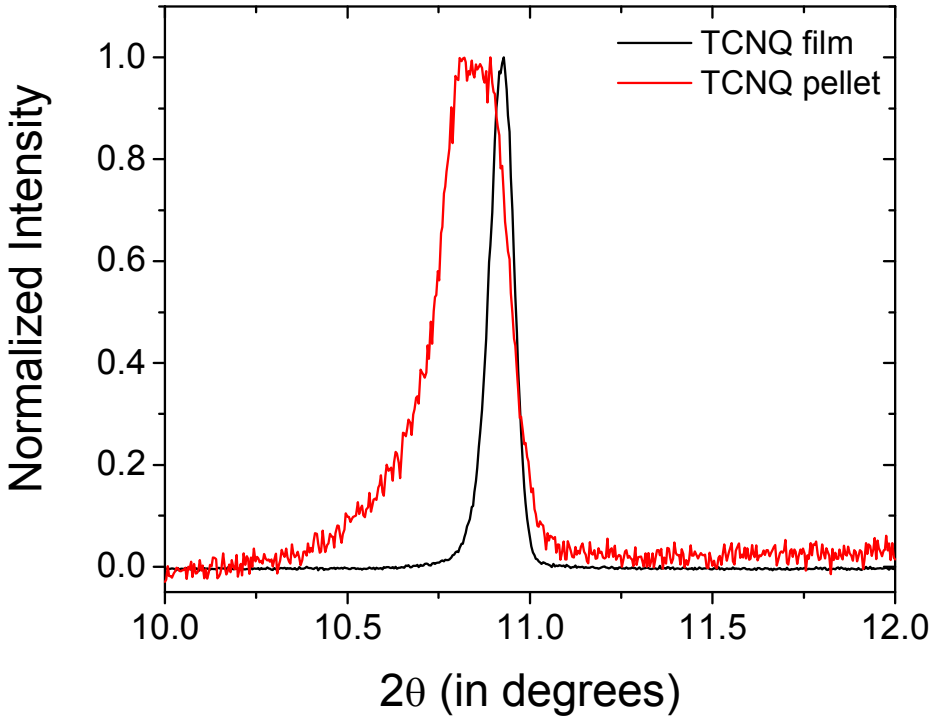

Fig 3.7 X-ray diffraction spectrum of TCNQ pellet and TCNQ polycrystalline film on Cu plate.

formation of defect free crystals is a key requirement for obtaining narrow line THz absorption spectra.

Taking a molecule called TCNQ as an example we have analysed the pellet sample as well as waveguide film using X-ray diffraction to determine the extent of crystallinity and orientation. Fig 3.7 shows the X-ray diffraction (XRD) spectrum of TCNQ pellet and TCNQ polycrystalline film on Cu plate. It is clearly evident that the XRD lines for waveguide films are at least three times narrower than that of the pellet suggesting a better degree of surface orientation in the waveguide film. Possible reasons also may be due to the process of making a pellet. Grinding the analyte, mixing with the transparent host and then compressing under high pressure may produce great deal of distortions (disorder) in the crystalline lattice of the analyte. Whereas on the other hand, the microcrystals formed on the metal waveguide plates yield sharp XRD lines associated with greater degree of crystallinity as well as orientation.

3.4 Study of dependence of THz absorption spectra on crystal morphology on the waveguide metal surface for Tetracyanoquinodimethane (TCNQ).

The THz vibrational modes of many molecules can be either intramolecular (internal) or intermolecular (external) modes of the molecules. The intramolecular modes are dependent on the structure of the molecule and originate from the internal motion of the molecule whereas the intermolecular modes have their origin from the collective motion of the group of molecules forming the crystal lattice. This implies that inter molecular modes show a significant amount of dependence on the crystal size, shape and

morphology. Taking 7, 7, 8, 8 - tetracyanoquinodimethane (TCNQ) as an example we have studied the dependence of THz absorption on micro crystal size and morphology on the waveguide plate.

TCNQ is a well known electron acceptor widely used to prepare charge transfer salts, which have applications in the area of molecular electronics [38]. It was first reported to have been synthesized in 1962. In 1973 it was discovered that a combination of TCNQ (electron acceptor) and tetrathiafulvalene (TTF) formed a strong charge-transfer complex and was referred to as TTF-TCNQ. The complex is formed in solution and can be crystallized into a well formed crystalline solid. These crystals exhibit metallic conductance and was the first purely organic electrical conductors discovered [39].

The size and morphology of the polycrystalline thin film obtained on the metal surface can be controlled by varying the method used to cast the film. By varying the concentration of the solution used and also by altering the method of solution growth of the crystal one can tailor the kind of crystals obtained. In this study, Polycrystalline thin films of TCNQ were made by dropcasting, spincasting, and by sublimation. The drop and spincast films were made using solutions with solute concentrations between 1.0 and 5.0 mg/ml in acetone. The mass of the films was estimated to be approximately 100 μg (using UV/Vis absorption). Films made on Al and Cu waveguide plate surfaces yielded visually similar film morphologies. For sublimation films, an Al waveguide plate was mounted onto the cold finger of a sublimation jar a few centimeters above a small quantity of TCNQ powder placed at the bottom of the jar. The sublimation jar was then evacuated and the bottom heated to induce sublimation onto the waveguide surface.

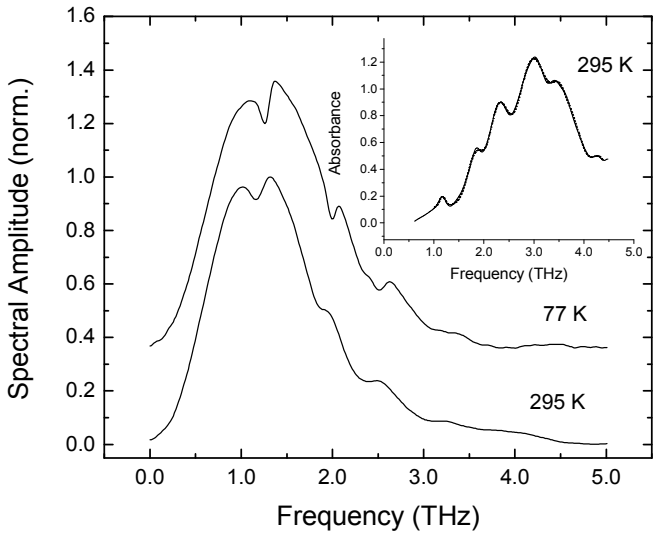

Fig 3.8 THz transmission spectra of a TCNQ pellet at 295K and 77K [publication P2]

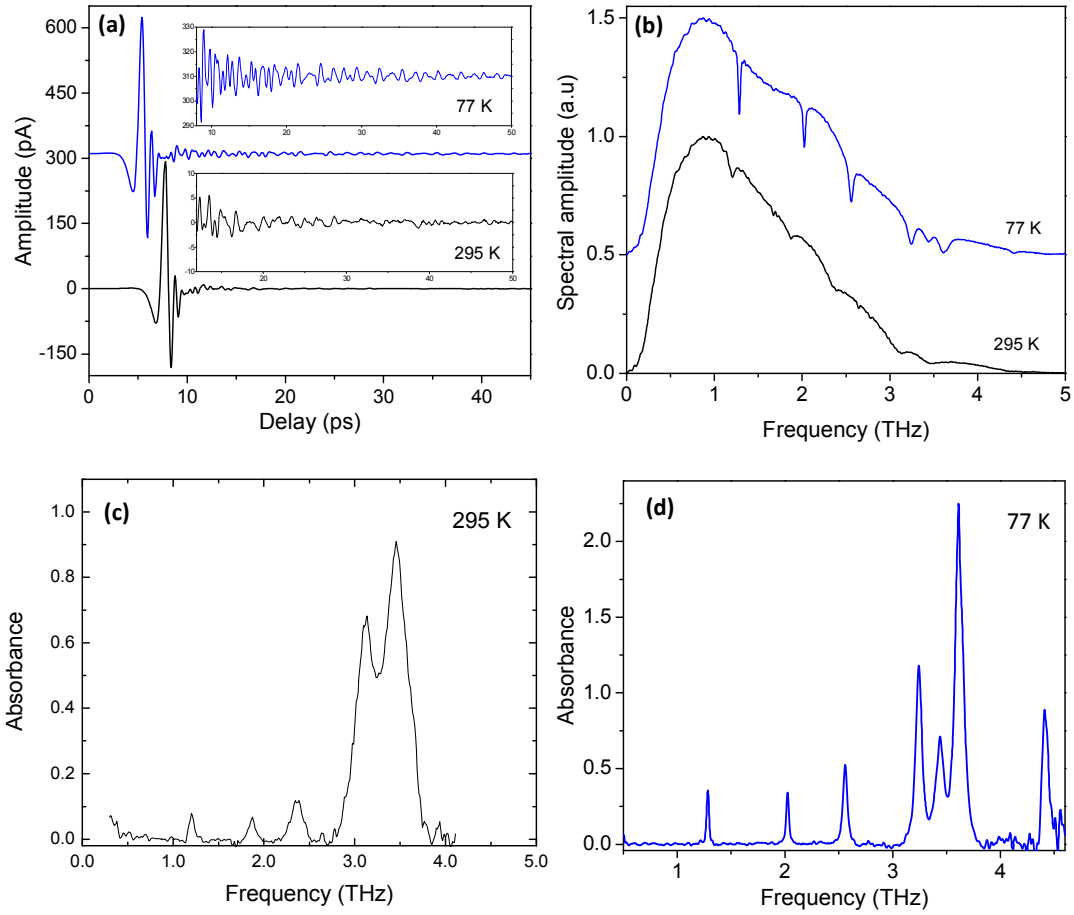

Fig 3.9 (a) Transmitted THz pulse through a copper waveguide with dropcast TCNQ film at 295 K and 77 K, **(b)** corresponding transmission spectra, **(c)** absorbance at 295 K and **(d)** absorbance at 77 K. [publication P2]

Table 3.1. Line-Center Frequencies and FWHM linewidths (within parentheses) for TCNQ pellet and TCNQ dropcast film in the waveguide [a] [publication P1]

Pellet Sample		Dropcast film	
295 K	**77 K**	**295 K**	**77 K**
1.16 (0.13)	1.27 (0.12)	1.20 (0.08)	1.28 (0.03)
1.83 (0.83)	1.99 (0.18)	1.87 (0.10)	2.02 (0.04)
2.28 (0.43)	2.50 (0.27)	2.36 (0.20)	2.56 (0.07)
2.97 (0.75)	3.04 (0.50)	3.13 (0.27)	3.24 (0.11)
3.47 (0.32)		3.46 (0.34)	3.44 (0.13)
3.70 (0.60)			3.61(0.11)
4.31 (0.35)			4.41 (0.08)

[a] All values are in THz

Fig 3.9 (a) shows the measured transmitted THz pulse through a copper waveguide with dropcast TCNQ film at 295 K and 77 K. The shift to earlier times at 77 K is due to the temperature dependent refractive index of the Si lenses [33]. The observed ringing in the time domain corresponds to sharp features in the corresponding transmission spectrum obtained by a numerical Fourier transform of the complete pulse measurements. The absorbance at 295 K and 77 K is shown in fig 3.9 (c) and (d). In contrast to the TCNQ pellet (Fig 3.8), the three lowest frequency vibrational bands in the waveguide film are well resolved, even at room temperature. Table 3.1 list the line centers and linewidths for both pellet and waveguide films.

At room temperature as can be seen from Fig 3.9 (b) and (c), five features are observed between 1.0 and 4.0 THz with line widths ranging between 0.08 and 0.34 THz. The line widths of the three lowest frequency lines are almost 2 - 4 times sharper than corresponding line widths for the pellet at 295 K. Cooling the waveguide results in

narrowing of the vibrational lines buy a factor 2-3. The relatively high S/N achieved for the 77 K measurements clearly resolves seven vibrational lines. In particular, the relatively broad doublet between 3.0 and 4.0 THz observed at 295 K has split into three relatively sharp lines. The narrowest line widths occur for the lowest-frequency lines. For example, the 1.28 THz mode narrows to a FWHM width of 0.03 THz and the 2.02 THz mode narrows to a FWHM width of 0.04 THz, which is a narrowing of about four times relative to the corresponding lines in the pellet.

3.4.1 Dependence of THz absorption spectra on crystal morphology

For TCNQ three different kinds of film preparation techniques were employed to prepare the polycrystalline film required for waveguide measurement, namely dropcast, sublimation and spin coating. It was observed that each of these film preparation technique resulted in a slightly different crystal morphology on the waveguide surface. It was also noted that for the dropcasting technique alone the microcrystal morphology depended on the concentration of the solution used to dropcast.

In Fig 3.10 the optical micrographs of the polycrystalline films obtained by different methods and also the corresponding waveguide THz absorbance spectra measured at 77 K are shown. Parts (a) - (c) of Fig 3.10 show how the microcrystal shape depends on the solute concentration when dropcasting is used to cast the film. At a relatively low TCNQ concentration (1.3 mg/ml), a dendritic structure is obtained with largest microcrystals having dimensions of ~30 μm. The corresponding absorbance spectrum is the same as in Figure 3.9 (d) and is reproduced in Fig 3.10 (a) for comparison. Higher TCNQ concentrations (2.4 mg/ml) result in TCNQ crystallizing as

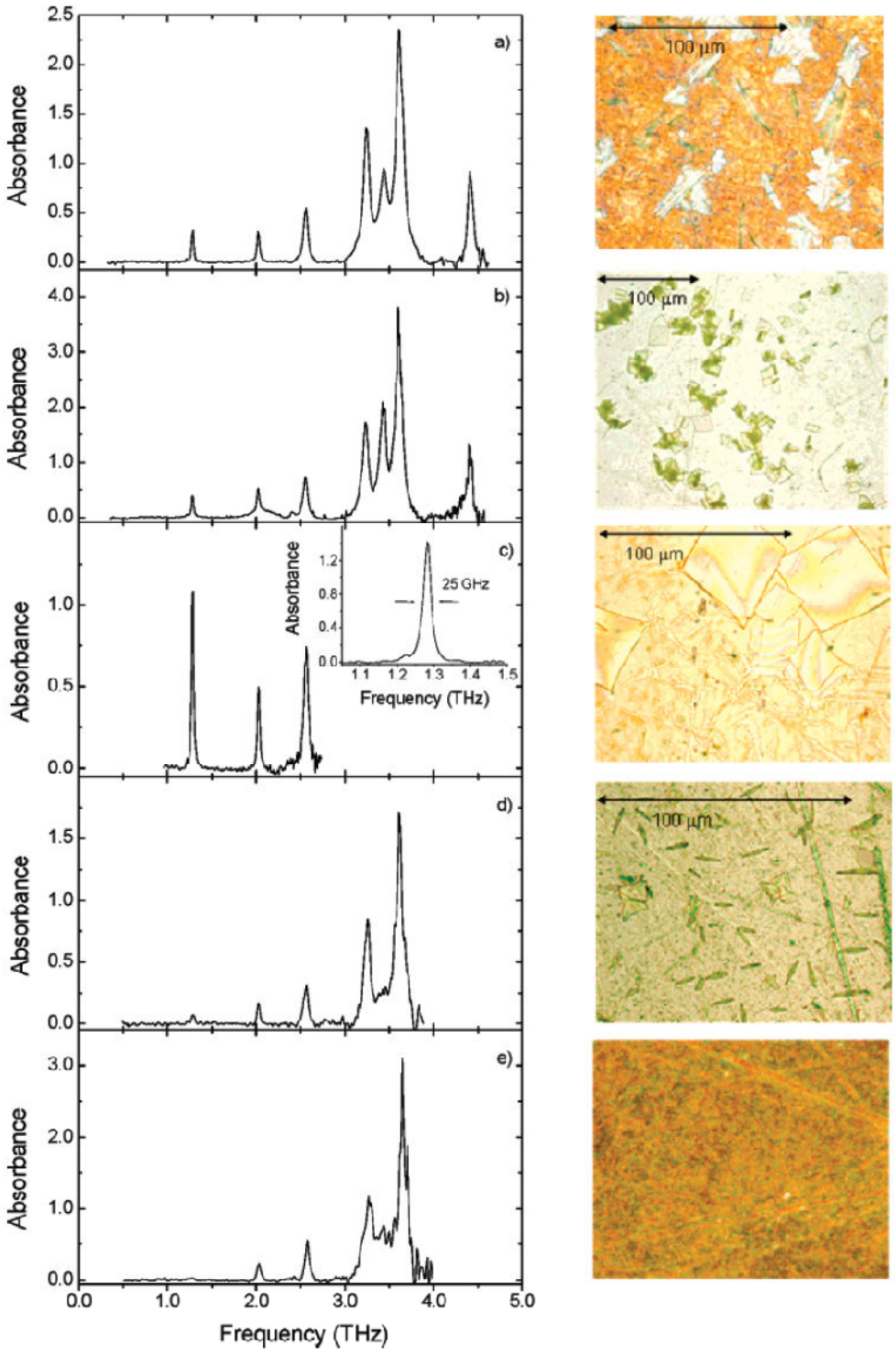

Fig 3.10 THz absorbance spectra for TCNQ waveguide films prepared using different methods and their corresponding optical micrographs, **(a)** Drop cast film on Cu (1.3 mg/ml) **(b)** Drop cast film on Al (2.4 mg/ml, **(c)** Drop cast film on Cu (5.0 mg/ml), **(d)**.Spin cast film on Al (2.0 mg/ml) **(e)** Sublimed film on Cu [publication P2]

small rhombic plates with various size distributions as shown in Fig 3.10 (b). The largest rhomboidal crystals have sides of about 15 - 20 μm in length. Only minor changes in the vibrational spectrum are observed for this film and occur mainly in the relative intensities of the group of three lines near 3.5 THz. Fig 3.10 (c) shows the morphology of a dropcast film made from a relatively concentrated TCNQ solution (5mg/ml). The largest microcrystals are formed here with sides more than 50 μm in length. In addition, the film also contains smaller rhombic plates and some dendritic structures. The absorbance spectrum in this case shows a significant increase in the relative intensity of the 1.28 THz mode. This film morphology also produced the narrowest line width (FWHM) 25 GHz for the 1.28 THz mode, which is shown in the inset of Fig 3.10 (c). The high frequency features were not measured in this case because of the strong absorption of the thicker film, which required 100μm spacers and also reduced spectral transmission towards the high frequencies through the PPWG.

The TCNQ absorbance spectrum was significantly different for spincoated and sublimated films (Fig 3.10(d) & (e)). Spin coating resulted in mainly needlelike microcrystals with average lengths of about 10μm. In addition to these, a small fraction of microcrystals resembled triangular platelets in shape. The strong contrasts in the vibrational spectrum of spin coated microcrystals are the reduced intensities of the 1.28 THz and the 3.44 THz features with respect to the other lines. Sublimation produced the smallest microcrystals and they were smaller than could be resolved using 100X magnification. The vibrational spectrum is similar to that of the spin-coated film, with the exception that the intensity of the 1.28 THz mode is almost totally attenuated.

Clearly, a wide range of microcrystal shapes and sizes were obtained depending on the method and specific methods of film preparation. The positions of the vibrational frequencies and their line widths did not change for the different morphologies shown in Fig 3.10, however significant differences in relative line intensities is seen. In particular, the modes at 1.28 and 3.44 THz are highly sensitive to the size of the microcrystals. Both modes exhibit significantly weaker relative intensity for films containing the smallest microcrystals, while the 1.28 THz mode shows increased relative intensity for the largest rhomb microcrystals. This dependence on morphology suggests that these modes have substantial external vibrational character and are associated with long range order of the crystal lattice.

3.4.2 Determination of microcrystal orientation on the waveguide surface using X-ray diffraction:

The X-ray diffraction analysis of the polycrystalline films used in this study was done by Dr. Joseph Melinger at Naval Research Labs and provides more insight into the degree of orientation and crystallinity of the polycrystalline samples. The following description was a part of the publication P2 and is reproduced here to substantiate the fact that the polycrystalline films obtained are of high quality and are aligned in a planar fashion. [publication P2]

The planar order obtained for the polycrystalline films on the surface of the metal plates allow for polarization effects to be observed for the vibrational modes in waveguide THz-TDS. Knowing how the microcrystals are oriented on the metal plate in turn lets us know the angle the crystal axes make with respect to the propagating THz

field. This knowledge allows us to assign line intensities for the different modes observed and can assist in assignment of vibrational modes to different motions of the molecule within the crystal lattice.

To determine their orientation and degree of planar order, TCNQ films were characterized using reflection X-ray diffractometry. This was done for dropcast TCNQ films on both Al and glass substrates that yielded the dendritic and rhombic plate morphologies shown in parts (a) and (b) of Fig 3.10, respectively. For a given TCNQ solution concentration, both the Al and glass substrates produced very similar microcrystal morphologies under inspection with an optical microscope.

TCNQ is known to crystallize in the monoclinic system having space group *C2/c* and with four molecules per unit cell [40]. The X-ray diffraction pattern observed for dendritic TCNQ microcrystals is shown in parts (a) (on glass) and (b) (on Al) of Fig 3.11. For both substrates, diffraction peaks due to TCNQ at $2\theta = 10.93°$, 21.94°, and 33.15° (and 44.68° for TCNQ on glass) dominate the spectrum. In fig 3.11 (b), strong peaks at $2\theta = 38.42°$ and 44.62° are due to the Al substrate. The positions and relative intensities of the TCNQ peaks were compared to a simulated X-ray diffraction spectrum of TCNQ using Mercury [41] and are found to be consistent with diffraction from the *(00l)* planes of the unit cell (with $l = 2$, 4, 6, and 8). Considering the absence of strong peaks due to other TCNQ planes, the data strongly suggest that the film has a dominant orientation where the *c - axis* of TCNQ unit cell points upward from the substrate surface, making an angle of 8.5° with respect to the surface normal, and that the *(001)* plane of the unit cell is aligned parallel to the waveguide surface. Consequently, for the polycrystalline sample film, the distribution of *c - axes* of the individual microcrystals defines a cone with an

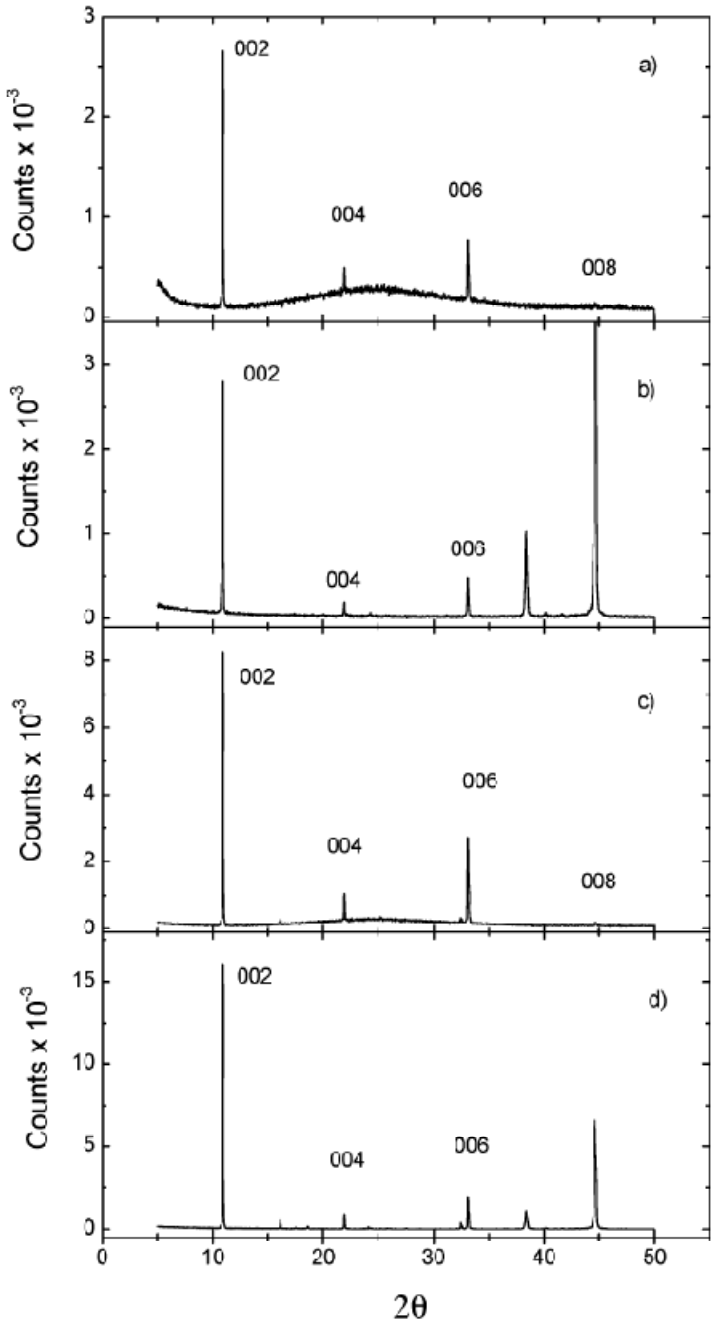

Fig 3.11 X-ray diffraction spectrums for TCNQ films on glass and polished Al surfaces. **(a)** Dendritic microcrystals on glass. **(b)** Dendritic microcrystals on Al. **(c)** Rhombic microcrystals on glass. **(d)** Rhombic microcrystals on Al. Peaks due to Al substrate are at 2θ = 38.42° and 44.62°. [publication P2]

angle of 8.5° about the THz polarization. The diffraction spectrum of the film on Al shows a few relatively weak lines that are just resolvable from the baseline, which are due to other TCNQ crystal planes and which indicate that other orientations are present to a minor extent. The higher degree of roughness of the Al surface relative to the glass surface may account for more variation in microcrystal orientation. The X-ray diffraction pattern corresponding to the rhombic plates is shown in Fig 3.11 (c) and (d). Here the diffraction peaks of the *(00l)* planes again dominate the spectrum, however, there is a somewhat stronger contribution from diffraction from other planes, particularly for the film on Al. The film of rhombic plates is cast from a relatively concentrated TCNQ solution (2.4 mg/ml), which produces a thicker film than that for the dendritic microcrystals. Partial stacking of the plates in the thicker film is likely to produce a greater fraction of microcrystals with different orientations with respect to the substrate.

A schematic of the TCNQ unit cell showing its orientation on the substrate and with respect to the experimental electric field polarization is shown in Fig 3.12. In addition, the molecular axes *(X, Y, and Z)* for an individual TCNQ molecule are also defined. *The X axis* is perpendicular to the plane of the TCNQ molecule, while the *Y* and *Z axes* are in the plane and are oriented as shown. A table of proportionality factors for band intensities along the *a, b, c,* and *c* (⊥ ab) axes* of the unit cell is reproduced from data from ref 58. With the *(001)* plane aligned parallel to the waveguide surface, the *a* and *b axes* are perpendicular to each other and are in the plane of the waveguide, and the *b* and *c axes* are perpendicular. The *c*- axis* is parallel to the electric field polarization. In this configuration, internal vibrational modes that are polarized along the *Y* and *Z*

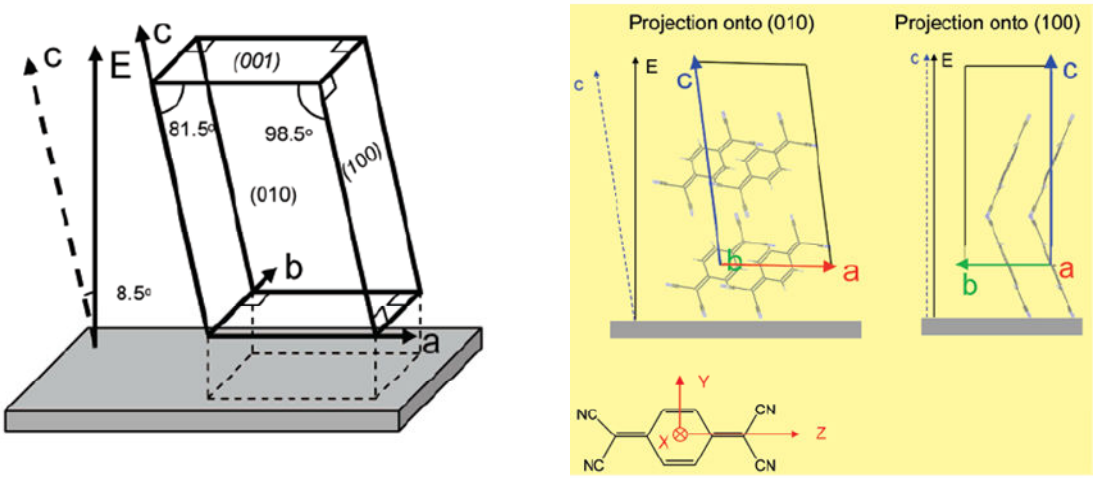

Crystal Direction	X	Y	Z
a	0.00	0.56	0.43
b	0.84	0.07	0.09
c	0.16	0.49	0.35
c * ***(⊥ ab)***	0.16	0.35	0.49

Fig 3.12 (Left panel) Schematic of the TCNQ unit cell showing its orientation on the metal PPWG surface and with respect to the electric field polarization. The electric field is polarized perpendicular to the PPWG surface. **(Right Panel)** Projection of the TCNQ unit cell onto the *(010)* plane (top, left) and *(100)* plane (top, right) and with respect to the experimental electric field. For the projection onto *(010)*, the two molecules on the left have their centers at $a = 0$ and $b = 0$, while the two molecules on the right are displaced one-half of a lattice translation along *b*. The *c-axis* of the unit cell makes an angle of 8.5° with the electric field polarization vector. With the *(001)* plane aligned parallel to the waveguide surface, the *a* and *b axes* are perpendicular to each other and are in the plane of the waveguide, and the *b* and *c axes* are perpendicular. The molecular axes of an individual TCNQ are shown. The *X axis* is perpendicular to the plane of the TCNQ molecule, while the *Y* and *Z axes* are in the plane and are oriented as shown. The table gives the proportionality factors for band intensities along the crystal axes. [publication P2]

molecular axes have greater projections along the *c* axis* and are expected to show enhancement in the waveguide film. A comparison of pellet and waveguide film spectra at 295 K (Fig 3.8 and 3.9 respectively) suggests that the vibrational mode near 3.5 THz gains relative intensity in the waveguide film spectrum, whereas modes near 1.87, 2.4, and 3.0 THz lose relative intensity.

Previous vibrational work done on the molecule differs in assignments of low frequency vibrational spectrum [42 - 44]. An earlier study indicates that the lowest three lines observed as external phonon vibrations [42]. This means these modes have their origins from vibrations external to the molecule itself and are associated with lattice vibrations, translations and intermolecular liberations. Some other study showed that the low frequency modes had a mixed character meaning both intra and inter molecular motions.

Considering the three low frequency lines as intermolecular corresponding to external vibrations, then the results above suggest that the vibrational modes at 1.87 and 2.36 THz do not have strong projections onto the *c* axis* because their relative intensities are attenuated in the oriented waveguide film spectrum. Ref 42 assigns the mode near 3.0 THz (100 cm^{-1}) to an out-of-plane ring bend (along *X*), which has a relatively weak projection onto the *c* axis*, and the mode near 3.5 THz (115 cm^{-1}) as an in plane bending of the NC-C-CN groups (along *Z*), which has a relatively strong projection onto the *c* axis*. The enhancement in relative intensity in the waveguide film near 3.5 THz appears to be consistent with this assignment of internal vibrational motion. Clearly, an angle dependent THz characterization of an oriented single TCNQ crystal would be valuable to more confidently assess polarization effects in waveguide THz-TDS. [publication P2]

3.5 Demonstration Sub-10 GHz resolution capability of waveguide THz-TDS in determining the vibrational modes using 2, 4-dinitrotoluene (24DNT)

In the preceding sections it was clearly demonstrated that using metal PPWGs one can significantly reduce inhomogeneous broadening and achieve very narrow line widths for the vibrational modes of the molecules under study. The molecules were then cooled to liquid nitrogen temperature, quenching the effect of thermal broadening mechanisms which further reduced the linewidth of the resonances and resulted in obtaining a very precise narrow linewidth vibrational spectrum. It is anticipated that cooling much below 77 K would allow us to further reduce thermal effects and achieve much narrow linewidths for these vibrational modes. Experimentally it was observed that cooling below 77 K to 10 K had a very great effect on the line shape and linewidth of the modes. The additional sharpening with further cooling implies that our polycrystalline thin films have very strong planar order and with the individual microcrystals containing a high degree of crystallinity. We can therefore obtain measurements approaching the quality of single crystals, but with the easy to cast polycrystalline sample films.

The instrument resolution of the waveguide THz-TDS technique is limited by the maximum temporal scan length one can perform before encountering strong reflections from numerous optics within the system. The major reflections in the system arise primarily from the cylindrical Si coupling lens for the PPWG and the Si windows of the chamber housing the waveguide. The first strong reflection is due to the 6.56 mm thick high resistivity Si coupling lenses at 150 ps corresponding to a *spectral resolution of 6.7 GHz (0.22 cm^{-1})*. This is the limiting instrument resolution of the system.

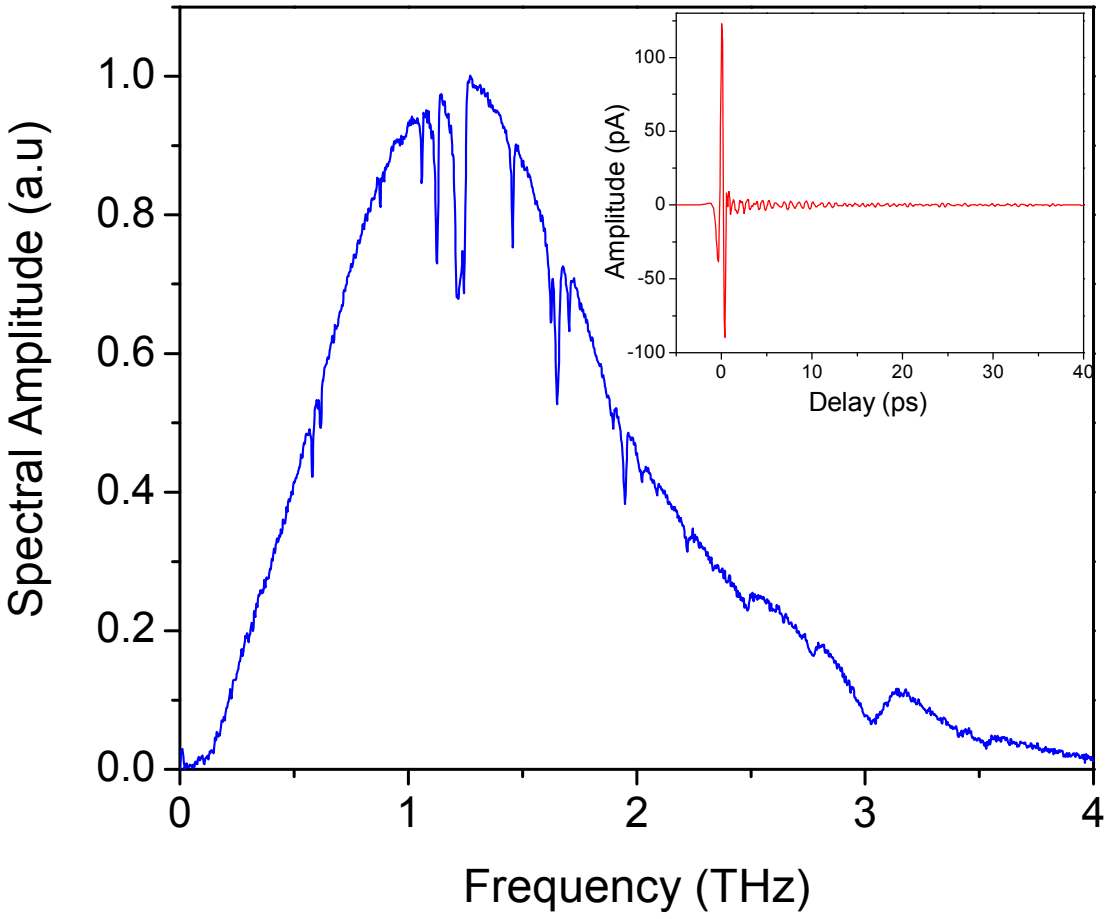

Fig 3.13 Output terahertz amplitude spectrum of dropcast 24DNT film within an Al PPWG at 11 K. **(Inset)** Time domain trace of the terahertz pulse through the 24DNT waveguide at 11 K. [publication P5]

2,4-dinitrotoluene (24DNT) is an explosives related solid and is a precursor as well as a byproduct of the degradation of the explosive 2,4,6-trinitrotoluene (TNT). This compound has been characterized earlier and pellet data for this molecule is available in literature. 24DNT pellets were made by mixing 32 mg of sample powder in 330 mg of polyethylene powder and then compressed at a pressure of 11 metric tonnes. The 24DNT waveguide film was obtained by drop casting 100 μl of a 2.5 mg/ml acetone solution onto a polished Al plate. The thick edges were removed by a solvent soaked swab, to obtain a uniform film with an estimated mass of less than 100 μg, compared to 32 mg of 24DNT used for the pellet sample. Alternatively another film was cast from a concentrated solution of 8mg/ml. The pellet as well as the two films was investigated using the standard THz-TDS setup.

Fig 3.13 shows the transmission spectrum of a 2.5 mg/ml 24DNT film within an Al PPWG at 11 K. Fig 3.14 shows the temperature dependence of the vibrational modes in both the pellet as well as the waveguide film. For the pellet, a strong broad resonance is seen at 1.06 THz. Upon cooling to 11 K, features sharpen moderately with only a minor change below 80 K, resulting in 7 observable features at 11 K. the features also blue shift during cooling.

The waveguide film on the other hand has a dramatic response to cooling. In sharp contrast to the pellet, there is substantial sharpening of the features at lower temperatures, particularly below 80 K. At 11 K, this sharpening resolves 19 observable vibrational lines. This is nearly 3 times the number of lines observed with the pellet and corresponds to a substantial increase in information obtained about the vibrational modes of this material as well as the precision of their identification. Spectral data, including line

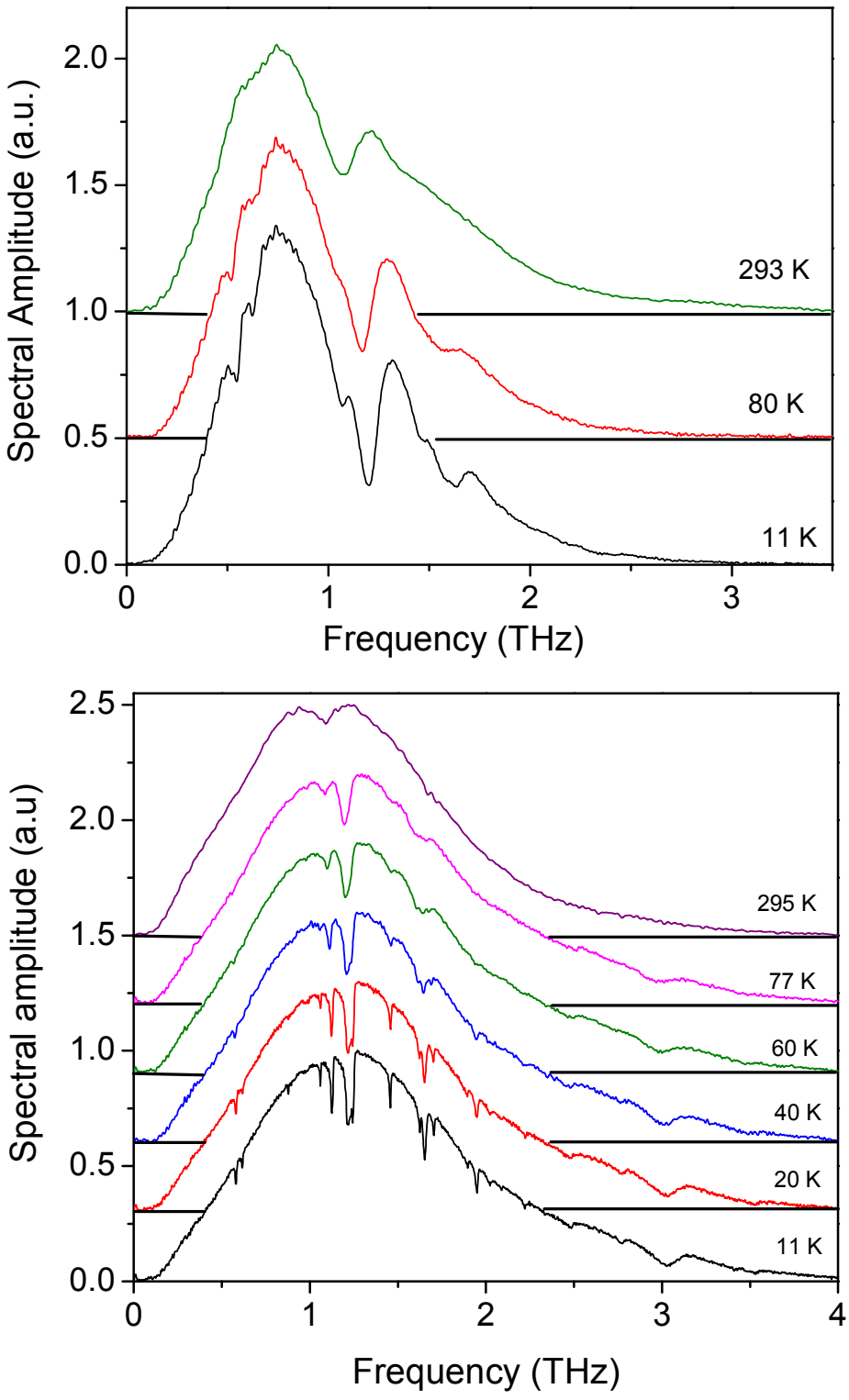

Fig 3.14 Amplitude spectra of THz transmitted through **(top)** 2,4DNT pellet and **(bottom)** waveguide film, as a function of temperature. [publication P5]

frequencies and line widths, for both the 24DNT pellet sample as well as the waveguide film are collected in Table 3.2 for comparison.

The amplitude absorbance of both the 24DNT pellet and waveguide at 11 K is shown in Fig 3.15. The dramatic difference between the waveguide and pellet absorbance is clearly seen. The waveguide clearly resolves the doublet near 1.1 THz, the doublet near 1.5 THz and the broad feature near 1.9 THz, corresponding to a narrowing by a factor of 5, 10 and 20, respectively. Of the 19 lines, 11 have a measured linewidth of less than 15 GHz (0.5 cm^{-1}). The limiting resolution being 6.7 GHz, we can expect that the intrinsic linewidths of some of these lines to be much narrower. Table 3.2 compares the present data to work previously carried out by other groups on this molecule. Previous work has measured up to five broad features in this frequency range, compared to the 19 narrow lines measured in this work with the low temperature waveguide [45-48]. The narrowest lines so far measured with the waveguide technique having a linewidth of 7 GHz are at 0.88 and 1.06 THz, indicated in Fig 3.15.

As evident from Fig 3.15 some of the absorption modes especially towards the higher frequencies are weak and almost disappear into the noise floor. In order to bring out these features a concentrated (8mg/ml) solution was used to dropcast the film. Fig 3.16 compares the absorbance of the two films. Clearly all the features are stronger and the high frequency modes are more clearly evident with new lines coming in between 2.2 and 3 THz. Another prominent change is that the second feature at 0.62 THz is missing and the cluster around 1.25 THz is now merged into one strong resonance and is no longer clearly resolved. This may be due to the fact that these resonances are somehow

Table 3.2. Comparison of line center frequencies (THz) of 24DNT for this study and previous work [publication P1]

This Study Waveguide 11 K	This Study Pellet 11 K	This Study Pellet 295 K	Liu et al. Pellet (45) 295 K	J. Chen et al. Pellet (46) 295 K	Y. Chen et al. Pellet (47) 295 K	Hu et al. Pellet (48) 295 K
0.58 (0.008)	0.55 (0.034)	-	0.43	0.43	-	-
0.62 (0.010)	0.63 (0.045)	-	0.66	0.66	-	-
0.88 (0.007)	-	-	-	-	-	-
1.06 (0.007)	1.07 (0.11)	-	-	-	-	-
1.12 (0.014)	-	-	-	-	-	-
1.22 (0.043)	1.20 (0.08)	1.06 (0.18)	1.08	1.08	1.08	1.08
1.24 (0.010)	-	-	-	-	-	-
1.46 (0.008)	1.46 (0.10)	-	-	-	-	-
1.62 (0.012)	1.60 (0.13)	-	-	-	-	-
1.65 (0.018)	-	-	-	-	-	-
1.70 (0.010)	-	-	-	-	-	-
1.89 (0.008)	-	-	-	-	-	-
1.95 (0.015)	1.92 (0.24)	-	-	-	-	-
2.03 (0.017)	-	-	-	-	-	-
2.22 (0.009)	-	-	-	-	-	-
2.48 (0.050)	-	-	-	-	-	-
2.77 (0.040)	-	-	-	-	-	-
3.02 (0.130)	-	-	2.52	2.54	-	-
3.46 (0.150)	-	-	-	-	-	-

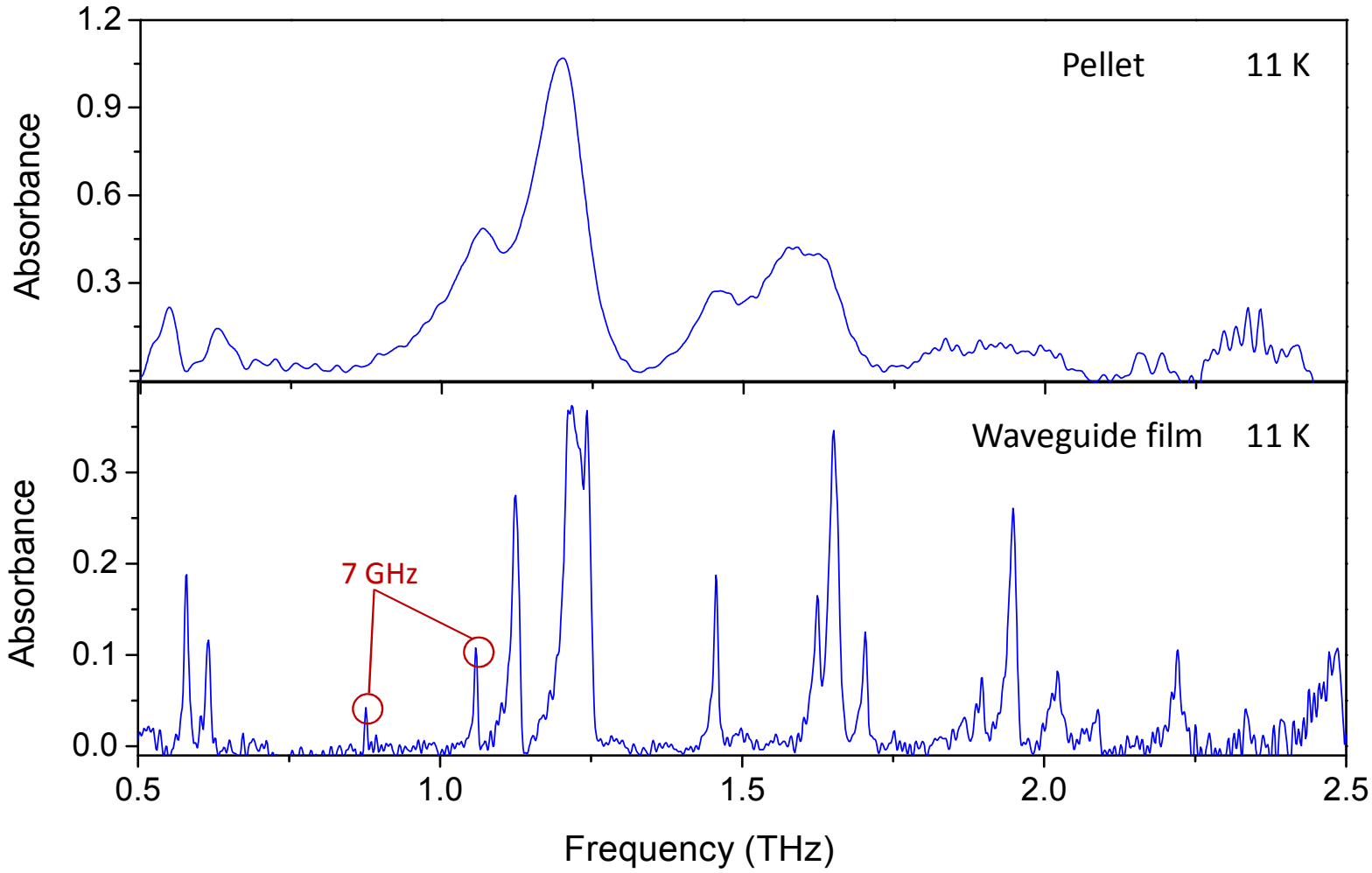

Fig 3.15 Comparison of Absorbance for 24DNT pellet and waveguide films. [publication P5]

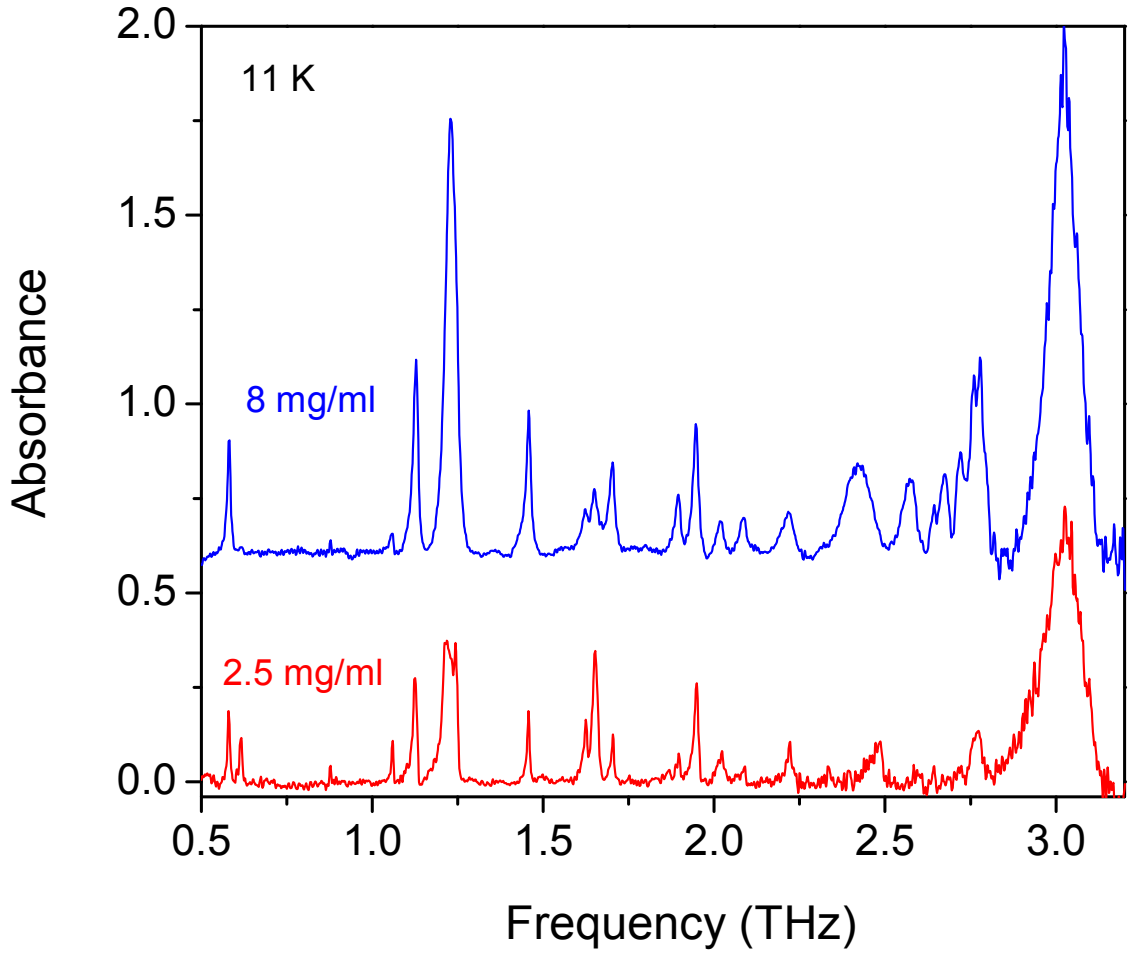

Fig 3.16 Comparison of absorbance for 2.5mg/ml (dilute) and 8mg/ml (conc) polycrystalline films of 24DNT on Al PPWG.[publication P5]

associated with short range order and when larger crystals are formed with a concentrated solution, they go away. Similar behavior was seen with TCNQ.

24DNT crystallizes in the *P21/n* space group with 8 molecules per unit cell [49]. Density functional theory of an isolated molecule [47] has attributed the vibrational modes in this frequency range to that of phonons. There are 6B-3 phonon modes predicted for a unit cell containing B molecules, thus for 24DNT 45 phonon modes are anticipated with 21 being infrared range to phonons. Also the low frequency intermolecular modes also occur in this frequency range. Given these theory predictions it is not surprising that waveguide THz-TDS revealed 19 modes at 11 K. It's possible that high precision THz measurements such as provided here can help refine theoretical modeling [14, 50] of THz vibrational spectra in the crystalline state. [publication P5]

As clear from the above discussion, the limiting factor for the frequency resolution is the reflection from the Si optics in the system. In Chapter 6 we will discuss about different coupling schemes and how these reflections can be avoided and how one can fully utilize the capabilities of waveguide THz-TDS.

3.6 4-Iodo-4-nitrobiphenyl (4INBP): demonstration of 1 GHz precision in vibrational line center determination

One of the driving reasons to study 4INBP using waveguide THz-TDS was the fact that this molecule exhibits a series of well resolved individual vibrational lines at cryogenic temperatures. Using the highly resolved 4INBP spectrum we can demonstrate

how the high resolution and high sensitivity of the waveguide THz-TDS technique can be used to determine line-center frequencies to a precision of upto 1 GHz.

Polycrystalline thin films of 4INBP were cast from 2 mg/ml solutions in chloroform on copper as well as Al. The optical micrograph of 4INBP/Al in Fig. 3.17 shows a morphology consisting of needlelike microcrystals. The X-ray diffraction spectrum confirmed the integrity of the 4INBP film and indicated two strongly preferred orientations, with the *(004)* and *(020)* crystal planes of 4INBP parallel to the plane of the waveguide surface. The waveguide films were measured at room temperature and the films did not reveal any noticeable vibrational structure. But upon cooling to 11 K the films on both Cu as well as Al revealed 10 well separated vibrational features.

The great S/N of the technique allows us to determine the line center frequencies with a precision as high as 1 GHz. To demonstrate this capability each individual temporal scan was zero padded to 2667 ps and Fourier transformed and the absorbance calculated for each of these spectral amplitudes. For a 150 ps temporal scan the data points in the spectrum are separated by 6.7 GHz. Interpolation to 2667 ps results in a 0.37 GHz separation between points in the spectrum.

In Fig 3.18 we plot the absorbance spectra of both Cu and Al waveguide films. The lowest frequency mode of the 4INBP/Cu film generated from seven independent zero-padded waveforms is plotted in the inset. The uncertainty of ± 0.5 GHz about the zero-padded average of 0.8061 GHz is the spectral region that contains all of the line-center frequencies of the individual zero-padded absorption spectra and is

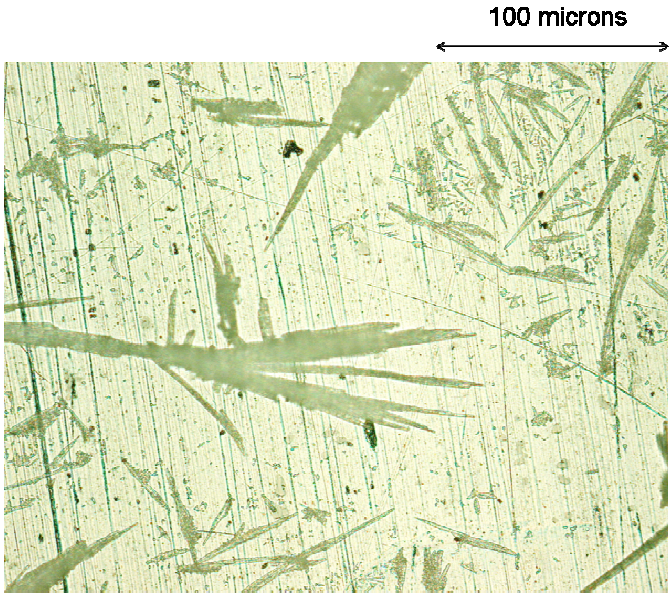

Fig 3.17 Optical micrograph showing needlelike morphology for the 4INBP on Al PPWG plate.

[publication P6]

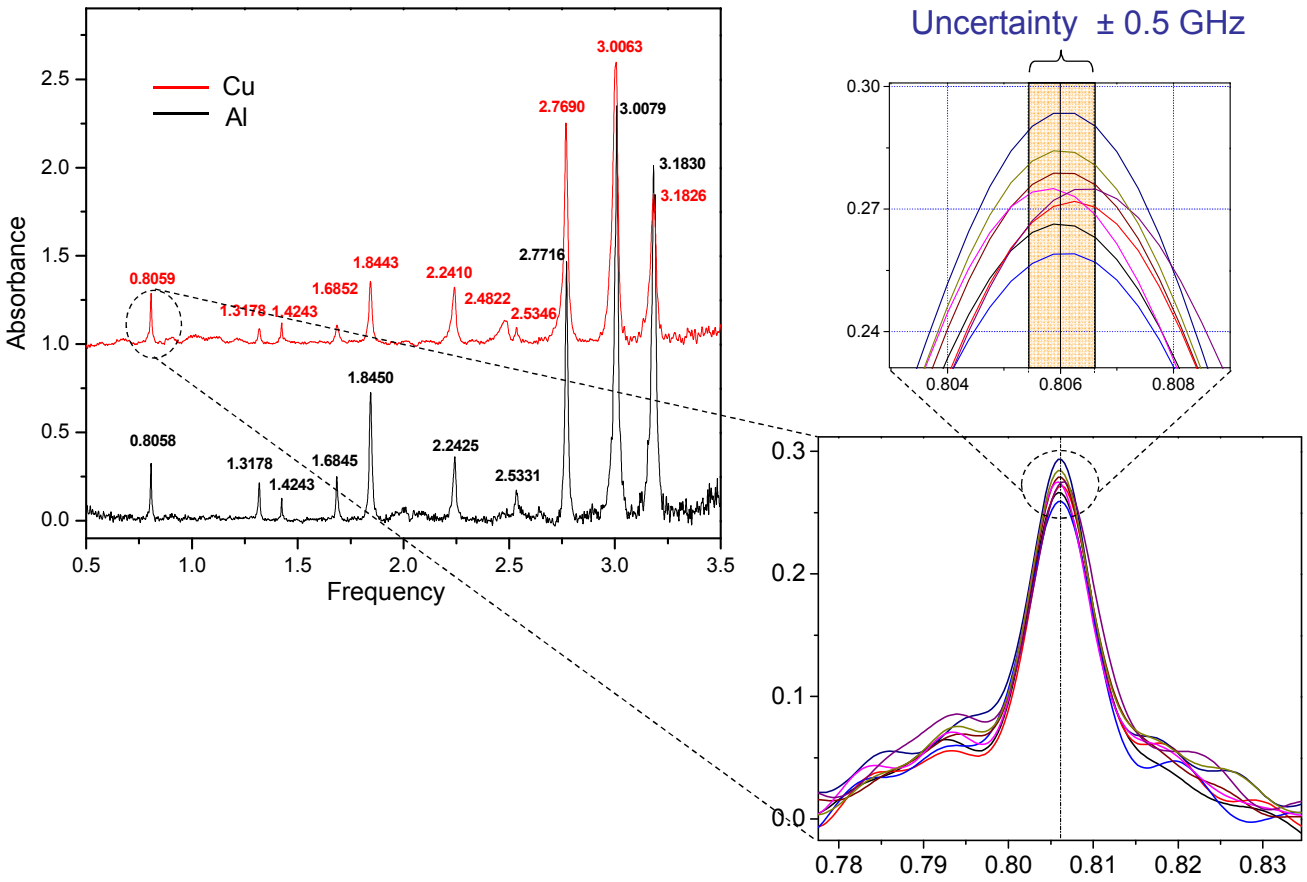

Fig 3.18 (left) Comparison of absorbance spectra for 4INBP/Al and 4INBP/Cu films measured at 11 K and 12 K, respectively. The absorbance spectrum for 4INBP/Cu has been set off for clarity. **(Right)** Absorbance spectra of the lowest frequency mode of the 4INBP/Al film generated from seven independent zero-padded waveforms [publication P6].

Table 3.3. 4INBP line center frequencies and uncertainties for films and pellet sample. FWHM linewidths are in parenthesis. All values are given in THz. [P6]

4INBP/Al 11 K	4INBP/Cu 12 K	Pellet 12 K
0.8061 ± .0005 (0.008)	0.8059 ± .0005 (0.010)	0.820 (0.032)
1.3178 ± .0005 (0.010)	1.3178 ± .001 (0.013)	1.29
1.4243 ± .0006 (0.008)	1.4243 ± .0007 (0.010)	-
1.6845 ± .0005 (0.011)	1.685 ± .0015 (0.021)	1.67
1.8450 ± .0009 (0.014)	1.8443 ± .001 (0.018)	1.82 (0.076)
2.2425 ± .0009 (0.016)	2.241 ± .0015 (0.021)	2.20
-	2.482	2.32
2.533 ± .002 (0.017)	2.535 ± .001	-
2.7716 ± .0015 (0.013)	2.769 ± .0025 (0.020)	2.68 (0.10)
3.0060 ± .003 (0.016)	3.006 ± .005 (0.030)	2.93 (0.12)
3.183 ± .005 (0.025)	3.183 ± .005 (0.032)	3.08 (0.13)

illustrated in the inset. The precision is dependent on the S/N and the linewidth. Larger S/N and narrower linewidths result in increased precision.

This high precision in the measurement of the line centers results in remarkable reproducibility of the data for independent film measurements. The absorbance spectra depicted in Fig 3.18 shows data where 4INBP/Cu was prepared and characterized more than one year after the 4INBP/Al. One difference between the two data sets is a shorter scan time of 100 ps for 4INBP/Cu (due to an interfering reflection for this film), compared with 150 ps for 4INBP/Al. Both spectra were obtained by zero-padding the temporal scans. The line-center frequencies and FWHM linewidths are summarized in Table 3.3.

Fig 3.18 and the data in Table 3.3 clearly demonstrate the high reproducibility of the technique, where most of the line-center frequencies for the two films agree to within 1 GHz. There is one deviation, where a small and relatively broad feature appears in the 4INBP/Cu spectrum but not in the 4INBP/Al spectrum. We also note the general agreement in relative line intensities exhibited by the two films. The broader linewidths for 4INBP/Cu is due to its shorter temporal scan. The minor variations in relative line intensities, linewidths, and extra feature in 4INBP/Cu are likely due to slight variations in the polycrystalline properties of the two films produced by drop casting. [P6]

3.7 Substrate independence of THz vibrational modes in waveguide THz-TDS

The key requirement to achieve line narrowing within a PPWG using waveguide THz-TDS is the ability to cast a polycrystalline film of the analyte on the metal surface of one of the plates comprising the PPWG. The film so formed on the metal surface has a high degree of planar order and this significantly reduces inhomogeneous broadening which plagues the traditional pellet samples used in the far infra red and THz-TDS techniques. The increased resolution and narrower features often result in a significant increase in the wealth of vibrational data that can be obtained from far infra red spectroscopy.

But given the fact that metals are reactive and when in solution readily give out ions, make them a reactive substrate for growing sample films. Hence, there may be chances that metal ions get incorporated in the crystalline lattice of the polycrystalline film formed on the metal surface. But, it is our assumption that this kind of incorporation, even if it occurs is limited to the few thin initial layers of the polycrystalline layer which comes in contact with the metal surface and is not entirely throughout the crystalline lattice. A recent article by C. Guadarrama -Perez et.al, model and analyze the crystallization of the molecule RDX on the Al surface. In this paper, the authors predict the formation of metal-RDX complex mediated by the oxygen-Al bonding leading to the formation of RDX-Al complex which also results in a conformal change within the RDX molecule. The authors then predict that this resultant interaction is one of the reasons for the additional modes resolved using the waveguide THz-TDS technique [51]. But in recent studies conducted by us, RDX was characterized using the waveguide THz-TDS technique on two different substrates namely Au coated Cu and Al, and we have

observed that the THz vibrational spectrum does not change, indicating that there was no evidence of interaction between the substrate (Al) and RDX significant enough to influence the THz measurement.[P6] Our only case of metal-analyte interaction was observed with tryptophan on Cu during our earlier attempts to characterize biological samples, wherein the white crystalline films turned green suggesting an interaction with Cu. This reaction was observed only when water was used as a solvent, and the crystallization process occurred over a period of few hours (days in some cases), compared to less than a minute for a solution made from volatile solvents like chloroform, acetone or any alcohol. This increased contact time between the metal substrate and the solvent and the fact that the solvent was water, are some of the reasons for the interaction with Cu. We found that the incorporation of Cu ions greatly affects the THz spectrum and only one of the four resonances observed at 77 K survives. This specific reaction to Cu was isolated and never happened when a volatile solvent was used or when Al was used as a substrate [P3]. When tryptophan films where cast from a methanol solution, no color change or interaction was observed. Moreover when the tryptophan films where cast from water, as well as methanol solutions on an Al substrate, the two sets of absorption lines matched, showing no significant metal-analyte interaction. [P3]

In order to address this aspect of solvent, sample and substrate interaction, a detailed experimental investigation of whether or not there is any substrate dependence of the observed vibrational modes with waveguide THz-TDS was done. In order to study the substrate dependence of the vibrational modes, three different metal surfaces were chosen namely gold, copper and aluminum. In addition, these three metallic substrates

were compared to two neutral substrates, a dielectric (2.5μm thick Mylar) coated aluminum waveguide plate and a self-assembled mono layer (SAM) passivated Au coated Si insert incorporated within a Cu PPWG. These two passivated substrates represent two different passivation techniques namely a simple mechanical passivation using a dielectric and the other a much more controlled, molecule specific passivation through SAMs. The well-ordered arrays and ease of functionalization of the untethered end of the molecule, makes SAMs ideal for substrate passivation and can also provide a controlled crystal nucleation center and facilitate better orientation of the polycrystalline layer. The SAM used here is cast from 11-hydroxy-undecanethiol on an Au-coated Si chip. The sulphur end of the molecule bonds with the Au surface whereas the hydroxyl end faces away from the Au surface and forms an ordered monolayer. Salicylic acid is chosen as a test material as it is known have distinct and well separated vibrational modes at THz frequencies and for the ease with which it crystallizes to form a polycrystalline film using the dropcasting technique. Four different substrates namely Al, Cu, Au and a dielectric (2.5 μm thick mylar) are used to cast the polycrystalline films. Polycrystalline thin films were cast on these substrates from a 10mg/ml salicylic acid/acetone solution. The PPWG was reassembled in each case and the test carried out using the procedure described earlier. For the case of the mylar the waveguide was assembled as shown in Fig 3.19. Each of the waveguides were cooled to 13 K using a He cryo cooler and their THz absorption spectrum was compared.

The amplitude transmission through the PPWGs made of four different materials namely Al, Cu, Au coated Cu and mylar coated Al, and with no sample in place are compared in Fig 3.19. All the metal PPWGs exhibit good TEM mode propagation, with a

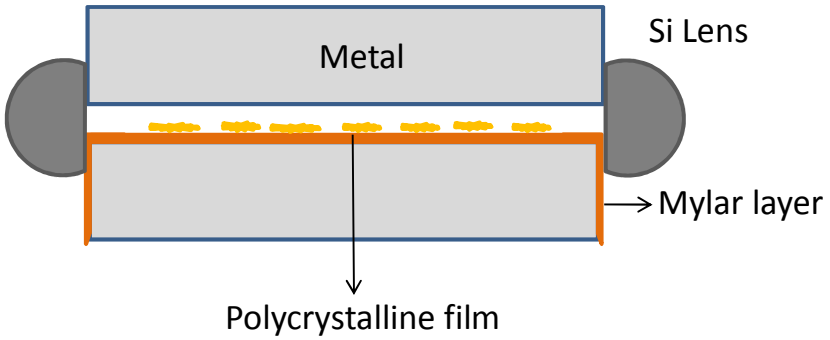

Fig 3.19 Metal PPWG with mylar passivation layer

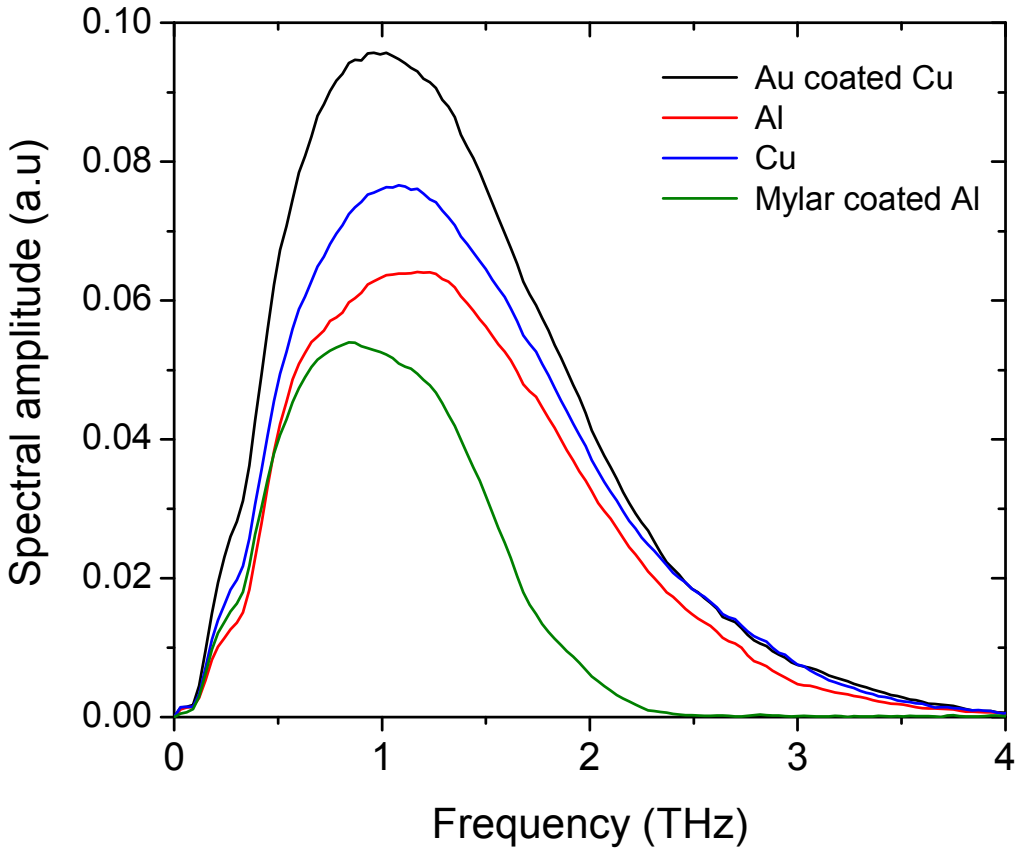

Fig 3.20 Comparison of spectral amplitude transmission through the PPWG with different substrates.

spectral throughput extending all the way up to 4 THz. The Au coated Cu PPWG has the maximum spectral amplitude transmission. The mylar coated PPWG supports single TEM mode propagation and only introduces a minor dispersion and broadband absorption above 1 THz due to the 2.5 μm thick layer. The high frequency components are attenuated by the mylar layer, and we obtain measurable amplitude transmission only up to 2.5 THz. But the clean TEM mode propagation through this PPWG provides for an easy way to make a neutral substrate for waveguide THz-TDS.

The absorbance spectrum extracted from each measurement are collected and compared in Fig 3.21. As evident from the data (13 K) shown in Fig 3.21, we have achieved a remarkable reproducibility of the vibrational modes for all substrates including mylar and SAM, suggesting that no metal-analyte interaction occurs and the modes observed are indeed that of the analyte (salicylic acid). In order to further confirm these results the comparison of microcrystals on the various substrates and XRD measurements of each of these films was performed to verify their crystal structure and orientation with respect to the substrate. The optical micrographs of these films on all the substrates are shown in Fig 3.22. Comparing the optical micrographs of microcrystals of salicylic acid on each of the substrates, we can see a strong similarity in the microcrystal shape and sizes. Clusters of thin, long, needle like crystals of length ~200-300 μm are obtained. This similarity is confirmed by the XRD data which shows an identical 2θ spectrum. The XRD data is presented in Fig 3.23. Salicylic acid crystallizes in the monoclinic system having a space group *P21/a* with 4 molecules per unit cell [53]. The films on all the substrates show strong orientation along the *(110)* direction with a corresponding strong peak at 10.96^{o} and the next stronger peak at 17.22^{o} corresponding

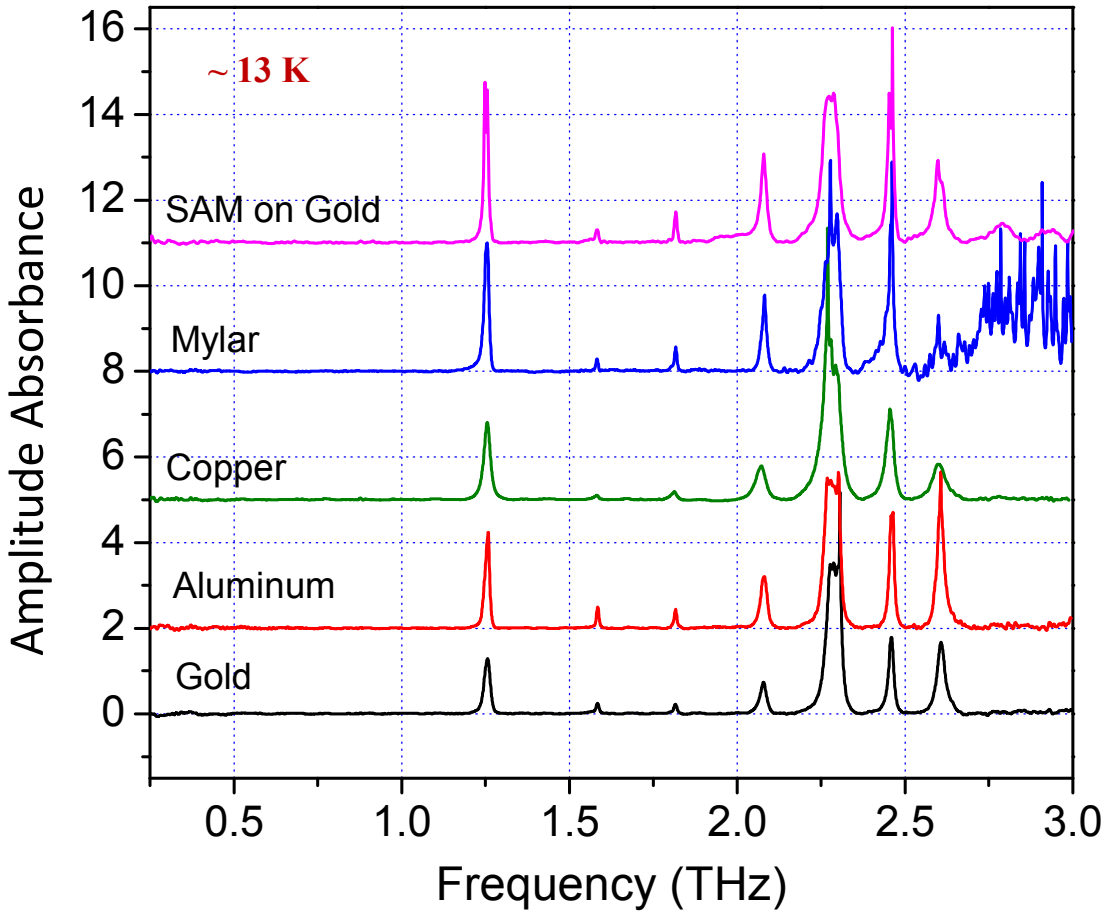

Fig 3.21 Comparison of the THz vibrational modes for salicylic acid obtained using waveguide THz-TDS for different substrates within the PPWG. The absorbance plots are shifted vertically for better clarity. [publication P12]

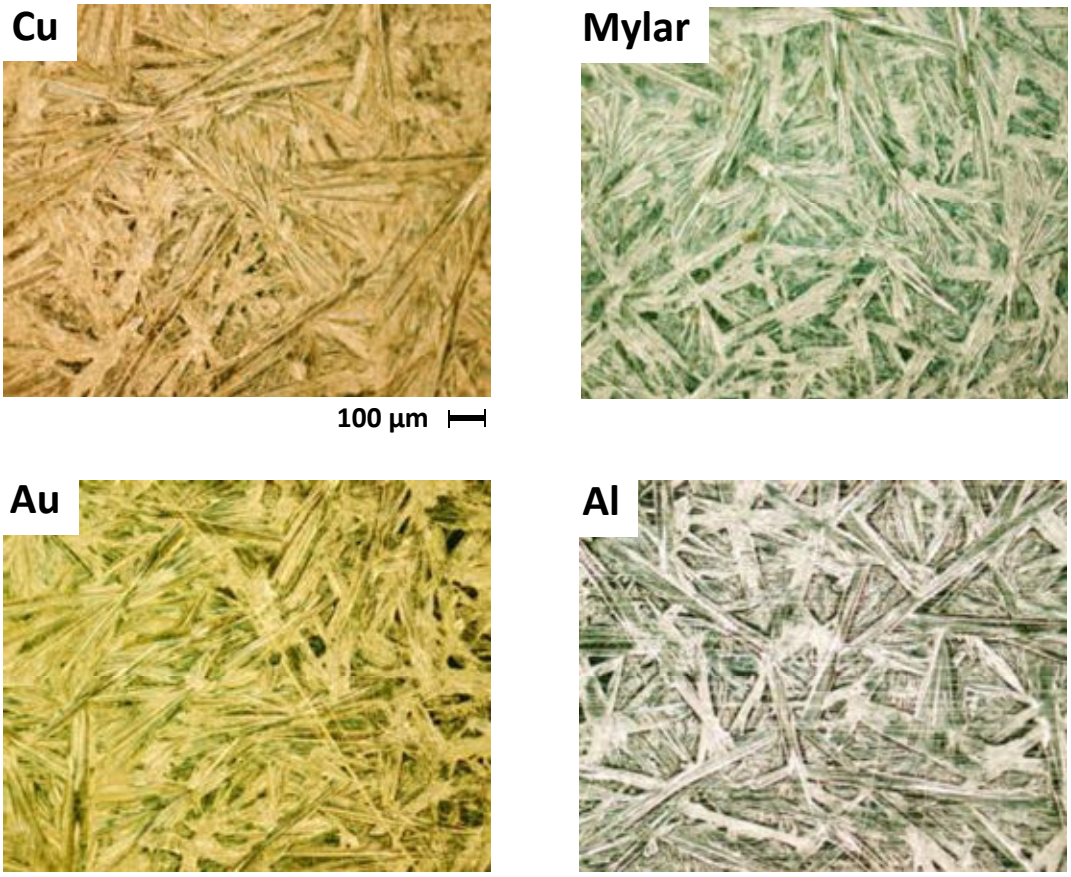

Fig 3.22 Optical micrographs of salicylic acid dropcast films on four different substrates namely Cu, Mylar, Au and Al. Scale bar applies to all the micrographs.[publication P12]

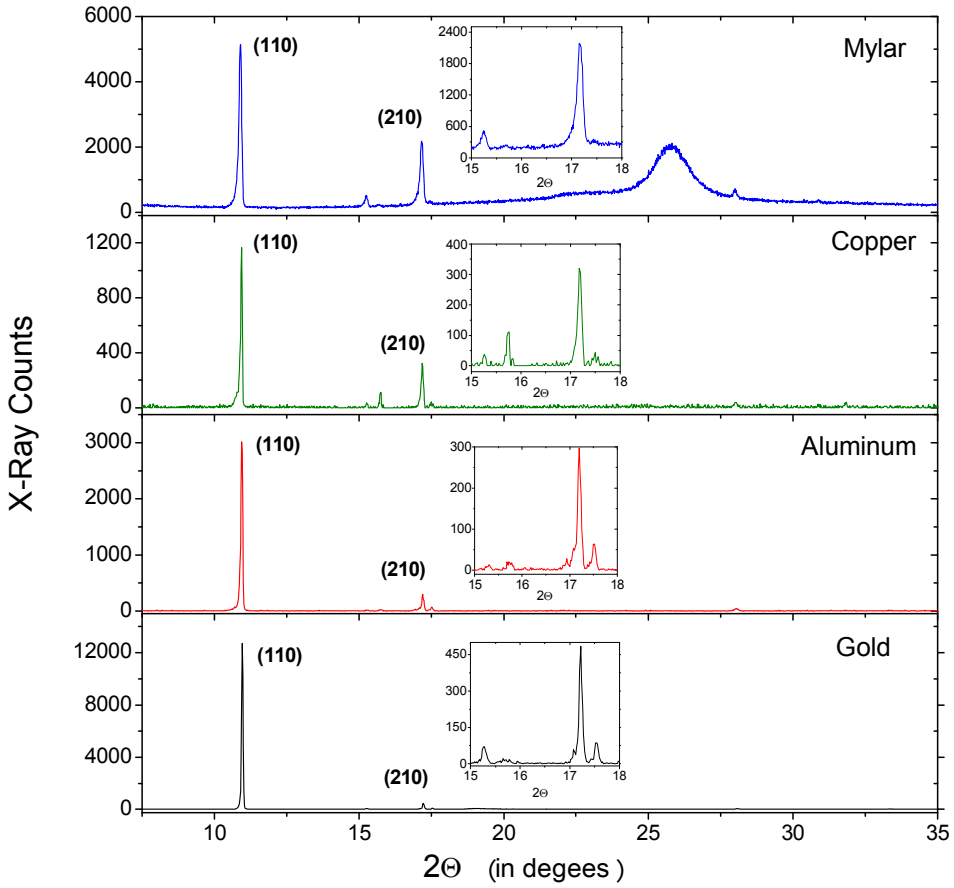

2θ (Database)	2θ (Observed)	Crystal plane
11.05	10.96	(110)
15.37	15.26	(210)
15.81	15.74	(020)
17.30	17.22	(210)
17.60	17.56	(120)
28.19	28.08	(320)
33.47	33.34	(330)

Fig 3.23 Comparison of the XRD data obtained for the salicylic acid polycrystalline film on various substrates. The table compares the XRD line centers observed to that from a database and the respective crystal planes are also listed. [publication P12]

to the *(210)* planes. We also see very weak peaks at 15.26^{o}, 15.74^{o}, 17.56^{o}, 28.02^{o} and 33.34^{o} which closely match to the data base values observed for pure salicylic acid. Upon careful observation we see that except in the case of mylar all the XRD results match up very well suggesting similar crystalline structure and orientation. For mylar we observe a broad scattering peak centered around 27^{o} and it is probably due to the mylar itself. Apart from this all the other lines match up and suggest similar crystalline environment for all the films which is also confirmed by the THz data.

The results of this controlled experiment for salicylic acid are consistent with our previous observations of substrate independence of organic films on different metal surfaces. The results presented here indicate that in most cases during the crystallization of the analyte on the metal surface there is minimal interaction with the metal surface. Moreover, the metals usually used for waveguide THz-TDS, Al and Cu are known to develop an oxide passivation layer which is few atomic layers thick when exposed to the atmosphere. Also, before dropcasting any sample, the waveguide plates are cleaned in oxygen plasma, to form an oxide passivation layer on the metal surface. From the literature, it is known that exposing a Cu surface to oxygen plasma for about 15 min generates an oxide layer of the order of 50 nm. Since, the Cu plates in our case were oxygen plasma treated for 2 minutes, this oxide layer should be of the order of few nm. [52].Also, even if there is some metal analyte interaction, it is our understanding that it is restricted to the layers within the interfacial region between the substrate and analyte and does not influence the subsequent layers which crystallize over it. The THz radiation transmitted through the waveguide does not respond to these initial layers, which is clearly evident from the waveguide data.

Chapter 4

Characterization of polycrystalline films of molecular solids using high resolution Waveguide THz-TDS

4.1 Introduction

This chapter presents the work done in applying the technique of high resolution waveguide THz-TDS to characterize a wide array of molecules ranging from organic, biological, pharmaceutical and explosive compounds in the form of polycrystalline solid state films. This is done to show the versatility of the technique in characterizing molecular samples belonging to all classes and establish it as a new tool for high resolution spectroscopy. The molecules chosen for this demonstration are the organic molecules Tris and melamine, biological molecules deoxycytidine and D-glucose, pharmaceutical molecule aspirin and explosive RDX. These molecules have been chosen based on their known activity in the THz frequency domain and as representatives of different types of molecules which are usually studied using far-infra red spectroscopy. Far infrared studies of some of these molecules have been reported in literature. Applying the waveguide THz-TDS technique, the most precise and narrow linewidth absorption

spectrum to date of these molecules is obtained and facilitates in establishing a very accurate vibrational spectral fingerprint. [publications P1-P12]

4.2 Organic molecules

4.2.1 Melamine – harmful food additive

Food additives are substances added to food during the manufacturing process for its preservation and in some rare cases to mimic the presence of certain nutrients. However, some of them are harmful when accumulated in our body. For example saccharin is often added to soft drinks and ice cream and has been proven to cause uterine cancer in rats. Thiabendazole and o-phenyl phenol, which are preservatives often applied on the surfaces of grapes, bananas, and lemons, are reported to induce chromosomal aberrations in mice. EDTA-2Na (ethylenediaminetetraacetic acid disodium salt dehydrate) is often added to mayonnaise and canned food and research suggests that it is related to low blood pressure and digestive trouble when consumed regularly [54].

In the summer of 2008, it was found that a harmful organic material called melamine was being added to pet food, milk powder and even chocolate [55]. Melamine and its derivatives are of great interest for industrial applications. Melamine is combined with formaldehyde to produce melamine resin, a very durable thermosetting plastic. It is also often added to polymers such as nylon to improve its fire resistance and mechanical properties [56]. These molecules are rich in nitrogen and are known to release nitrogen when burnt or charred, which helps in retarding fires. Since these chemicals are nitrogen rich they are found to be added to food items to mimic the presence of proteins. Ingestion of melamine in pets and cattle is known to lead to serious health disorders related to the

reproductive system and kidney and in some cases lead to death. Recently there have been many reports about deaths of many babies who consumed melamine tainted milk powder in China [57]. In order to aid its detection and identification, this molecule has been characterized using the pellet technique as well as waveguide THz-TDS.

The melamine pellet was prepared by mixing 25 mg of melamine in 230 mg of polyethylene host and compressing the resultant powder mixture into a pellet. The THz transmission of this pellet was measured in a standard THz-TDS setup at 295 K and 77 K. The polycrystalline melamine film was prepared by dropcasting from a water solution onto a polished copper waveguide plate. Many concentrations and solvents were tried in order to obtain a suitable and working polycrystalline film for waveguide THz-TDS. It was found that dropcasting from a saturated solution (10mg/ml) of melamine in de-ionized water yielded a very thick highly crystalline film (macroscopic triangular crystals). The optical microscope image of the film is shown in Fig 3.6. But this film was too thick to fit in to a 50 μm gap in the waveguide. Hence a 100μm gap was used. But this film despite being crystalline, when examined in a THz-TDS setup yielded a featureless transmission spectrum at 295 K as shown in Fig 4.1. Upon cooling to 77 K a very weak evidence of a absorption feature emerges around 1.8 and 2.1 THz. This suggested that the absorption spectrum of melamine is highly dependent on microcrystal size as well as orientation on the metal surface (long/short range crystal order).

A 100 μl dropcast from a 2.1 mg/ml solution in de-ionized water was found to yield an ideal thin polycrystalline film (see Fig 4.2 (inset)), which easily fit within the desirable 50μm gap of the Cu PPWG. The metal sample plate was then incorporated into

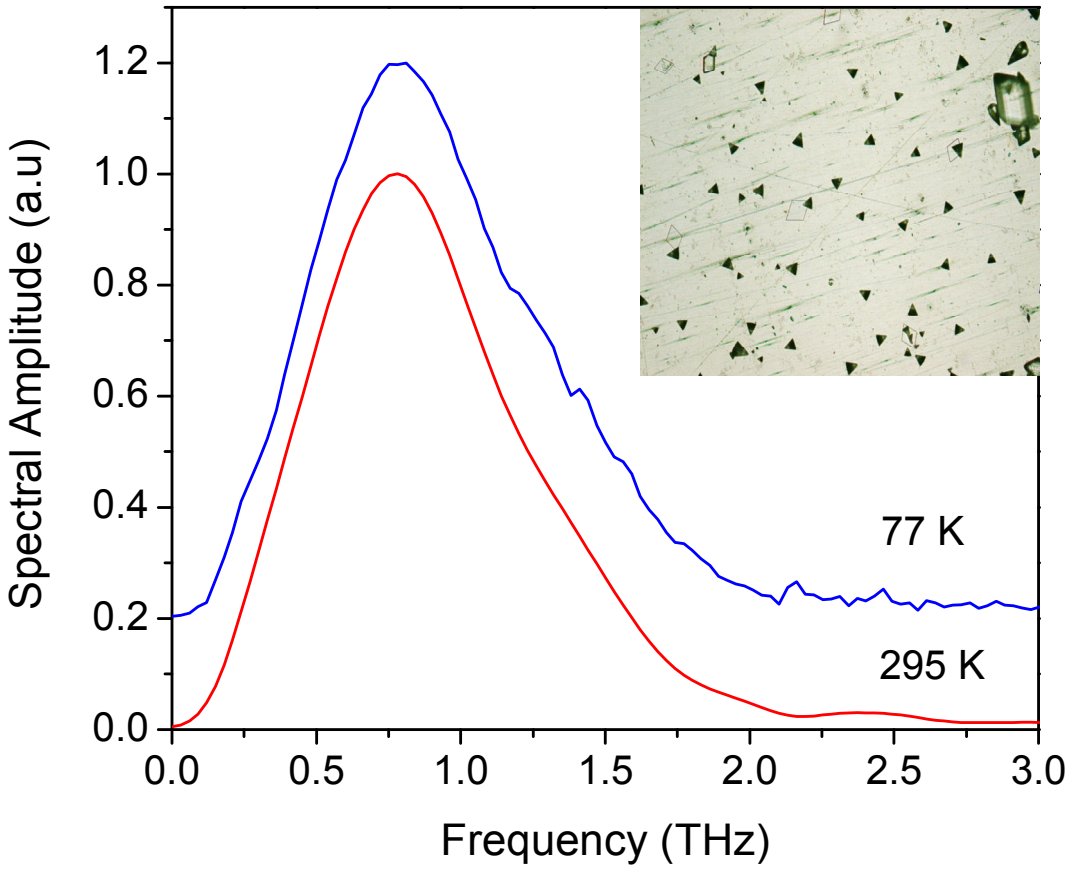

Fig 4.1 (Inset) Optical micrograph of polycrystalline melamine film dropcast from a concentrated solution (10mg/ml). Corresponding THz transmission spectrum at 295 and 77 K.

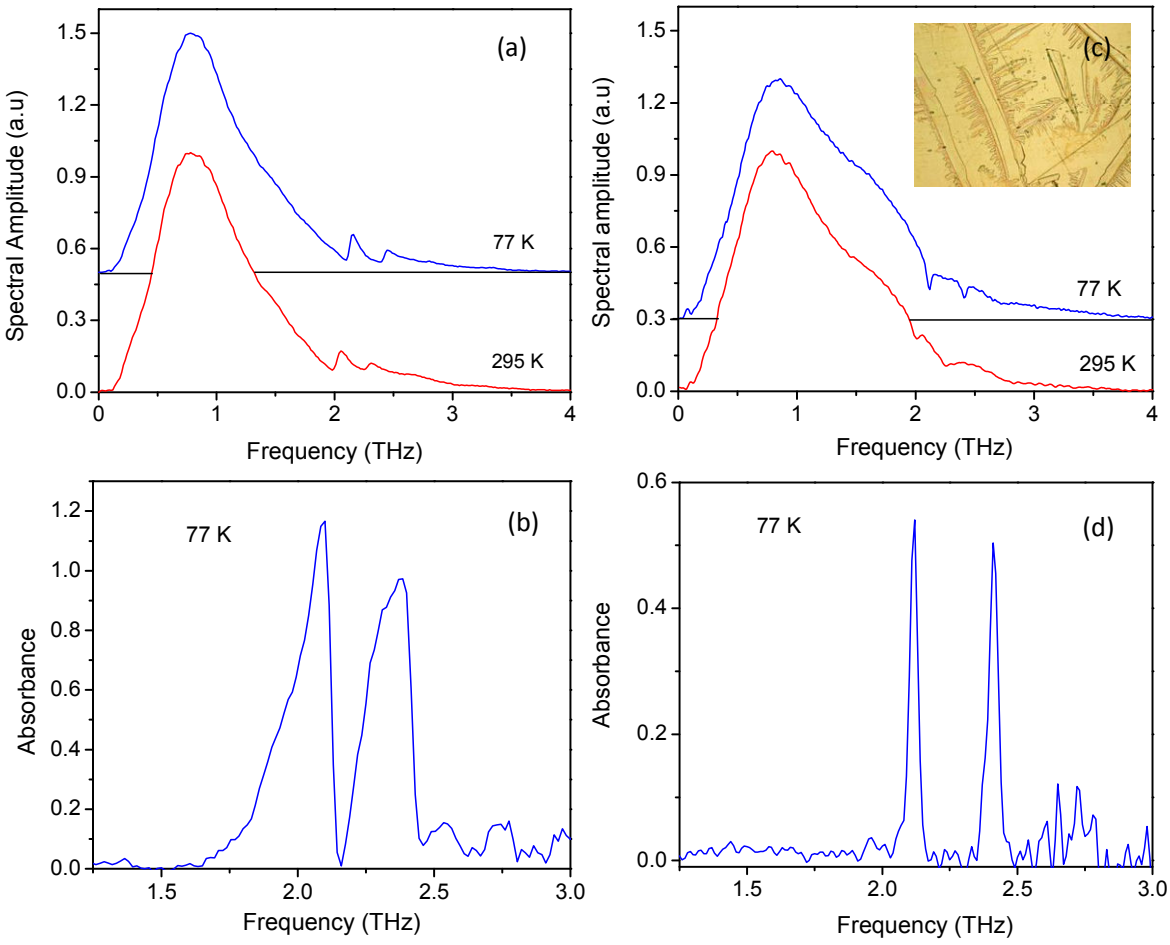

Fig 4.2 (a) Spectra of THz pulses transmitted through melamine pellet at 295 K and 77 K respectively. **(b)** Absorbance Spectrum of melamine pellet at 77 K. **(c)** Spectra of THz pulses transmitted through waveguide containing melamine film at 295 K and 77 K respectively. **Inset** shows optical micrograph of the melamine film on Cu waveguide. **(d)** Absorbance spectrum of waveguide film at 77 K. [publication P11]

a parallel plate waveguide with a 50 μm gap between the plates. The THz transmission of the melamine PPWG was measured both at 295 K and at 77 K. The amplitude spectra of the THz pulses transmitted through the melamine pellet at 295 K and 77 K is shown in Fig 4.2 (a). The absorbance spectrum at 77 K is shown in Fig 4.2 (b). Two spectral features are seen at 1.98 THz and 2.25 THz at 295 K, which have been previously reported at the same frequencies [58]. These lines marginally sharpen when cooled to 77 K. The FWHM linewidths at 77 K are 150 GHz at 2.1 THz and 180 GHz at 2.39 THz.

In contrast the transmission spectrum of the waveguide film exhibits sharper features at 2.01 THz and 2.26 THz, even at 295 K. Cooling of the waveguide to 77 K yields dramatic sharpening of these features resulting in two sharp spectral features at 2.12 THz and 2.41 THz, each having a FWHM linewidth of 37 GHz. It is also observed that the spectral features both in the pellet as well as the waveguide film shift by more than 100 GHz to higher frequencies upon cooling to 77 K. A similar strong line shift to higher frequencies with decrease in temperature was observed in 1,2DCB [P1].

This application of waveguide THz-TDS to melamine shows that it has the potential to generate well resolved absorption features and can be used as an important experimental technique to establish high resolution spectral finger prints to aid in its detection. [publication P11]

4.2.2 Tris (hydroxymethyl) aminomethane - temperature dependence line centers of vibrational modes

Tris (hydroxymethyl) aminomethane (Tris) is an amino alcohol extensively used in biochemistry and molecular biology as a component of buffer solutions since its first introduction by Gomori in 1946 [59-60]. Commonly known as Tris or THAM, it is a stable white crystalline powder having high solubility in water. Since its first use as a buffer component, this molecule has proven to have other important applications, such as in the field of medicine as well as in thermal energy storage [61-62].Tris is used as a component of buffer solutions, such as in TAE (Tris-acetate-EDTA) and TBE (Tris-borate-EDTA) buffer, especially for solutions of nucleic acids. Tris has a pKa of 8.06, which implies that the buffer has an effective pH range of [63-65]. The useful buffer range for Tris of 7-9 coincides with the typical physiological pH of most living organisms [59-60]. This and its low cost make Tris one of the most important buffers used in biology and biochemistry [62-66]. This widely used buffering agent has also been shown to act as an inhibitor of acetocholine, a neurotransmitter found in both the peripheral nervous system and the central nervous system in many organisms, including humans. At concentrations ranging from 5 to 10 mM, it has been demonstrated to function as a potent inhibitor of both excitatory and inhibitory responses to iontophoretically applied acetylcholine [65, 67]. More recently, Tris has been used in the field of medicine as a drug to cure metabolic acidosis in acute lung injury [61, 62, 68].

This molecule was chosen to be studied as a consequence of our attempts at studying bacteriorhodopsin thin films in the waveguide. Bacteriorhodopsin was suspended in a TRIS buffer solution. When it was attempted to dropcast a polycrystalline

thin film of bacteriorhodopsin, a white crystalline substance precipitated out. Bacteriorhodopsin is a purple colored membranous substance and clearly the white crystals which precipitated out were not bacteriorhodopsin. The bacteriorhodopsin suspension consisted of the Tris buffer as well as some amount of sucrose left behind from its extraction. Hence, the decision was made to characterize Tris. Also, Tris being a common buffer component used in many biological samples, it's important to know its THz vibrational response (far-infrared modes) to avoid erroneous assignment of modes belonging to Tris to that of the actual sample being studied. Bacteriorhodopsin itself when measured in the waveguide, never showed any features and only a broadband absorption was obtained. Bacteriorhodopsin being a membrane protein is known to be active in the THz region and calculations have shown that this molecule has very closely placed vibrational modes. This also may be one of the reasons for it to express continuum absorption behavior.

Tris (99% pure) in white crystalline powder form was purchased from Sigma Aldrich and was used without further purification. Tris pellets were made by mixing 330 mg of polyethylene powder with 20 mg of Tris, and the mixture was pressed into pellets of thickness 2 mm and diameter 1 cm. For the films used within the PPWG, the inner surface of the waveguide plate was first cleansed with solvent and then plasma-cleaned before casting the films. Two different film preparation techniques namely, dropcasting and sublimation were employed to get different microcrystal morphologies on the waveguide plates. Dropcasting from a solution of the sample gave macroscopic crystals, whereas sublimation yielded a uniform film with very small microcrystals. The dropcast film was made by placing ~200 μl of Tris solution in water (10 mg/ml) on the polished

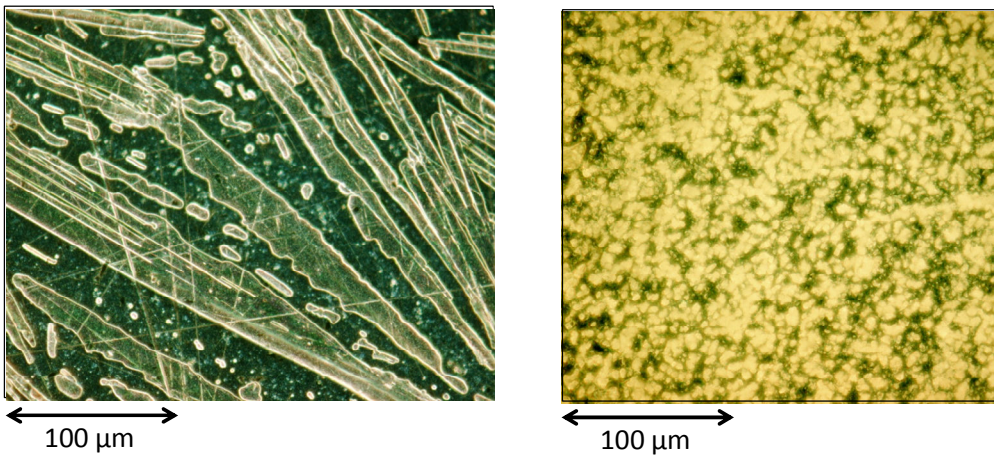

Fig 4.3 Optical micrographs of the Tris dropcast film on the **(left panel)** and the sublimated film on the **(right panel)**. [publication P8]

inner surface of the Al waveguide plate. The solution was allowed to evaporate overnight to obtain a planar distribution of fairly large microcrystals on the waveguide plate. Following evaporation, the relatively thick areas of the film along the outer edges were removed using a solvent soaked swab to leave a visually uniform film. Alternatively, ~100-200 μg of the sample was placed in a glass sublimation unit, with the waveguide plate attached to the cold finger. The unit was then evacuated and then heated to deposit a uniform film of Tris on the waveguide plate. Similar to the dropcast film, the outer edges were swabbed to obtain a rectangular patch of uniform film. This method yielded very small sized microcrystals, in comparison to the dropcast technique. The optical micrographs of both films are shown in Fig 4.3. A typical film mass was estimated to be ~ 60 - 80 μg. All the samples, the pellet as well as the waveguide films were then cooled to 13.6 K and the temperature dependent THz absorption spectrum was recorded.

Fig 4.4 shows the amplitude spectrum transmitted through the pellet as well a dropcast film in the waveguide at 13.6 K. The transmission through the pellet had spectral components all the way up to 4 THz (fig 4.4 (a)). The transmission spectra at room temperature showed the presence of four absorption features at 1.23, 1.45, 1.75, and 2.11 THz. At 13.6 K, these features showed minimal narrowing and developed into features at 1.31, 1.57, 1.76, and 3.14 THz. The narrowest feature at 13.6 K had a FWHM linewidth of 150 GHz for the 1.76 THz line.

For the waveguide film, as evident from the temporal data which exhibits a long ringing tail extending all the way upto 130 ps, many sharp resonances in the frequency domain were observed. The transmission through the waveguide has spectral components extending all the way up to 4 THz, as shown in Fig 4.4 (b). The transmission spectra at

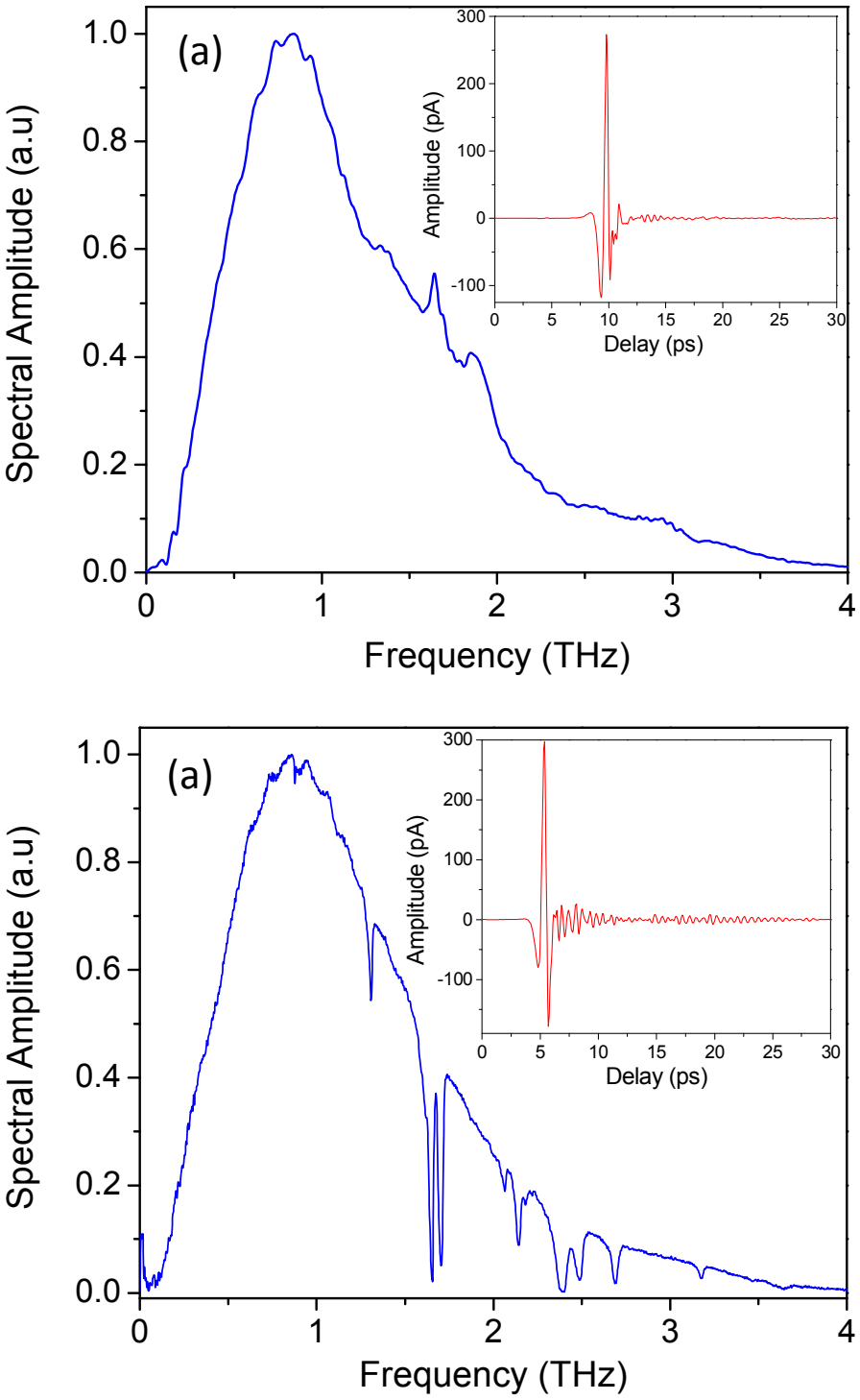

Fig 4.4 Output terahertz amplitude spectrum of Tris pellet **(a)** and Tris film within an aluminum PPWG **(b)** at 13.6 K **Inset**: Time domain trace of the terahertz pulse through the Tris pellet at 13.6 K. [publication P8]

room temperature showed the presence of three absorption features at 1.5, 1.78, and 2.22 THz. In contrast to the pellets, upon cooling the waveguide film to 13.6 K, various thermal broadening mechanisms were quenched, and the transmission spectra evolved to reveal 12 highly resolved and narrow resonance features, as shown in Fig 4.4 (b).

Fig 4.5 compares the absorbance spectra at 13.6 K for sublimated and dropcast films and clearly compares the difference in evolution of spectral features for both the films with temperature. The sublimated film does not show resonances at 1.308, 2.064, 2.489, and 3.640 THz. The features at 2.173, 2.392, and 2.712 THz with linewidths 39, 25, and 39 GHz are broader than the corresponding features seen with dropcast film at 2.142, 2.393, and 2.691 THz with linewidths 27, 39, and 27 GHz, but the sublimated film shows three features that do not show up in the dropcast film: namely, at 1.629, the broad feature at 1.92, and 3.471 THz. At 13.6 K, the cluster of lines around 1.65 THz resolves into only two features at 1.655 and 1.706 THz with linewidths of 17 and 23 GHz in the dropcast film, whereas in the sublimated film, the cluster resolves into three features at1.629, 1.647, and 1.70 THz with linewidths of 15, 12, and 20 GHz, respectively. The line at 1.647 THz is the narrowest, having an FWHM linewidth of 12 GHz. The line at 2.484 THz in the sublimated film is very weak as compared to its dropcast counterpart.

Sublimated films are composed of microcrystals that are much smaller than the ones obtained by dropcast, as evident from Fig 4.3. The disappearance of some of the modes in the sublimated film may be due to the fact that these modes are dependent on the long range order of crystallinity as we had discussed with the case of TCNQ in chapter 3. There is also a possibility that when the thin films of Tris are formed by the two different methods, the microcrystals may be oriented slightly differently in the two

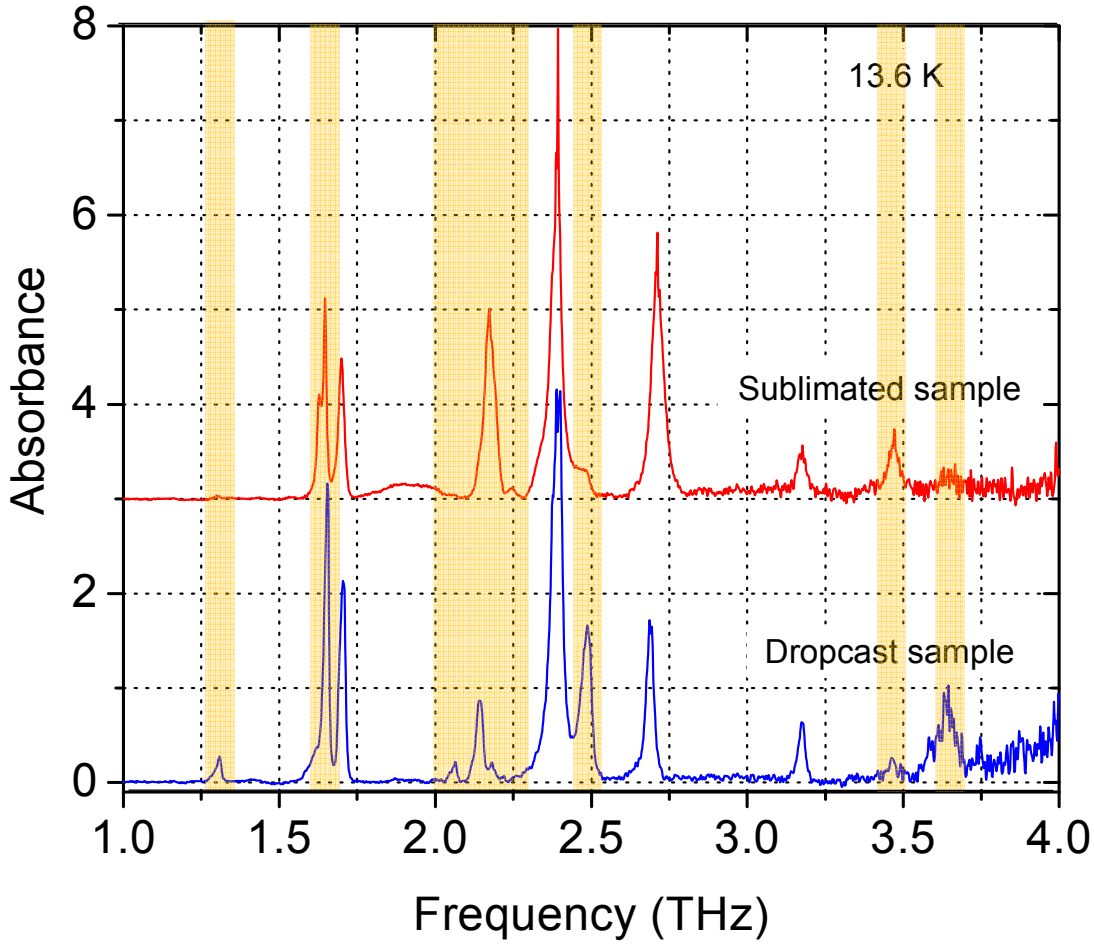

Fig 4.5 Comparison of the absorbance of dropcast and sublimated Tris thin films within a polished aluminum PPWG at 13.6 K. The colored bands indicate the difference between the two absorbance spectra. [publication P8]

Table 4.1: Line-center frequencies and FWHM linewidths (within parentheses) for the Tris Pellet and Tris Film Samples[a] [publication P8]

Pellet [b]		Dropcast film [b]		Sublimated film [b]	
295 K	**13 K**	**295 K**	**13.6 K**	**295 K**	**13.6 K**
1.23[w]	1.31[w]	-	1.308(0.021)	-	-
-	-	-	-	-	1.629(0.015)
1.45 (0.21)	1.57(0.16)	1.50 (0.07)	1.655(0.017)	1.51(0.07)	1.647(0.012)
1.75[w]	1.76 (0.15)	1.78 (0.12)	1.706(0.023)	1.80(0.14)	1.701(0.020)
-	-	-	-	-	1.918(0.165)
-	-	-	2.064 [w]	-	-
-	-	-	2.142(0.027)	-	2.173(0.039)
-	-	-	2.181 [sh]	-	2.246 [w]
2.11(0.21)	-	2.22(0.21)	2.393(0.039)	2.14 (0.18)	2.392 (0.025)
-	-	-	2.489(0.040)	-	2.484 [sh]
-	-	-	2.691(0.027)	-	2.712 (0.039)
-	3.14[w]	-	3.176(0.026)	-	3.177 (0.031)
-	-	-	3.465 [w]	-	3.471 (0.033)
-	-	-	3.640(0.083)	-	-

[a] All values are in THz
[b] "w" represents weak absorption line. "sh" represents shoulder.
[P8]

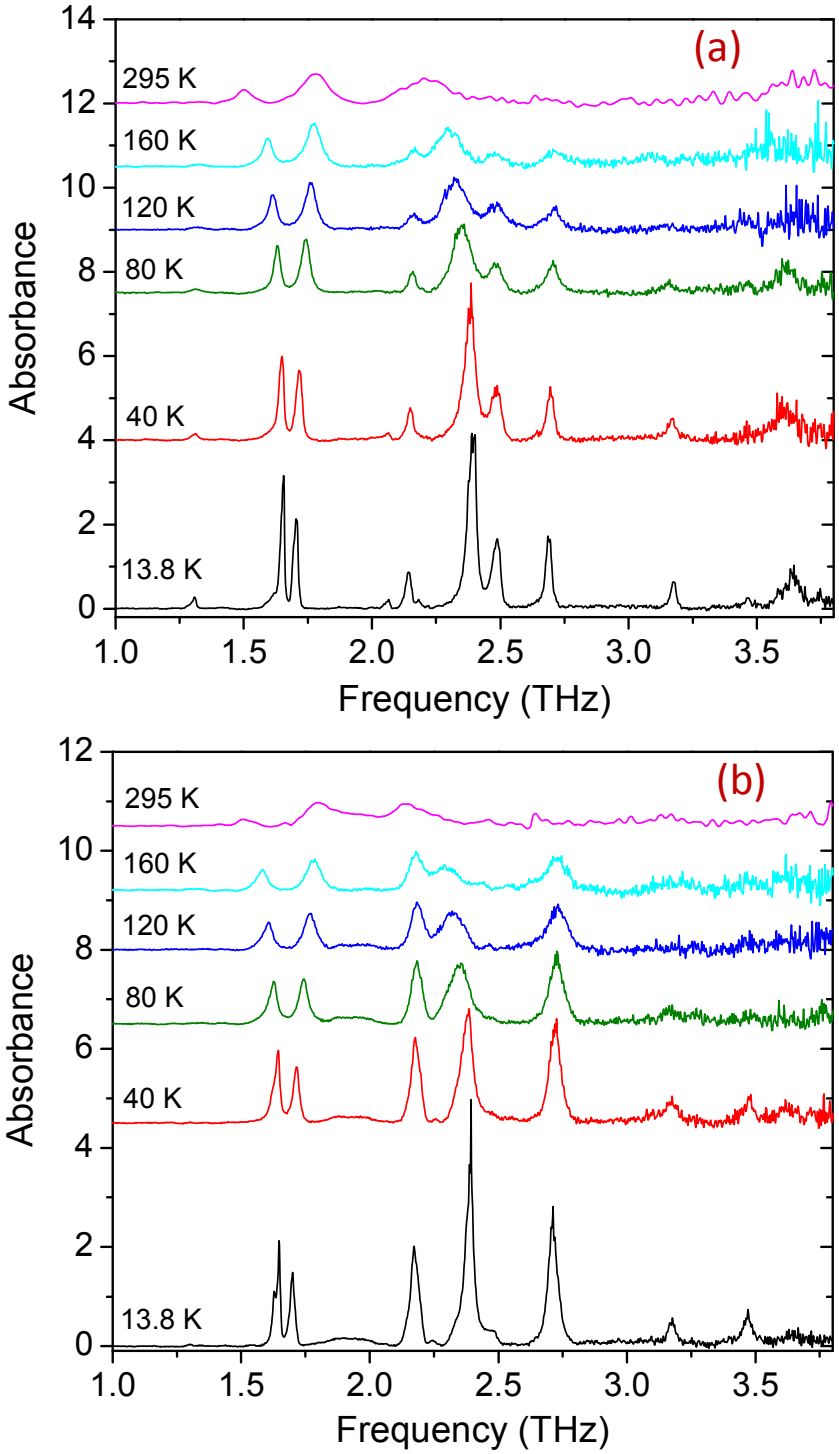

Fig 4.6 Absorbances as a function of temperature for **(a)** dropcast Tris thin films and **(b)** sublimated films within polished aluminum PPWG. For clarity, the spectral amplitudes and absorbances from 40 to 295 K are offset. [publication P8]

films, and consequently, some of these modes, such as 1.308 and 2.484 THz in the sublimated film, may be diminished or totally absent due to the polarization dependence of the modes with respect to the propagating THz field.

Temperature dependence of THz vibrational modes:

The temperature dependence of the THz vibrational modes for the sublimated film and the dropcast film is shown in Fig 4.6. It is clear from the figure that the spectral features undergo a frequency shift upon cooling. This frequency shift may be towards the high frequency side called the *"blue shift"*, or towards the low frequencies called the *"red shift"*.

The features beyond 1.704 THz experience very negligible frequency shift. For the two specific resonances at 1.656 and 1.704 THz (at 13.6 K), the frequency shift is large but of a different sign. The resonance at 1.656 THz is seen to *blue-shift* from its room temperature value of 1.50 THz, and the one at 1.704 THz undergoes a red shift from 1.78 THz. This opposite shift of these two adjacent resonances is clearly tracked in Fig 4.6. The fractional shift in frequency of these two resonances for dropcast as well as sublimated films is summarized in Fig 4.7. This fractional shift for 1.656 THz (blue shift) and 1.704 THz (red shift) is seen to follow a quadratic dependence with change in temperature.

In previous work, [65, 69] Tris has been shown to crystallize in the orthorhombic system having $Pn2_1a$ space group with four molecules per unit cell. Tris crystallizes in a layered structure with strong hydrogen bonding within each layer and weak hydrogen bonds between layers. The blue frequency shift is, in part, due to compression of the

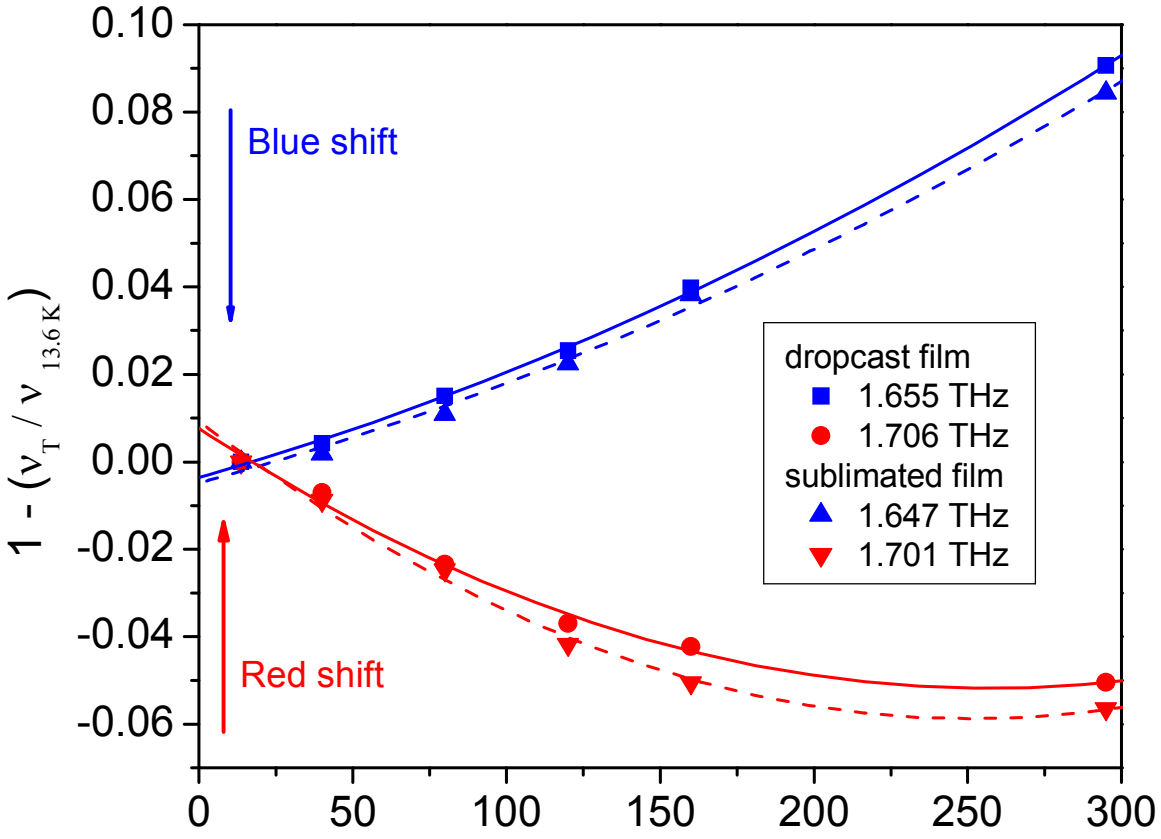

Fig 4.7 The temperature-dependent frequency shift for two vibrational modes of Tris dropcast and sublimated films. The *y* values are plotted as the fractional shift of the line frequency, υ_T, at temperature, *T*, from the line frequency, $\upsilon_{13.6K}$, measured at 13.6 K. The mode frequencies in the legend are the values measured at 13.6 K. The solid (dropcast film) and dashed lines (sublimated film) are quadratic fits to the data points. [publication P8]

crystalline lattice upon cooling, which results in a steeper intermolecular potential. Anharmonicity of the vibrational modes may also contribute to the shift [70]. The anomalous red shifting with cooling temperatures has been reported for some hydrogen bonding solids and has been interpreted to be due to weak intermolecular forces (van der Waals forces) that soften the vibrational potential as the temperature is lowered [71,72]. The extensive hydrogen bonding within the crystal lattice with differential hydrogen bonding strengths within the plane compared to between planes is considered to play a role in the red shift of resonances [71, 72]. [publication P8]

4.3 Biological molecules

4.3.1 Deoxycytidine

Deoxycytidine (dC) is a deoxyribonucleoside and is one of the building blocks of the DNA. They are nucleosides containing a deoxyribose componenet attached to them. The other deoxyribonucleosides are deoxyadenosine, deoxyguanosine, thymidine and deoxyuridine. dC is chosen here to represent this class of biological molecules and to show that the waveguide technique can be successfully used to get its high resolution vibrational spectrum

The dC film was prepared by drop-casting a 12 mg/ml solution in deionized (DI) water onto an optically polished, plasma-cleaned Cu waveguide plate. The transmitted spectrum through the dC film at 295 K and 77 K is shown in fig 4.8. The spectrum at room temperature is featureless and does not show any evidence of the presence of any vibrational modes and is almost similar to the transmission of a bare waveguide with a

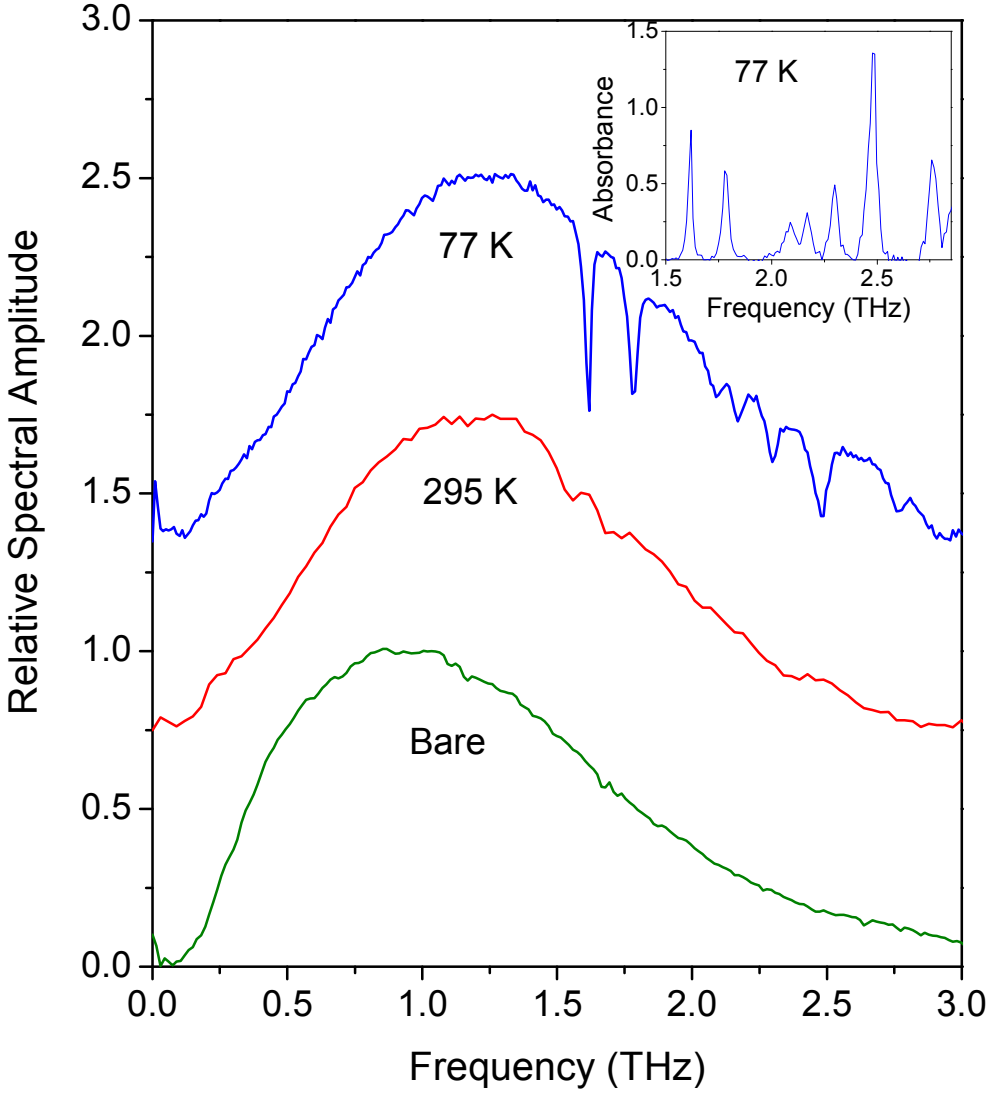

Fig 4.8 Measured transmitted spectrum for deoxycytidine films at 295 K and 77 K. The featureless spectrum at 295 K is compared to the transmission through an empty waveguide. [publication P3]

Table 4.2: Comparison of absorption line frequencies for deoxycytidine studied by waveguide THz-TDS and two other groups [publication P3]

Waveguide THz-TDS 77 K	Fischer et al. 10 K	Li et al. 10 K
-	0.85 (0.05)	-
-	1.55 (0.07)	1.54 (n.o.)
1.62 (0.02)	-	-
1.78 (0.03)	1.75 (0.10)	-
2.09 (0.05)	2.09 (0.13)	-
2.17 (0.03)	-	-
2.30 (0.04)	2.35 (0.09)	-
2.48 (0.04)	2.5 (0.06)	2.43 (n.o.)
2.76 (0.04)	-	2.76 (n.o.)
-	2.82 (0.06)	-

Values in parentheses are the FWHM linewidths. Both frequencies and linewidths are given in THz. Frequencies for Fischer et al. [73] and linewidths for both references [74] are estimated from corresponding figure. n.o - linewidths not obtainable.

broadband absorption. But upon cooling to 77 K a dramatic change is seen and strong sharp absorption features appear. The absorption lines sharpen significantly and linewidths of 20 – 50 GHz is measured for the observed features. One another observation made during the study was that these modes are highly dependent on the surface morphology of the film suggesting that these modes are very inter molecular in nature. The morphology of the film depended strongly on the humidity, with the best results resulting from the film drying in a high humidity environment (~ 80%).

dC has been studied previously in pellet form at 10 K by Fischer et al. [73] and Li et al. [74] The absorption line frequencies observed using waveguide THz-TDS is compared to those obtained by these studies in Table 4.2. From the table it is clear that the waveguide data obtained doesn't fully agree with the data at 10 K the first two lines observed by Fischer et. al is missing in the waveguide data at 77 K. this is probably got to do with the additional cooling required to resolve and develop these lines with waveguide THz-TDS. For many samples we have observed that cooling to 10 K beyond 77 K produces dramatic effects and resolution of many vibrational features. When these sample films were measured the capability to cool to 10 K wasn't in place and provided by the fact that the sample films of dC are very tough to make, efforts to cool to 10 K wasn't made. If the dC waveguide films were cooled to 10 K, it is expected that much more vibrational data could be resolved than that observed at 77 K. [publication P3]

4.3.2 D-Glucose

The D-Glucose film was prepared by sublimation onto an optically polished, water cooled Al waveguide plate. Attempts at making dropcast films from water solutions often resulted in amorphous glassy looking films, which showed no observable spectral features. The spectrum of the transmitted THz pulse through the waveguide containing sublimed film is shown in Fig. 4.9. Three absorption lines are observed at 1.89, 2.11, and 2.57 THz at 295 K.

The observed absorption features do not agree with previous results on dry D-glucose [75-77], but they agree with the absorption features observed with D-glucose monohydrate [78]. This might be due to the fact that the D-Glucose films were allowed to sit at ambient humidity for several hours before any hint of the visible crystal structure appeared in the films. This exposure to ambient humidity clearly led to water getting incorporated into the D-glucose film after sublimation resulting in a hydrated D-glucose film. On cooling to 77 K these 4 resonances significantly narrow. The low frequency line at 1.89 THz appears to red shift to 1.65 THz, while the rest blue shift. 2 new resonances are resolved at around 1.67 and 2.46 THz at 77 K. [publication P3]

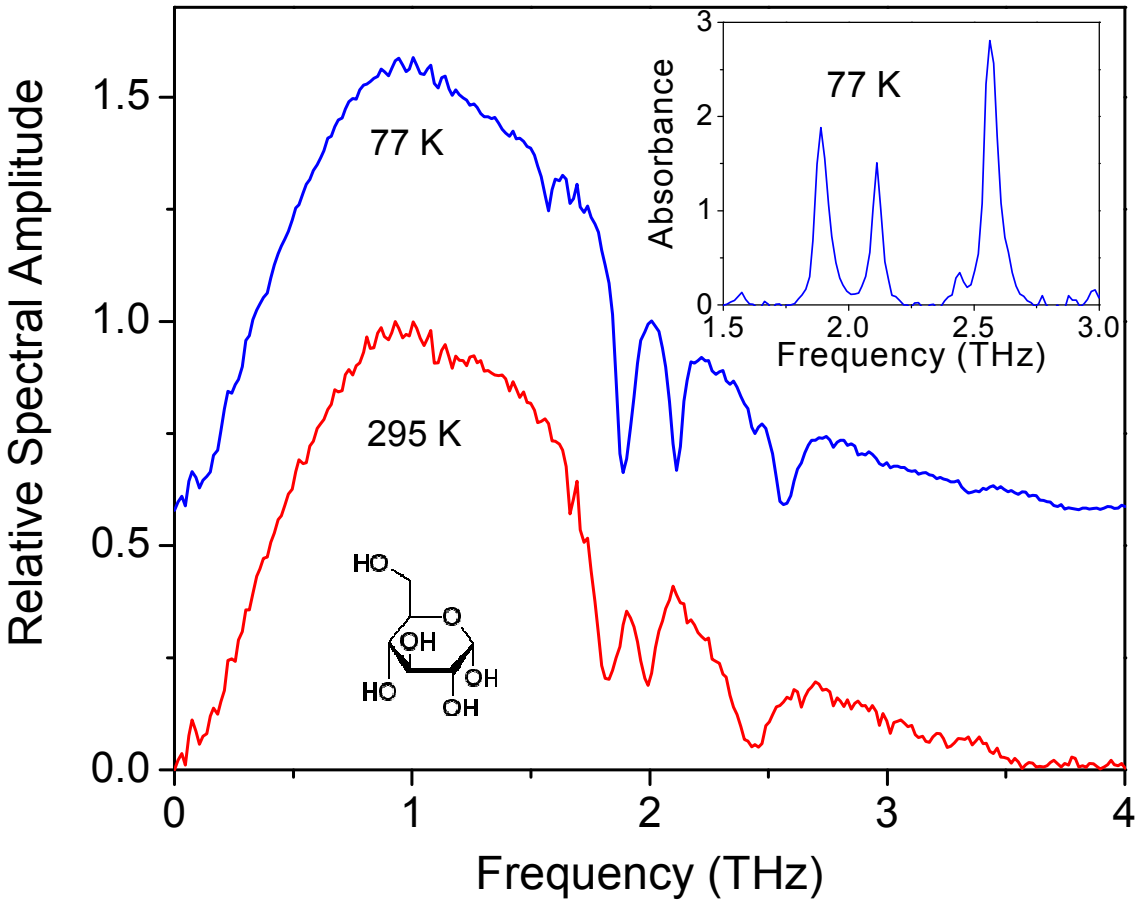

Fig4.9 Spectra of THz transmitted through the waveguide with D- glucose film (hydrated). Spectrum at 77 K is offset for clarity. **(Inset)** Absorbance spectrum at 77 K. Spectrum at 295 K is normalized to unity. [publication P3]

4.4 Pharmaceutical molecules

4.4.1 Salicylic acid and Aspirin

Aspirin and its precursor salicylic acid (2-hydroxy benzoic acid) come under the category of small organic molecules having important applications in biology, pharmaceutical and cosmetic industry. Salicylic acid is well known for its use in acne treatments and is a constituent of many skin creams and beauty products apart from being a precursor to the synthesis. Aspirin (acetylsalicylic acid) is a very popular and well studied drug, used primarily as an analgesic, antipyretic, and also for blood thinning (antiplatelet). The chemical structures for both the molecules are shown in fig 4.10.

The salicylic (2-hydroxybenzoic) acid waveguide film was prepared by drop casting a 10 mg/ml acetone solution onto a polished Cu waveguide plate, while the aspirin waveguide film was prepared by drop casting a 27 mg/ml methanol solution onto a polished Cu waveguide plate. The pellets for both the samples were made from a 28:330 mg mixture of analyte to polyethylene. The optical micrographs of the dropcast films for salicylic acid and aspirin are presented in Fig 4.11. Both images confirm the presence of a good crystalline film on the waveguide surface.

The absorbance of the waveguide films of both these compounds obtained using the pellet technique as well as the waveguide technique is compared in Figs 4.12 and 4.13. Also the vibrational lines observed for both the samples along with their FWHM linewidths is collected in Table. 4.3.

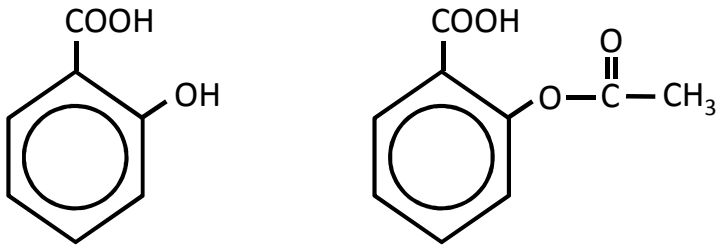

Fig 4.10 Chemical structure of **(a)** Salicylic acid and **(b)** Aspirin

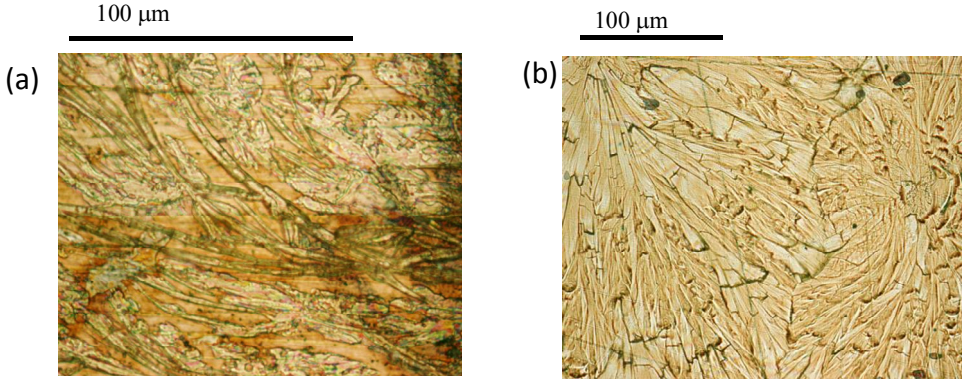

Fig 4.11 Optical micrographs of **(a)** Salicylic acid and **(b)** Aspirin [publication P4]

Table 4.3: Absorbance line frequencies and FWHM line widths (in parentheses) in THz at 77 K for salicylic acid and aspirin. [publication P4]

Salicylic Acid		Aspirin	
Pellet	**Waveguide**	**Pellet**	**Waveguide**
1.21 (0.05)	1.23 (0.04)	-	1.11 (0.05)
1.53 (0.04)	1.55 (0.03)	1.68 (0.25)	1.87 (0.06)
1.77 (0.05)	1.79 (0.06)	2.14 (0.37)	2.17 (0.06)
2.00 (0.06)	2.04 (0.07)	-	2.35 (0.11)
2.21 (0.10)	2.25 (0.07)	-	2.49 (0.05)
2.39 (0.06)	2.42 (0.04)	-	2.87 (0.12)
2.52 (0.12)	2.56 (0.07)	-	3.34 (0.23)
2.91 (0.10)	-	-	3.69 (0.11)

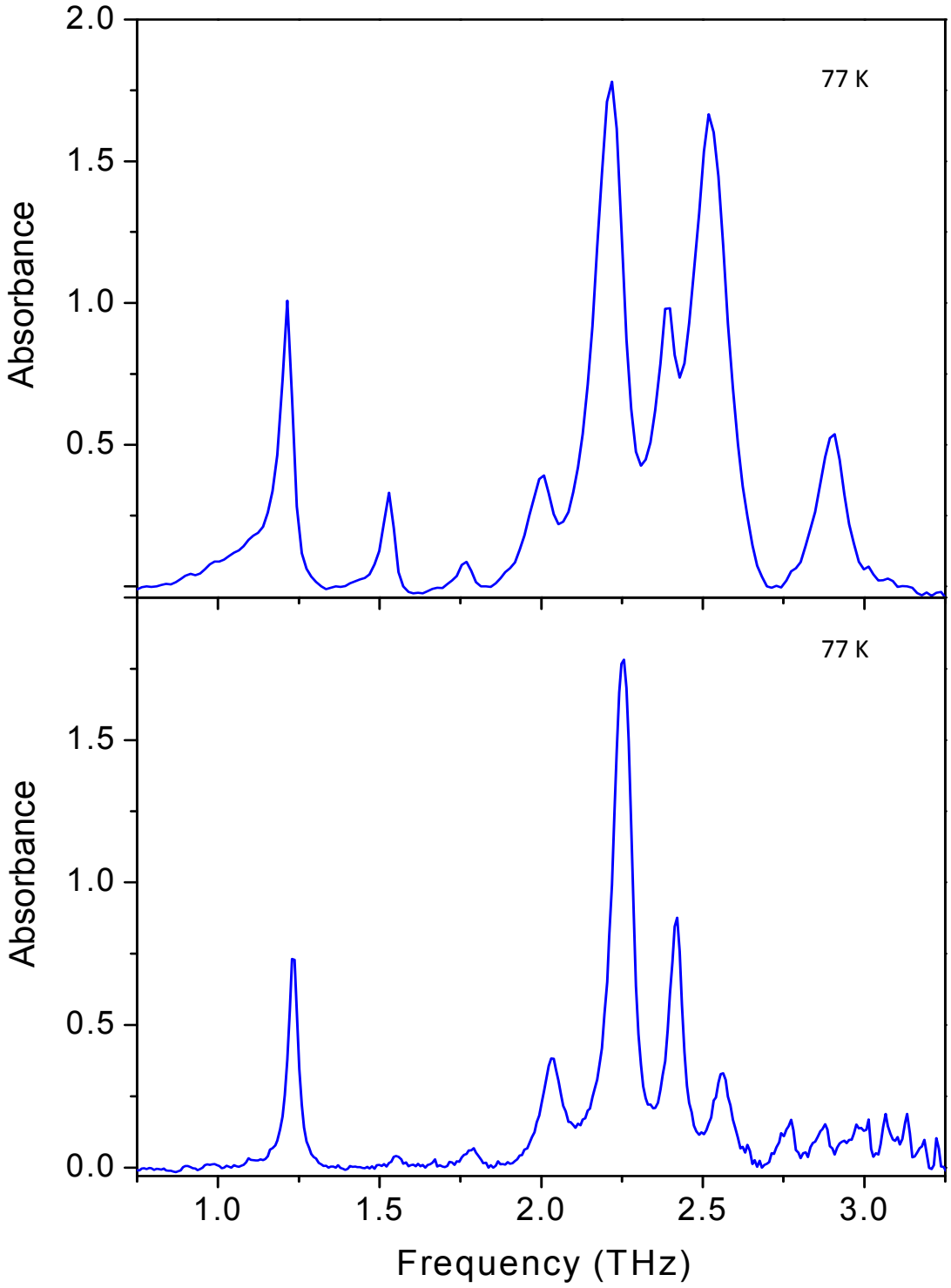

Fig 4.12 Absorbance of **(top)** salicylic acid pellet and **(bottom)** salicylic acid film in the waveguide at 77K [publication P4] .

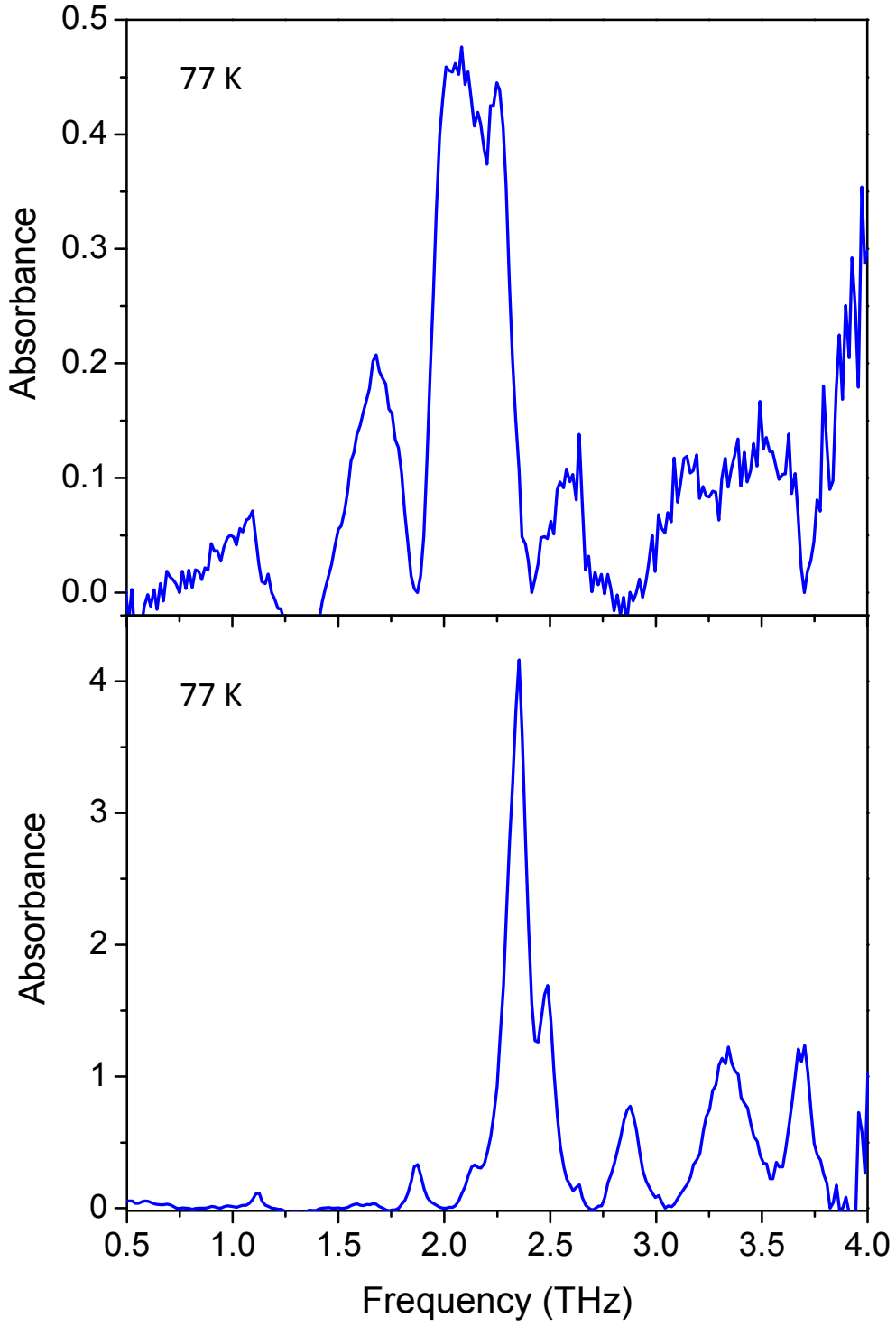

Fig 4.13 Absorbance of **(top)** Aspirin pellet and **(bottom)** Aspirin film in the Cu waveguide at 77K [publication P4]

For salicylic acid the cooled waveguide film reveals 7 features with linewidths ranging from 40 – 80 GHz. With the pellet the four features between 2.0 and 2.5 THz overlap somewhat, while with the waveguide they are distinct (see Fig 4.12). The lines at 2.2 and 2.5 THz for the waveguide film have a linewidth approximately one-half the value of the corresponding line in the pellet and are better resolved in the waveguide. The relative intensities of the absorption lines differ between the pellet and the waveguide. This is probably due to the greater planar ordering of the microcrystals on the metal surface, resulting in the electric dipoles associated with the absorption lines having a fixed orientation with respect to the THz electric field within the waveguide, in contrast to random orientations for the pellet. In particular, the 2.2 THz line is strongly enhanced for the waveguide, while the 2.9 THz line has vanished, suggesting that the corresponding molecular dipole might be along the waveguide surface (i.e., perpendicular to the THz electric field). For aspirin, a substantial line narrowing for the waveguide film is observed in comparison to the pellet. The pellet reveals just 2 two broad features at 77 K. But with the waveguide eight narrow features with linewidths ranging from 50 – 230 GHz. all of these lines have been observed in previous work [79], but with considerably different relative amplitudes. The line centers and linewidths for both salicylic acid and aspirin samples are collected in Table 3. [publication P4]

4.5 Explosives and energetic materials

4.5.1 RDX - Cyclotrimethylene-trinitramine

RDX and acronym for Research Department eXplosive is an explosive nitro amine widely used by the military and in industrial applications. Its chemical name is Cyclotrimethylenetrinitramine. It is a white crystalline solid, which is stable in storage and as an explosive used in mixtures with other explosives and plasticizers. It is one of the high explosives used by the military. One of the promising applications of THz-TDS is the detection and identification of explosive materials. In order for that to happen one needs a database of spectral finger prints, to which data on the field can be compared, to make an unambiguous identification. So, using waveguide THz-TDS it is demonstrated that a high resolution spectral fingerprint can be obtained for this class of compounds.

Thin polycrystalline films of RDX were formed by dropcasting from volatile solutions. RDX standard solutions (1 mg/ml in 1:1 acetonitrile:methanol) were purchased from Accustandards Inc., and concentrated to 2 mg/ml by slow evaporation under a vented chemical hood. 250µl of the concentrated solution was dropcast on the surface of Au coated Al and Al waveguide plates. An optical micrograph of the RDX film on an Au-coated waveguide plate is shown in Fig 4.14 and reveals a complex dendritic morphology for the film. A similar morphology is observed for RDX on Al.

The stable polymorph of the explosive solid RDX crystallizes in the space group *Pbca*, with eight molecules per unit cell (Z=8) [80]. The X-ray diffraction spectrum of

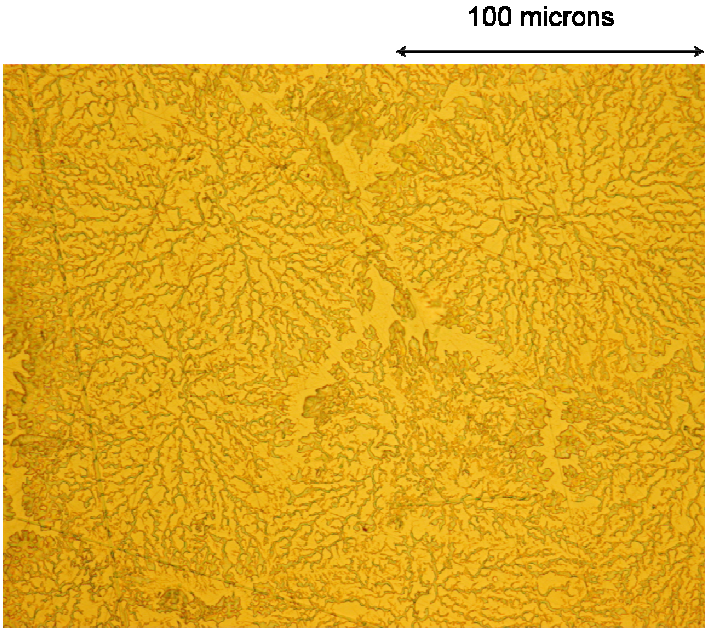

Fig 4.14 Optical micrograph showing a dendritic morphology for the RDX on Au. [publication P6]

RDX on both metal surfaces showed several peaks, all of which could be assigned to crystal planes of the *Pbca* unit cell, and confirmed that the film contained a single polymorph. The strongest diffraction peaks came from the *(111), (200), (201),* and *(021)* planes. Because of the presence of multiple diffraction peaks we conclude that the RDX film is not as highly oriented as other molecular films that were made by dropcasting, where the X-ray diffraction spectrum was dominated by diffraction from a single crystal plane [80, P2].

Both the films on Au as well as Al were incorporated within the PPWGs and their transmission spectrum was measured as a function of temperature. The waveguides were cooled to 13 K. The temperature dependent evolution of the transmission spectrum for both the films is shown in fig 4.15. Both the films reveal a broad absorption at room temperature which evolves into 21 lines at 13 K. The transmission through the Al waveguide had more bandwidth compared to the Au waveguide and hence 2 more lines could be resolved for the Al waveguide film.

Fig 4.16 compares the absorbance spectra of the two films at 13 K to a digitally reproduced data of a pellet from a reference [81]. The line-center frequencies and FWHM linewidths are collected in Table 4.4. The spectra of the two films show general agreement in terms of the number of lines, line frequencies, and relative intensities. All of the major lines are observed in both absorbance spectra at nearly the same line-center frequencies. The higher signal to noise for RDX/Al permits the observation of vibrational lines beyond 3 THz. It can be noted that many of the lines exhibit a tail on the red edge of the line shape. This effect is more pronounced for the RDX/Au film. This type of effect is commonly observed in THz spectra of polycrystalline pellet samples due to scattering

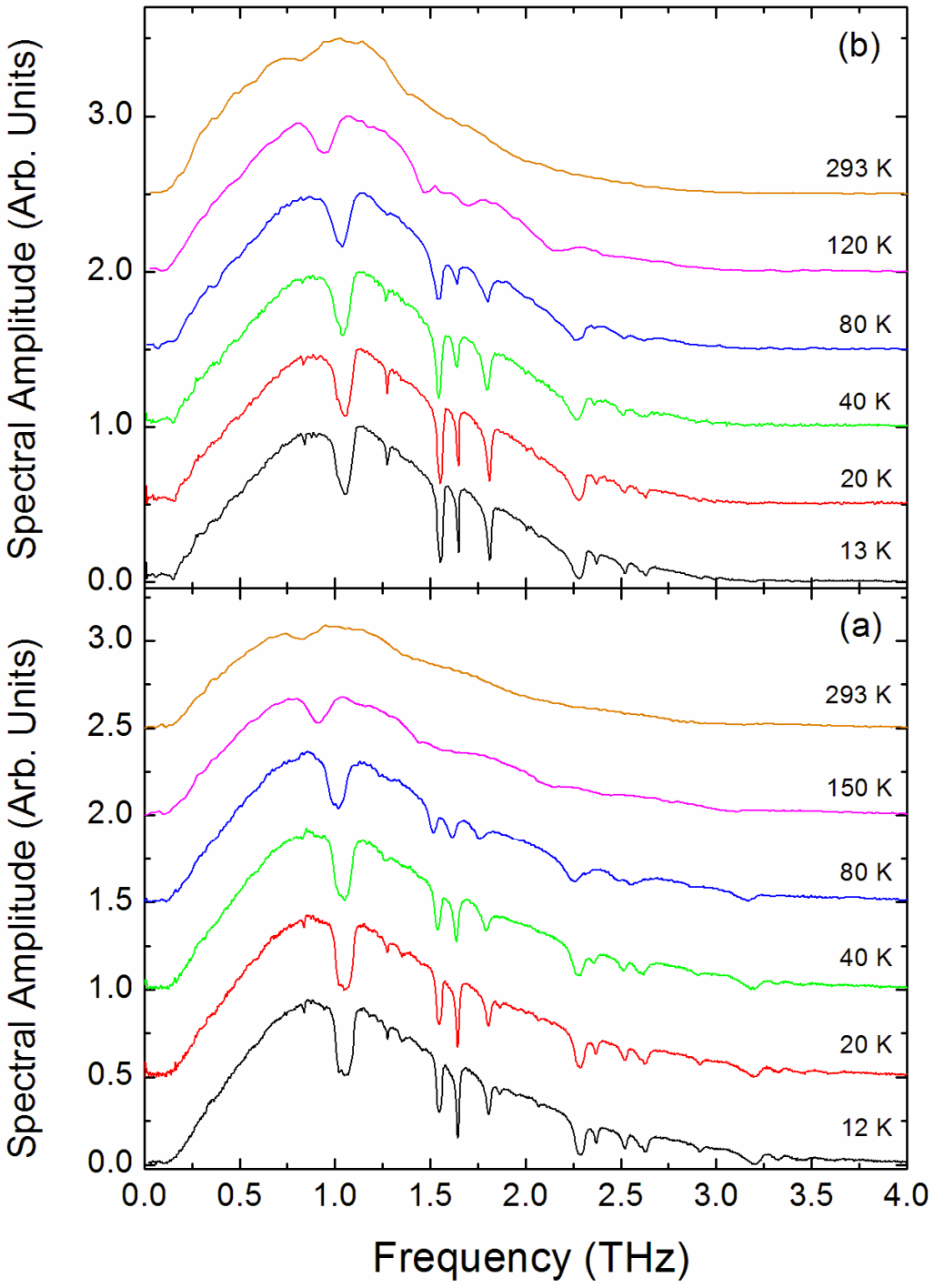

Fig 4.15 Spectral amplitudes as a function of temperature for RDX thin films. **(a)** RDX/Au. **(b)** RDX/Al. [publication P6]

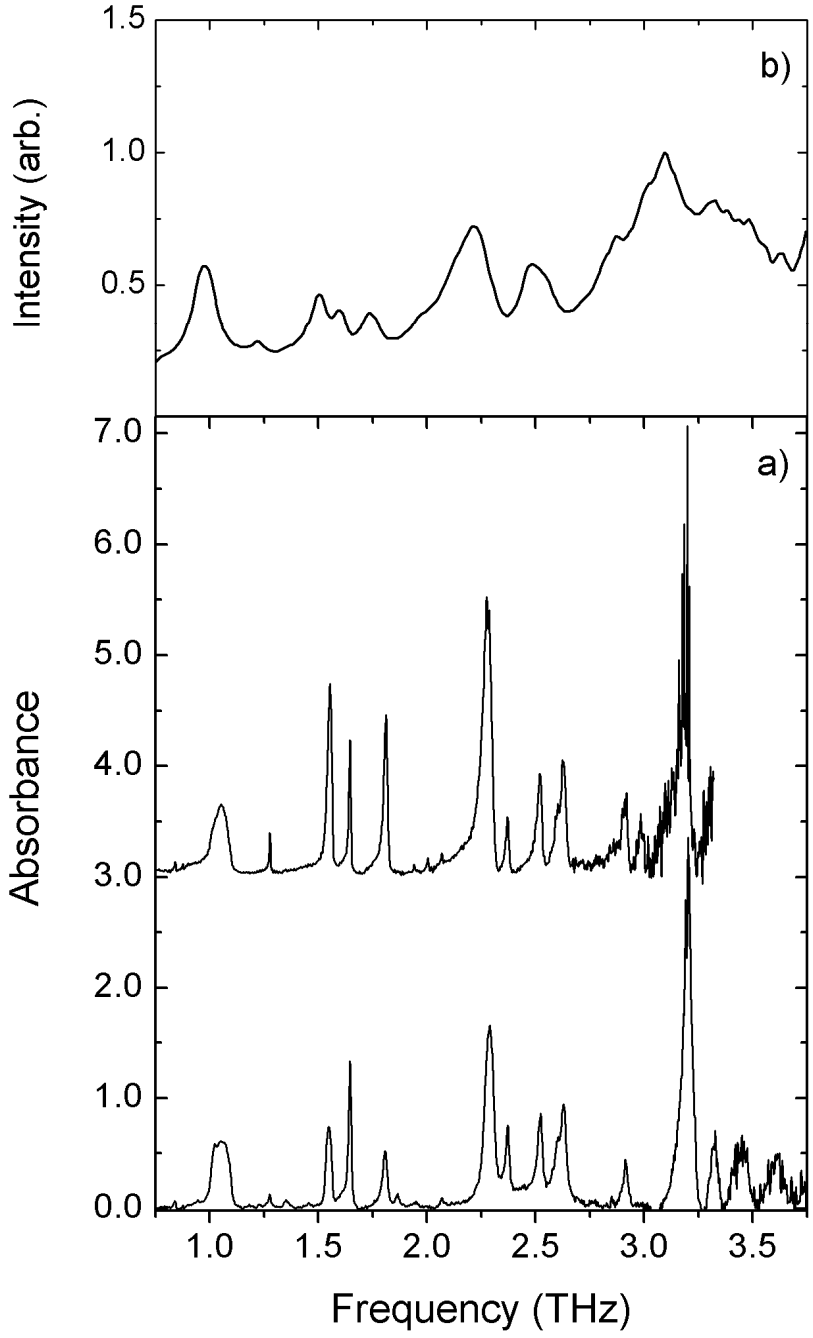

Fig 4.16 (a) Comparison of absorbance spectra of RDX/Al **(bottom curve)** and RDX/Au **(top curve)**. In both cases the broad absorption background has been removed. For clarity, the RDX/Al spectrum has been multiplied by 1.5 and the RDX/Au spectrum has been offset. **(b)** RDX pellet spectrum at 7 K, reproduced digitally from [81] [publication P6].

Table 4.4. Line center frequencies for the RDX films samples previous measurements of pellet samples. FWHM linewidths in parenthesis
[Publication P6]

RDX/Al film 12 K	RDX/Au film 11 K	RDX/Al film 295 K	D.GAllis et al. [81]Pellet 7 K	D.GAllis et al. [80]Pellet 298 K	J. chen et al. [82]Pellet 298 K	Y.Hu et al. [83]Pellet 298 K
0.839^{w} (0.010)	0.839^{w} (0.009)	-	-	-	-	-
0.876^{w}	0.877^{w}	-	-	-	-	-
1.04 (0.090)	1.04 (0.082)	0.85	0.99	0.81	0.78	0.81
1.276 (0.010)	1.278 (0.007)	1.06	1.23	1.05	1.05	1.05
1.351 (0.025)	-	-	-	-	1.35	1.35
1.548 (0.028)	1.553 (0.026)	1.40	1.50	1.38	1.44	-
1.642 (0.017)	1.646 (0.010)	1.55	1.62	1.53	1.56	1.56
1.808 (0.015)	1.810 (0.018)	-	1.77	-	1.77	-
1.864 (0.015)	-	-	-	-	1.92	-
1.943^{w}	1.941^{w}	-	-	-	-	-
-	2.005^{w} (0.009)	-	1.98	-	-	-
2.069^{w}	2.069^{w}	-	-	-	-	-
2.290 (0.046)	2.286 (0.050)	1.98	2.22^{sh}	1.98	-	-
2.370 (0.018)	2.370 (0.015)	-	-	-	-	-
2.524 (0.025)	2.520 (0.030)	2.23	2.49	2.22	-	-
2.603	2.600	-	2.55^{sh}	-	-	-
2.625 (0.028)	2.625 (0.030)	-	-	-	-	-
2.91 (0.027)	2.91	-	2.88	-	-	-
-	-	-	3.00	-	-	-
3.20 (0.040)	3.19	-	3.09	-	-	-
3.32 (0.042)	-	-	3.33	3.09	-	-
-	-	-	3.39	-	-	-
3.45	-	-	3.48	-	-	-
3.61	-	-	3.66	-	-	-

from the grains. In the RDX film the tailing effect is likely due to scattering from individual RDX microcrystals. Table. 3 also compares the waveguide data to the earlier work. It is clear that the waveguide results provide more exhaustive vibrational data compared to the earlier work involving pellets and single crystals.

A comparison of Figs. 4.16 (a) and (b) shows that the RDX waveguide films, generally exhibit much sharper linewidths than the pellet. For example, the 7 GHz linewidth for 1.278 THz mode of the RDX/Au at 13 K is at least a factor of 5 narrower than the corresponding line (1.23 THz) in the RDX pellet at 7 K. The sharper linewidths of the films result in a more informative vibrational spectrum. [publication P6]

Chapter 5
High Q THz Bragg waveguides

5.1 Introduction

In the previous chapter, we saw how metal PPWG can be employed for high resolution spectroscopy of various classes of molecules. In this chapter yet another adaptation of the PPWG for spectroscopy is explored. As discussed in chapter 2 metal PPWG are excellent guiding structures at THz frequencies due their low loss dispersion free propagation of the TEM mode [21]. This property and the ease with which active and passive components can be integrated within it, the PPWG has shown great potential as a THz interconnect device [24].

Propagation of electromagnetic radiation through periodic media often results in many interesting and potentially useful phenomena. Periodic structures such as photonic crystal bandgap materials and surface plasmon resonators are currently being researched extensively for their potential as frequency filters and high sensitivity sensors. Two-dimensional (2D) metallic THz photonic structures used as the bottom plate of a PPWG have shown sharp bandgap turn-ons with high dynamic range [84]. A 1D THz photonic metal PPWG with high throughput and well defined stopbands has also been

demonstrated [85]. Periodic deep grooves in one waveguide plate excited higher order propagating and non-propagating modes, thereby producing broad stop-bands with sharp turn-offs and turn-ons. Incorporating a defect produced a sharp 17 dB transmission resonance with a Q of 120 [85]. Structures like these which produce sharp high Q resonances often have applications in thin film detection as well as trace element detection. We have already demonstrated in the previous chapter that that application of PPWG for spectroscopy only requires only microgram sample quantities.

In this chapter the fabrication and incorporation of 1 μm thick dielectric THz Bragg gratings within a single TEM mode metal PPWG is discussed. Bragg gratings have long been used as frequency selective devices for integrated optics. Bragg gratings are capable of extremely sharp frequency responses and are commonly used in fiber optics for filtering and in semiconductor lasers as part of cavity resonators [86]. Optical Fiber Bragg grating sensors have been widely used in many sensing applications including temperature, strain, and pressure measurements [87, 88].

In this study, 2 different grating samples were fabricated and incorporated into a PPWG and experimentally demonstrate the resulting high-Q resonances. High resolution measurements of THz Bragg resonances of different strengths and linewidths were obtained. The application of these high-Q Bragg gratings for sensitive spectroscopy is also demonstrated. Ability to detect nm thick patterned structures is demonstrated.

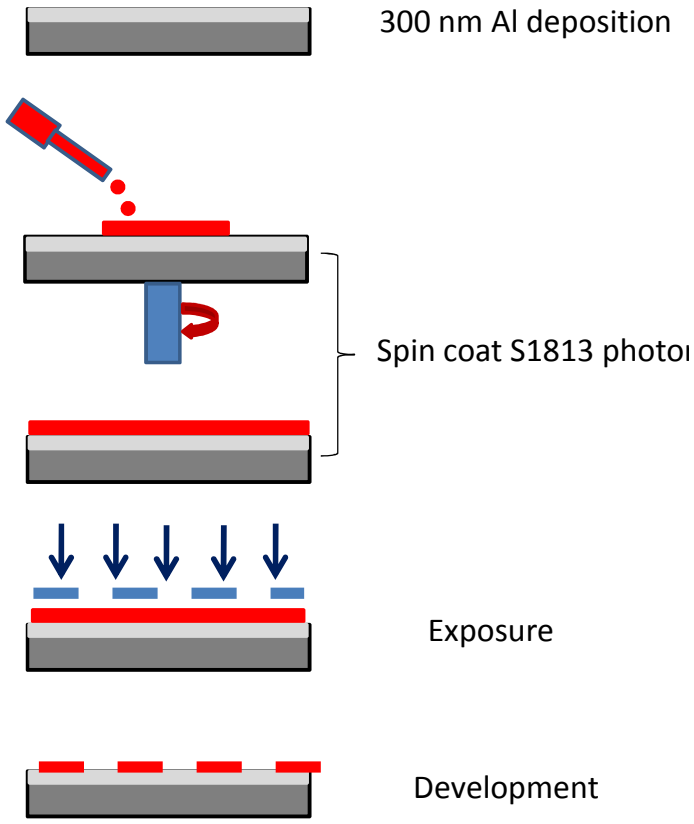

Fig 5.1 Fabrication of dielectric Bragg gratings using standard lithographic and metallization techniques

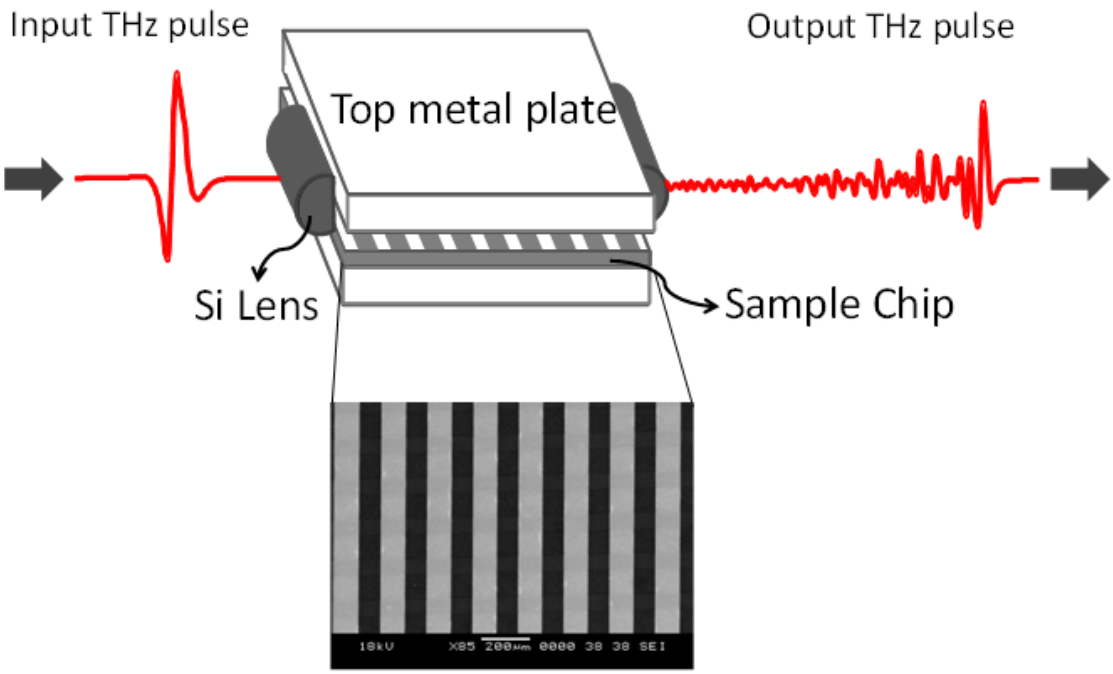

Fig 5.2 Cross sectional view of the PPWG assembly together with the sample Bragg chip.

[publication P7]

5.2 Fabrication and construction of High-*Q* Bragg PPWG

High quality one dimensional gratings were fabricated in a clean room using standard lithographic and metallization techniques (MEMS technology). An approximately 1 μm thick layer of Shipley S1813 photoresist was spun onto a high conductivity Si wafer which was previously coated with a 300 nm thick Al layer. With a custom designed lithographic mask, the photoresist film was exposed and developed. After the lithography, the soft photoresist gratings on the wafer were baked at 150 ^{o}C in a convection oven, which transforms the soft structures to permanent, hard polymer structures. These steps are illustrated in fig 5.1. The final thickness of the grating structure, measured using an atomic force microscope, was 900 nm (see Fig 5.3). The 0.3 mm thick wafer was diced into 15 mm wide x 30 mm long chips to fit the PPWG setup shown in Fig 5.2. Two different 1D grating sample chips were fabricated; symmetric Sample A with 80 μm of photoresist followed by 80 μm of space (160 μm period), and asymmetric Sample B with 75 μm of photoresist followed by 25 μm of space (100 μm period). The 1D THz Bragg PPWG was constructed by sandwiching a sample chip between the two polished Al plates of the original PPWG with the metalized face of the chip serving as the 30 mm long new bottom plate of the waveguide. 50 μm spacers separated the top Al plate and the sample chip. Two plano-cylindrical high resistivity Si lenses were used to in-couple and out-couple the THz pulses. The THz pulse propagation was perpendicular to the lines of the grating, with the THz polarization being perpendicular to the plates.

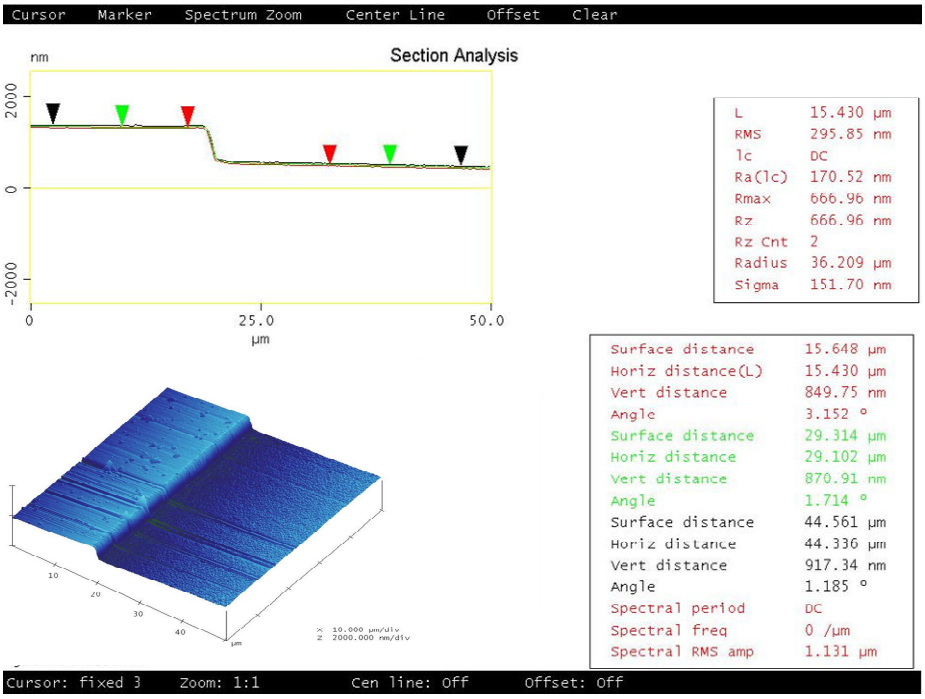

Fig 5.3 AFM thickness measurements of the Bragg samples (~ 900 nm)

5.3 Characterization

The resulting 1D Bragg waveguide assembly was then placed in the confocal beam waist of a photoconductively switched terahertz time domain spectroscopy (THz-TDS) system for characterization. An average of nine measured THz output pulses from the symmetric Bragg waveguide (Sample A), and an average of six for the asymmetric Bragg waveguide (Sample B) was used to obtain the THz transmission spectrum of each of the Bragg samples. The output amplitude spectrum of the symmetric Bragg sample is illustrated in Fig 5.4 and for the asymmetric sample in Fig 5.5. The experimentally determined linewidths were obtained from pulse train measurements extending to 150 ps, which determine the corresponding spectral resolution to be 6.7 GHz. The spectra of the transmitted THz pulses were calculated after zero-padding, i.e. the 150 ps data pulse was extended to 2667 ps by adding a train of zeros at the end of the pulse. An important consideration to be kept in mind while zero padding is that, a too early truncation of the time domain pulse and starting the zero-padding before the pulse has damped out, results in a broadened line shape accompanied by small spectral shifts. But when a time pulse signal has disappeared into the noise (as in our experiments), subsequent zero-padding should not affect the line shape and not produce observable frequency shifts.

The line centers were determined from the interpolated amplitude spectrum of the zero-padded average of nine independent transmitted THz pulse measurements for Sample A and six for Sample B. The indicated uncertainty of ± 0.5 GHz about the fundamental frequency $B_o = 0.9347$ THz for the zero-padded average of Sample A, is the spectral range that contains all the central frequency peaks of the nine individual zero-padded THz pulses. This same procedure was used for the six individual zero-padded

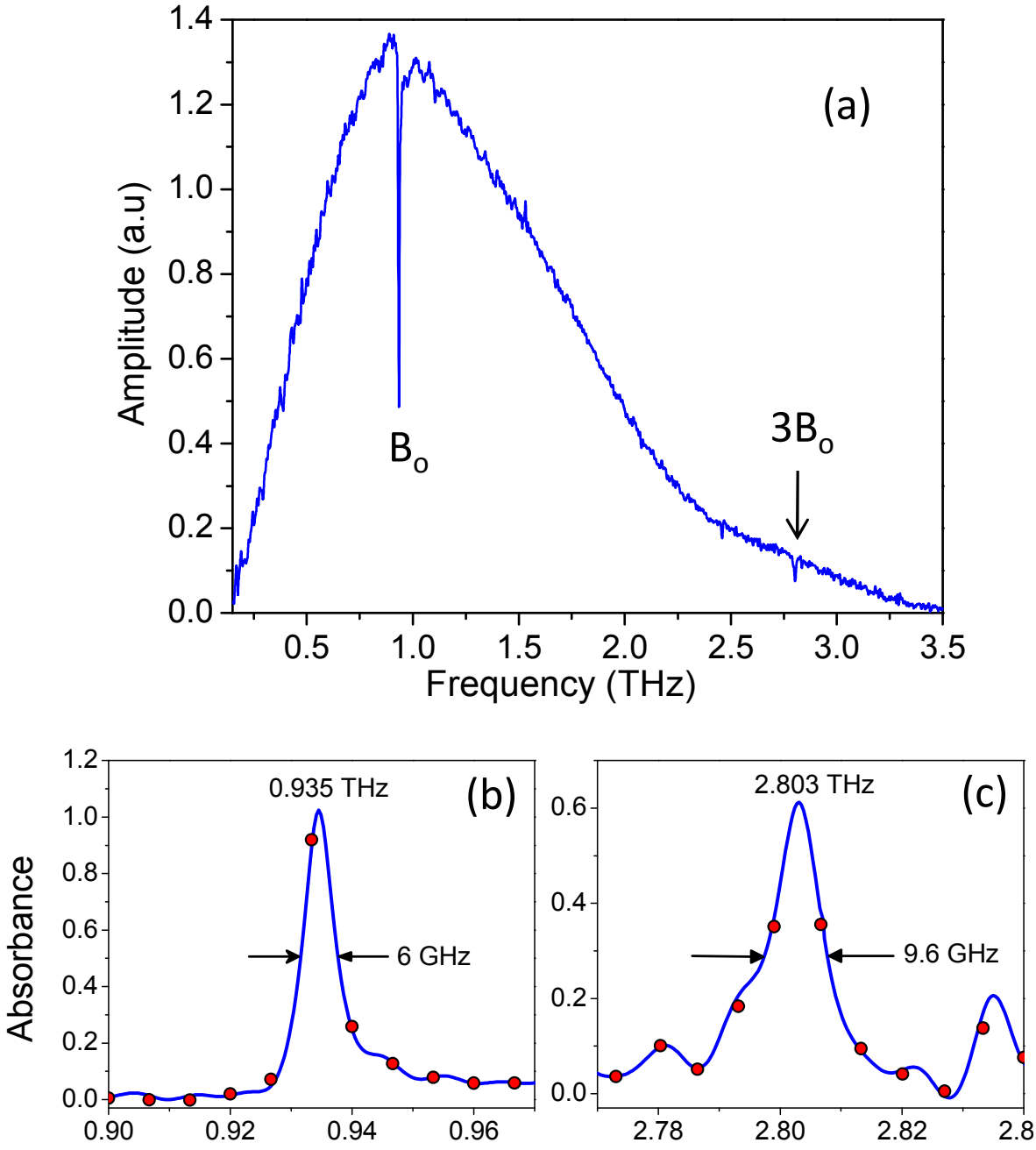

Fig 5.4 (a) Output transmission spectrum of type A Bragg waveguide **(b)** and **(c)** Waveguide absorbance spectrum zoomed in at the fundamental Bragg frequency B_o and its third harmonic $3B_o$. Open circles indicate non zero-padded data points separated by 6.7 GHz. [publication P7]

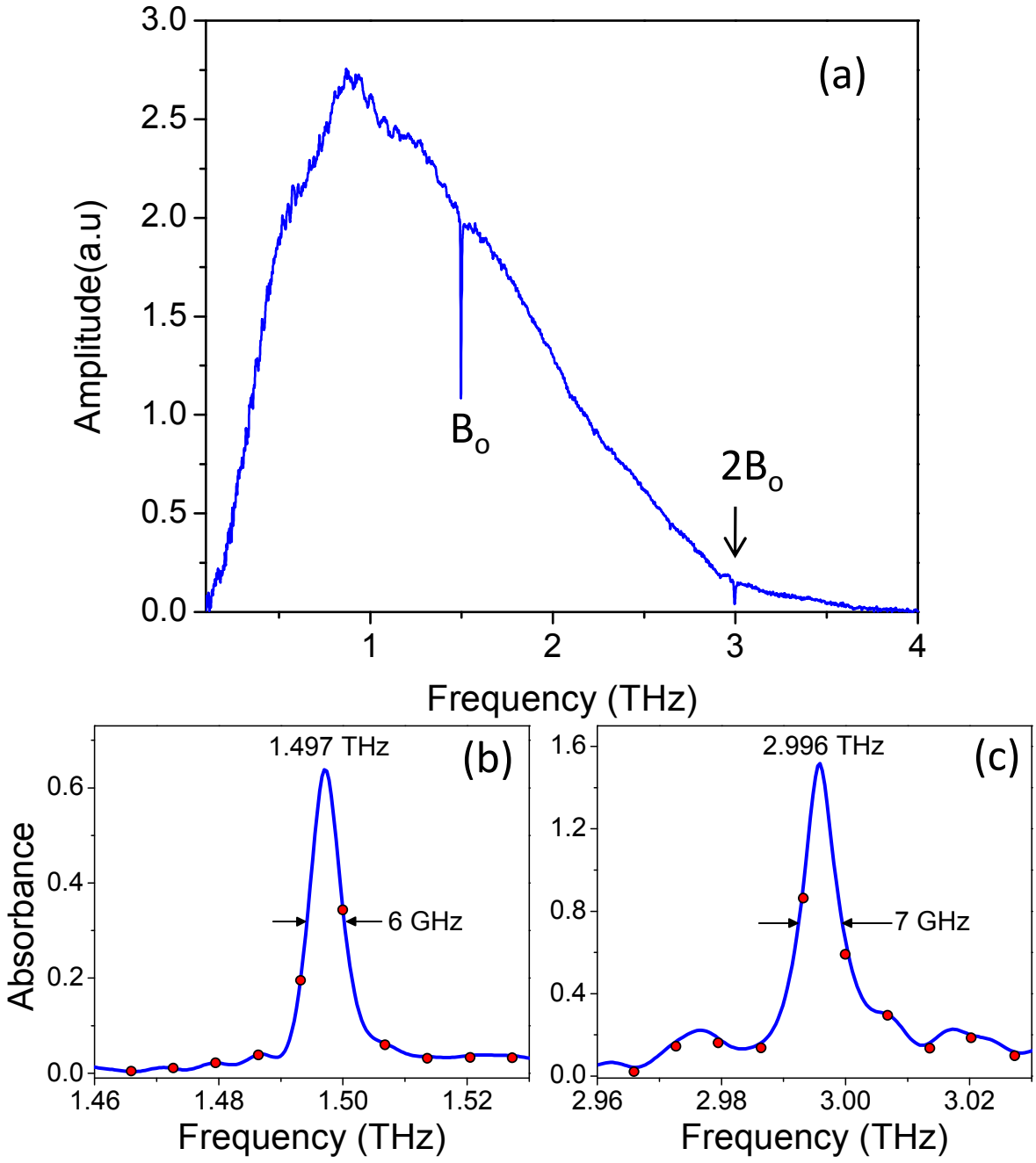

Fig 5.5 (a) Output transmission spectrum of type B Bragg waveguide **(b)** and **(c)** Waveguide absorbance spectrum zoomed in at the fundamental Bragg frequency B_o and its second harmonic $2B_o$. Open circles indicate non zero-padded data points separated by 6.7 GHz. [publication P7]

Table 5.1: The Bragg resonance frequencies v_o and their uncertainty, absorbance fwhm Δv and Q values listed for the two samples. [publication P7]

Waveguide	υ_o (THz)	$\Delta\upsilon$ (GHz)	$Q = \upsilon_o/\Delta\upsilon$
Sample A	0.935 ± 0.5 GHz	6.0	155
	2.803 ± 5.0 GHz	9.6	290
Sample B	1.497 ± 0.5 GHz	6.0	250
	2.996 ± 2.0 GHz	7.0	430

pulses of Sample B. This uncertainty is strongly dependent on the S/N ratio of the spectrum; as the S/N ratio increases, the corresponding uncertainty decreases, and vice versa. It is noteworthy that the B_o frequencies have been determined to a precision of ± 0.5 GHz, compared to the spectral resolution of 6.7 GHz. Hence, for sensor applications frequency shifts of 0.5 GHz or more should be measurable. The observed resonance frequencies and their uncertainty, their FWHM linewidths and *Q* factors are listed in Table 5.1. *Q* values are calculated using the relation $Q=\upsilon_o/\Delta\upsilon$, where υ_o is the line center frequency and $\Delta\upsilon$ is the absorbance fwhm linewidth of the resonance. The Q=430 measured for the second harmonic of sample B is one of the highest experimentally measured *Q* for a periodic structure incorporated within a metal THz PPWG.

5.4 Analysis

One important observation one makes when we look at the output spectrum from the Bragg PPWG is that the waveguide preserves TEM mode propagation despite the incorporation of the sub micron thick Bragg stack within the PPWG. This is because, the depth of the grating (Fig 5.3) of ~ 900 nm is about 2 % of the waveguide gap of 50 μm and the grating only acts as a small perturbation to the propagation of the TEM mode of the PPWG. An earlier demonstration by A. Bingham et.al wherein similar metal Bragg gratings where incorporated within the PPWG had depths of about 20 μm which was about 20% of the 100 μm gap. This kind of arrangement gave rise to complicated output spectrum consisting of strong band gaps and clearly excited multimode propagation [85]. In comparison to that result the present arrangement preserves pure TEM mode

propagation with the expression of clean high-Q Bragg resonances. This kind of output is desirable for thin film and trace material sensing.

The grating within the waveguide can be considered to be a simple thin Bragg stack of alternating regions of two types of hypothetical bulk material with indices of refraction of 1.0057 and 1.0000. For sample A, the Bragg stack equivalent would be alternating 80 μm long regions to achieve a total length of 30 mm and for sample B, it would be alternating layers of 75 μm of n_1=1.0057 and 25 μm of n_2=1.0000. Propagating through this Bragg stack, the terahertz pulse would be reflected by each interface plane. If the Bragg condition is not satisfied, the reflections from the subsequent interfaces become progressively out of phase and would eventually cancel out. When the Bragg condition is satisfied, the reflections from each interface add constructively in the backward direction to form a back-reflected peak and a corresponding forward absorption peak, both with the same center frequency.

One can use the principle of momentum and energy conservation to determine the center frequency of the Bragg grating. Energy is conserved as THz radiation propagates through the Bragg stack. For conservation of momentum the sum of the incident wavevector k_i and the grating wavevector K must be equal to reflected wavevector k_r.

$$k_i + K = k_r \tag{5.1}$$

When the Bragg condition is satisfied $k_r = k_i$, hence,

$$\frac{2\pi}{\lambda} n_{eff} + \frac{2\pi}{\Lambda} = -\frac{2\pi}{\lambda} n_{eff} \tag{5.2}$$

This can be simplified as,

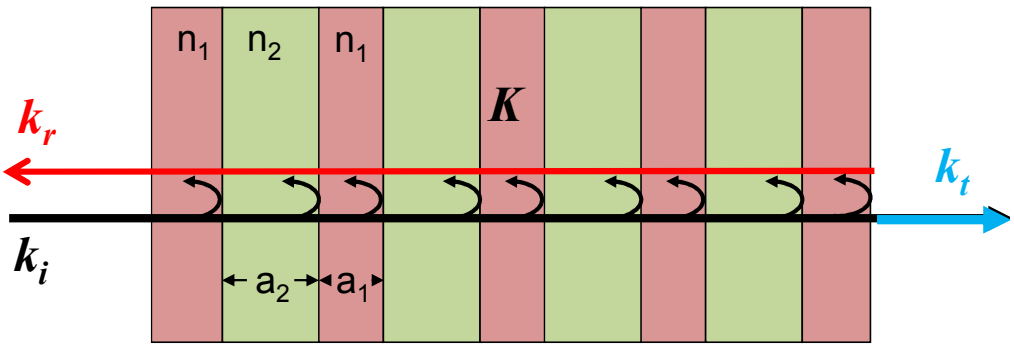

Fig 5.6 Illustration of the weak bulk equivalent of the Bragg stack structure within the PPWG. Region n_1 has an index contribution from the 900nm thick photoresist and 49 μm thick air region ($n_1 = 1.0057$) and region $n_2 = 1.0000$ (air).

$$\lambda_B = 2n_{eff}\Lambda \quad (5.3)$$

Where λ_B is the Bragg wavelength, Λ is the grating period and n_{eff} is the effective waveguide index. The first order Bragg condition in terms of frequency can be written as:

$$B_o = \frac{c}{2n_{eff}\Lambda} \quad (5.4)$$

where c is the speed of light

The refractive index of baked S1813 photoresist at 1 THz is 1.65. [89] In order to calculate the effective refractive index of the region comprising the photoresist and a gap of ~ 50μm we use equation 15 from ref [19].

Since we have a ~ 900 nm layer of photoresist and a gap of 50 μm, the effective refractive index of the region comprising the photoresist within the waveguide can be calculated to be 1.0057. This gives an effective index of 1.0028 and 1.0043 for types A and B Bragg waveguides, respectively. Using this refractive index, B_o for Λ=160 μm and 100 μm is calculated to be 0.934 and 1.492 THz. The experimentally determined resonances at 0.935 and 1.497 THz are in good agreement with the predicted values. The length of the Bragg waveguide is 30 mm. from this the intrinsic linewidth predicted can be calculated. Since we have assumed a weak Bragg stack the single reflection coherence length is 60 mm, which gives the expected linewidth to be 5 GHz. the experimental resolution is 6.7 GHz. Hence the Q predicted for the third harmonic resonance of sample B at 2.996 THz is ~ 600, whereas the experimentally obtained Q was 430.

5.5 Application of high-*Q* Bragg PPWG for sensing

High-*Q* resonant structures have great potential in sensing applications, which require narrow, easy to detect features. The 1D Bragg waveguides are ideal for such sensing applications, in particular refractive index sensing, which is important for biological and chemical detection of a number of substances. [90] One such application would be in the detection of antibodies and antigens [91]. Antibodies have preferential attraction toward antigens. Hence a dielectric grating of antigens formed on the metallized plate can be used to detect trace amounts of antibodies. When this grating is dipped in a solution containing antibodies, the binding of antibodies to antigens changes the effective index of the Bragg waveguide, thereby causing a shift in the Bragg resonance together with a large change in signal strength.

This capability can be achieved in 2 different ways:

1. Deposit the analyte layer on the opposite plate of the PPWG facing the Bragg stack (400nm detection limit)
2. The analyte itself is patterned as a Bragg stack (50 nm detection limit)

To demonstrate the first method sample B was used and S1813 photoresist was used as the analyte and thin films of different thickness was spin coated on the opposite plate of the PPWG. The PPWG was reassembled using 50 μm spacers. The THz transmission spectrum was measured for different film thicknesses. Fig 5.7 summarizes the results for 2 different film thicknesses of 1.5 μm and 3.7 μm obtained by varying the spin RPM and the time of spinning. The effective index for a 1.5 μm film can be calculated to be 1.0095 which estimates the new Bragg frequency of the loaded

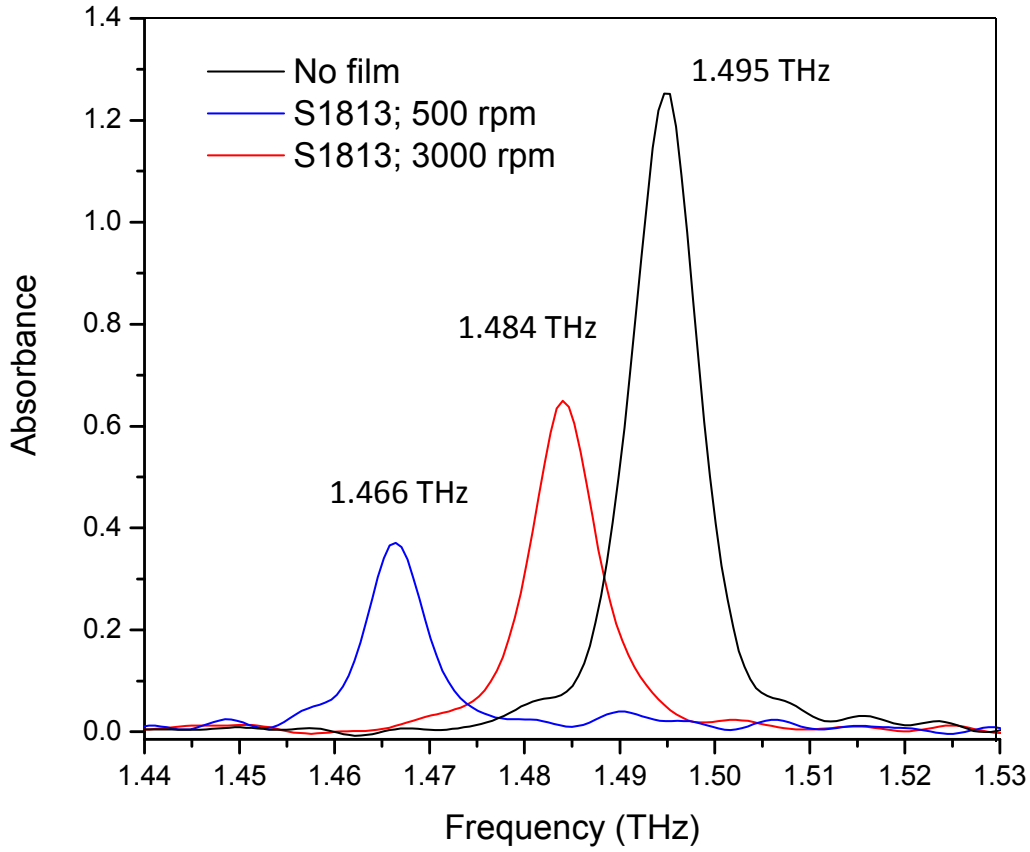

Fig 5.7 Shift in Bragg resonance for different film thickness on the opposite plate of the Bragg PPWG

waveguide to be 1.485 THz. The experimentally observed value is 1.484 which is very close to the calculated value. Similarly for the ~3.7 μm film the expected value is 1.470 THz and the experimental value is 1.466 THz. The experimental limit to the frequency shift that can be detected based is 0.5 GHz, which is the experimental uncertainty. A shift of 0.5 GHz in frequency domain translates to film thickness of ~ 400 nm which can be detected and sensed with the Bragg waveguide in this arrangement.

To demonstrate the second technique a sample chip (sample A) made of S1813 photoresist was taken and placed in plasma cleaner (asher) for 10 min. the plasma cleaner burns the photoresist and a small change in refractive index is also expected along with thickness change. After 10 min the sample chip was taken out and the depth of the Bragg stack was remeasured using the AFM. The final depth of the Bragg stack was found to be ~ 50 nm (see fig 5.8).

This Bragg chip was reincorporated as before into the PPWG with a 50 μm gap and the transmission spectrum was measured to see if any hint of the presence of the burnt Bragg structure was seen. No evidence of any Bragg resonance was seen at 50 μm. The gap was then lowered to 35 μm and the Bragg waveguide reassembled. The comparison between Sample A with 900 nm depth and 50 μm to the waveguide with 50nm depth and 35 μm gap is shown in fig 5.9. The expected line center for the depth of 50 nm and a gap of 35 μm is 0.936 THz and is very close to the observed value of 0.934 THz.

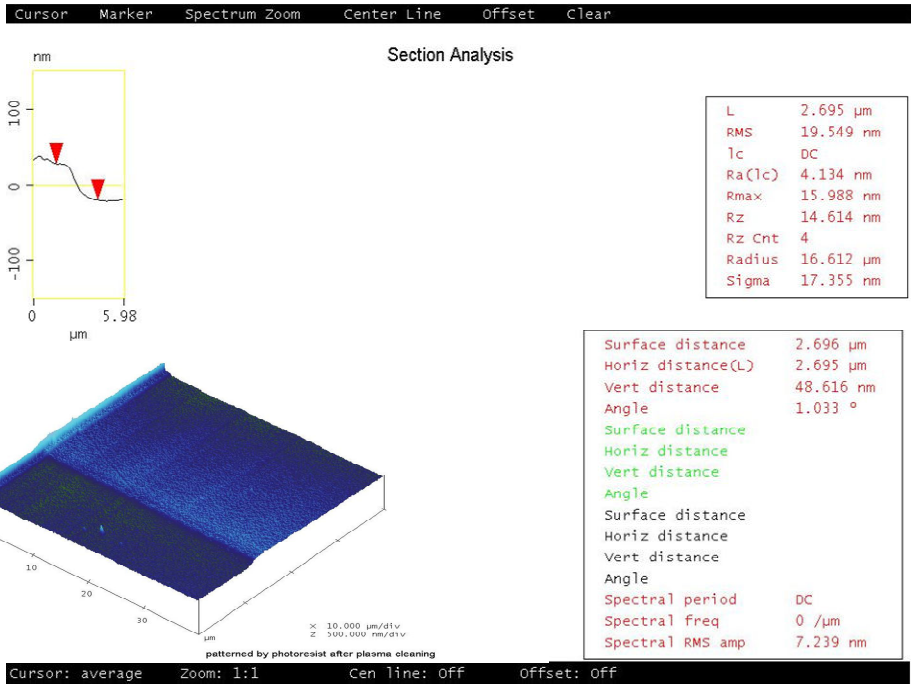

Fig 5.8 AFM thickness measurements of the plasma burnt Bragg samples for 10 min (~ 50 nm)

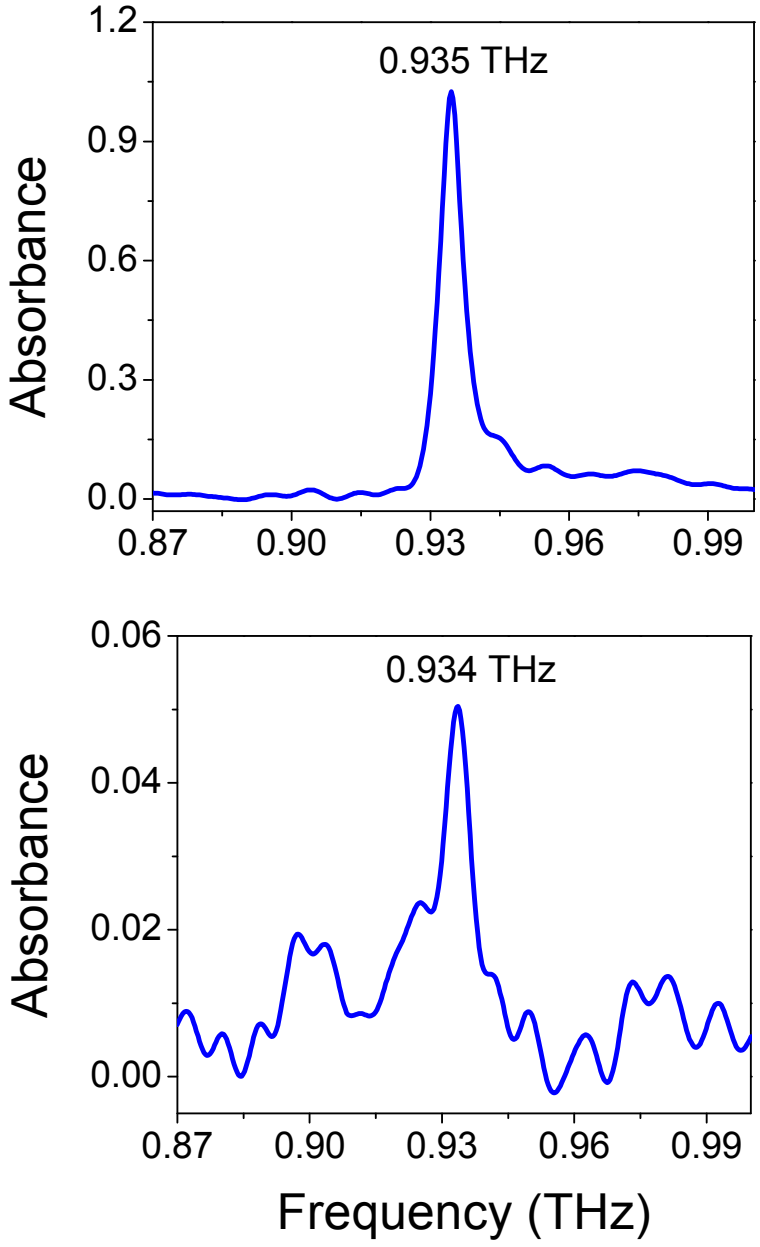

Fig 5.9 Comparison between Line frequencies of sample A **(top)** 900 nm depth **(bottom)** 50 nm depth

5.6 Bragg PPWG gas sensors

This demonstration clearly shows the power of the Bragg waveguides in the ability to detect sub 100 nm thick perturbations within the PPWG. With this capability it is possible to detect small changes in refractive index of the Bragg film as well as sample film on the opposite plate of the PPWG.

The refractive index change can be brought about my many physical phenomena like adsorption of gas molecules to certain specially designed polymers to certain films of antigen and antibody which have specific preference to each other. These phenomena often induce a very small index change which we believe can be detected by the Bragg technique.

Based on this proof of principle demonstration there are plans for construction of Bragg PPWG based sensors for threat gases and vapors. Certain specific polymers have a property of adsorbing or trapping vapors and gases of specific types. This trapping of gas molecules results in a measurable index change which can be monitored by the shift in the Bragg resonance. Patterned polymer films or unpatterned films on the opposite plate of the PPWG can be used to construct a PPWG based Bragg sensor for precise and sensitive identification of vapors and gases.

Chapter 6

Enhanced THz wave coupling using metal flares

6.1 Introduction

In the last few chapters, the adaptation of metal PPWGs for performing high resolution spectroscopy and sensing was discussed. The key feature which enabled this application was the fact that metal PPWGs can support low loss, distortion free and dispersion free propagation of broadband THz pulses in the lowest order TEM mode. The TEM mode is unique in the sense that it does not possess a frequency cutoff and thus supports propagation of broadband THz pulses.

The mode profile within the PPWG is described by the *y-component* of the electric field, which has a spatial dependence proportional to $cos[m\pi y/b]$ as given by equation (2.3) in chapter 2. This dependence results in an even uniform profile for the TEM mode (TM_0), an odd profile for the TM_1 mode and an even profile for the TM_2 mode. Hence, the next higher order mode, the y-polarized, on-axis input even Gaussian beam is going to couple into is the TM_2 mode. So, in order to sustain single TEM mode propagation through the PPWG, the gap spacing between the plates has to be chosen such

that the cutoff frequency of the TM_2 mode lies outside the range of the input spectrum. This condition dictates the maximum allowable gap for sustaining a single TEM mode propagation necessary for spectroscopic applications. For a gap of 50μm, the cutoff for TM_2 mode is 6 THz and for a gap of 100 μm this cutoff drops to 3 THz which is well within the available spectral range of the input signal (0-5THz). Also, we have observed that for a gap of 50 μm we achieve the best sensitivity for performing THz-TDS for the thin films. So for majority of the applications in this thesis, the gap size chosen is 50 μm and below.

But having such small gap sizes makes the coupling of THz pulses to these PPWGs challenging. One way to do it is to use the quasi-optic coupling technique of cylindrical lenses to shape and reduce the beam extent and make it suitable for coupling into the sub-wavelength gap.

6.2 Quasi-optic coupling using Si plano cylindrical lenses

The material chosen for the plano-cylindrical lenses was silicon, due to its low dispersion and absorption properties. PPWG with the Si lens assembly used for coupling is shown in Fig 6.1. The dimensions of the lenses chosen are: 15mm x 10mm x 6.56 mm with a radius of curvature of 5mm and focal length of 6.71 mm. The input Si plano cylindrical lens focuses the THz beam to an elliptical spot to the entrance of the PPWG. The lens produces a line focus, with a minor axis given by:

$$\omega_{02} = {}^{\lambda f}/_{\pi\omega_{01}} \tag{6.1}$$

Where λ is the wavelength, f is the focal length and w_{01} is the input beam radius. Hence at 1 THz, for a beam radius of 9 mm, and focal length 6.71 mm, ω_{02} = 150μm. Hence for a plano-cylindrical lens having a thickness of 6.56 mm with the focus just beyond its surface, focuses the 9mm beam at 1 THz down to a *1/e* diameter of 300μm at the input face of the PPWG. This arrangement dramatically improves freespace coupling to the PPWG and an identical plano-cylindrical lens at the output face out couples the THz beam on to the receiver.

The quasi-optical coupling of a freely propagating terahertz beam into the PPWG at the beam waist of a confocal terahertz system is surprisingly efficient over the entire bandwidth. Compared to the free-space system, the insertion of only the two cylindrical lenses separated by their focal lengths reduces the amplitude of the transmitted terahertz pulse by the multiplicative factor 0.4 = 0.8 x 0.5, where 0.5 is the Fresnel transmission through the uncoated Si lenses (due to the reflective losses of four surfaces), and 0.8 is the quasi-optical amplitude coupling (transmission) through the two confocal lenses. The introduction of 50μm air spaced 30mm long Cu PPWG reduces the transmission to 0.24 = 0.6 x 0.8 x 0.5, where the additional factor of 0.6 is due to the waveguide coupling loss with a smaller loss due to ohmic losses of the metal.

Three different Si lenses were tried and their performance was compared. Apart from the 6.56 mm thick lens another lens having the same design parameters but being slightly thicker at 7.07 mm was also used. Along with this a much thicker lens, almost double the thickness of the first 2 lenses at 15 mm (r = 10mm) was also used and the performance of all three lenses compared. The 6.56 mm lenses had an amplitude coupling ratio of 24 %, the 7.07 mm lenses had 18 % and the thick 15 mm lenses had 9%. One of

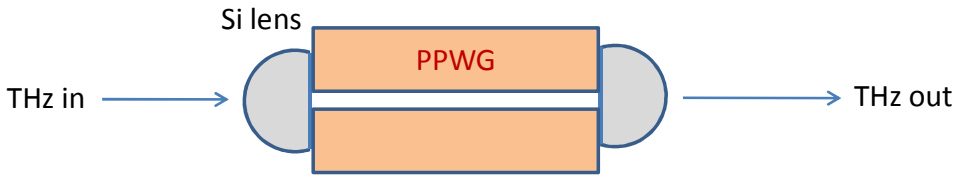

Fig 6.1 Metal PPWG with Si lens couplers

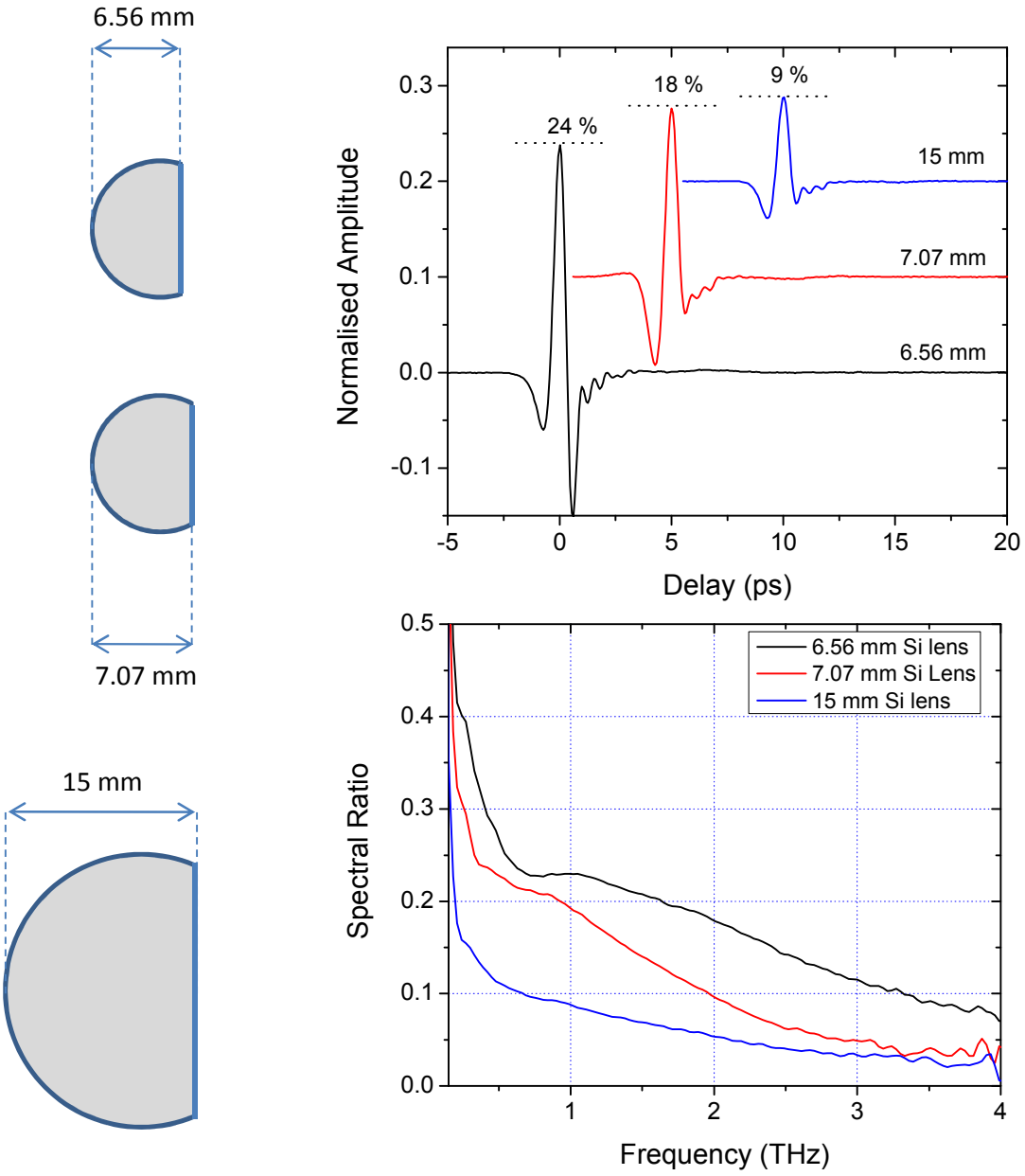

Fig 6.2 Comparison of the coupling performance of the Si lenses

the reasons the coupling characteristics of the thicker Si lens was studied, was to delay the reflection arising from the flat surface of the lens, which limited the maximum scan length for the waveguide THz-TDS which in turn limited the instrumental frequency resolution.

For the 6.56 lens the reflection occurred at 150 ps after the main pulse, which limited the instrument frequency resolution to 6.6 GHz. By using the 15 mm lens this reflection could be pushed back to almost 310 ps which doubled the frequency resolution that could be achieved. Of all the three lenses tested, the 6.56 mm lens performed the best in terms of amplitude coupling as well as the broadband performance and the lowest performance was from the 15mm lenses which had just 9% amplitude coupling ratio. The performance of the three lenses is summarized in fig 6.2. The frequency dependent coupling ratio is also shown.

Despite the good performance of the 6.56 mm lenses one cannot help but notice that the reduction in performance comes from the big Fresnel reflection which occurs due to the high refractive index of Si (n = 3.412). About 30% of the beam is reflected from each of the two lenses and subsequently induces a ~ 50% loss. As demonstrated the best amplitude coupling ratio achieved was 24 %. Hence any mechanism or new coupling scheme which betters this performance will lead to increased THz field coupling and concentration within the sub-wavelength gaps of the PPWG and thereby increase system performance as well as S/N of the measurement.

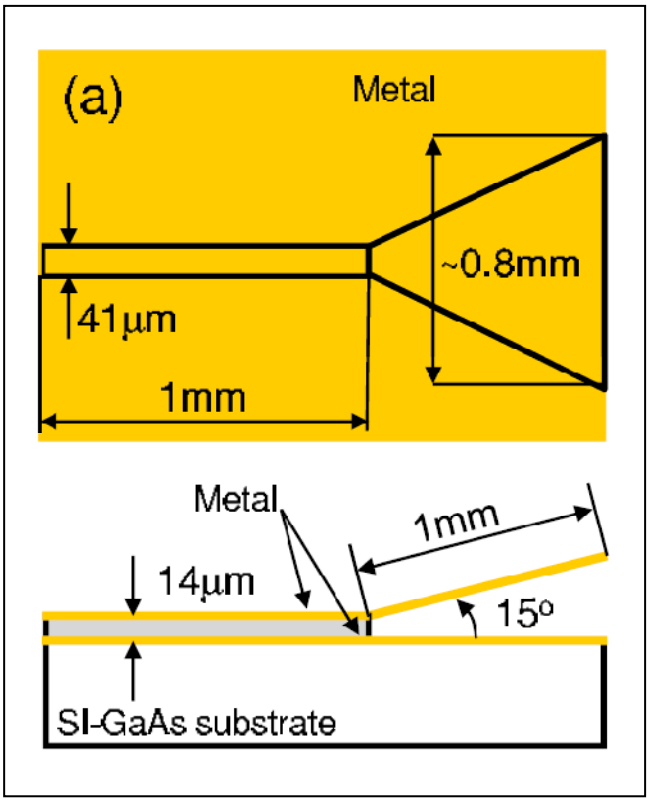

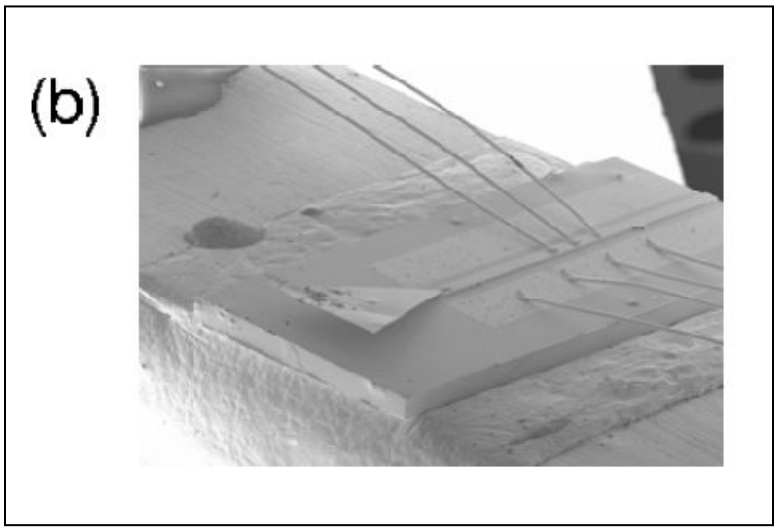

Fig 6.3 (a) Schematic of the horn antenna like structure used by W.Maineult et.al for coupling THz radiation between the QCL and freespace. (b) SEM picture of the same structure [93]

6.3 Adiabatically varying metal flares as an alternative coupling scheme

The inspiration to try an adiabatically varying metal flare as a coupling scheme for PPWGs came from the observation made by M.Theuer et.al [92] on THz pulse compression using a metallic cylinder over a coated metal sheet. The authors observed an unprecedented compression of the THz surface wave on the sheet when it encountered the metallic cylinder in its path. The authors measured a significant fraction of the incident radiation go through the gap between the metal cylinder and the sheet. The adiabatically varying gap between the cylinders efficiently compresses and funnels the THz radiation through the sub-wavelength gap. [92] This gave us an idea that a similarly varying adiabatic metal structure could be used as a coupler at the entrance of the PPWG. In fact, upon looking through literature we found at least 2 examples of this idea being implemented to couple THz waves into a wave guiding structure. The first demonstration was from W. Maineult et.al who implemented this horn antenna like structure to couple THz radiation from freespace to metal-metal waveguides for applications in construction of THz Quantum cascade lasers. The structure they implemented is shown in fig 6.3. [93] A much more recent demonstration was by S. H. Kim et.al, who applied this technique to the coupling of metal parallel plate waveguide. The authors used adiabatically varying machined plates having tapered end faces and demonstrated that for a 3^{o} slope angle to the taper they could achieve as high as 56 % coupling at 1 THz. [94] The coupling efficiency for Si lens coupled PPWG at 1 THz was about 24 %. So the tapered end coupling almost doubled the efficiency of the Si lens. J. Zhang et. al also demonstrated coupling into adiabatically compressed PPWG's using Si lenses. They could efficiently

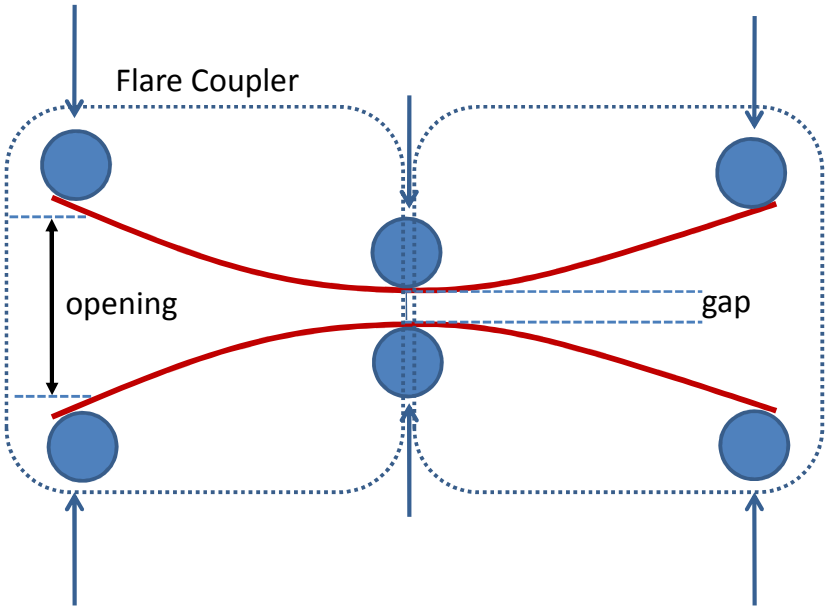

Fig 6.4 The metal flare assembly used to demonstrates the maximum coupling efficiency achievable using this configuration. The cylinders indicate the pressure points which could be moved in control fashion using a micrometer to control the opening and the minimum gap at the center. [92, publication P9]

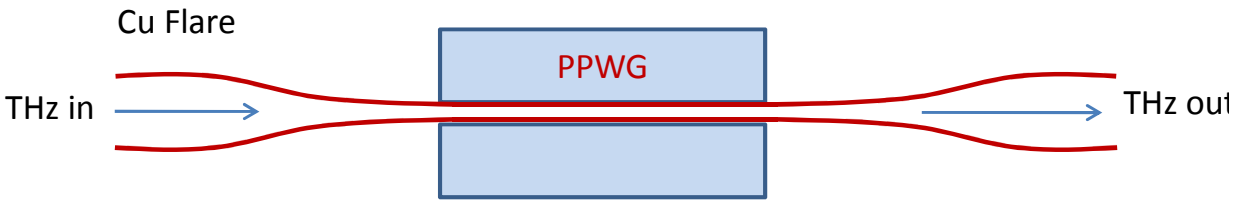

Fig 6.5 Adaptation of the metal flare coupler assembly to a 3cm long PPWG

couple in the THz radiation into the adiabatically varying gap and extract the THz radiation out only limited by the ohmic losses of the metal plates.[95]

Encouraged by the results with the cylinders and the recent demonstrations we decided to apply a simplified version of a horn antenna to the coupling of the PPWG. We manufactured adiabatically varying metal flares from commercially available copper shim. This in our opinion is a easy to use and a low cost alternative for achieving better coupling to the PPWG. The construction of the flares is simple and fast. Using a paper cutter, 15 mm wide strips are cut from a 9 cm diameter, 15 cm wide roll of standard commercial 100 μm thick copper shim. The strips are then slightly pressed and rolled using a metal cylinder to make them flat and to remove bends. To evaluate the coupling efficiency of this arrangement independent of the waveguide losses the experimental arrangement shown in Fig 6.4 is used. This introduces 2 symmetrical flare couplers back to back. With this arrangement the coupling efficiency of the flare coupler was studied as a function of flare opening as well as the minimum gap size. Two 25 mm diameter circular rods compress the copper shims together in the center, while the gap is kept open by the mechanical spacers outside of the THz beam. At the points indicated in the figure the cylinders could be moved back and forth using a micrometer to control the gap size or the flare opening. The results obtained from this investigation are presented in Fig 6.6. From the figure it is very clear that independent of the gap size, the best coupling ratio is obtained for an opening between 5 – 8 mm. In particular for the gap sizes we are interested in, i.e. 50 and 100 microns, the maximum coupling ratio of 39 % and 41 % respectively was obtained for a flare opening of 6.3 mm. This coupling is almost 15 % more than the maximum achieved using a 6.56 mm Si lens. All these efficiencies

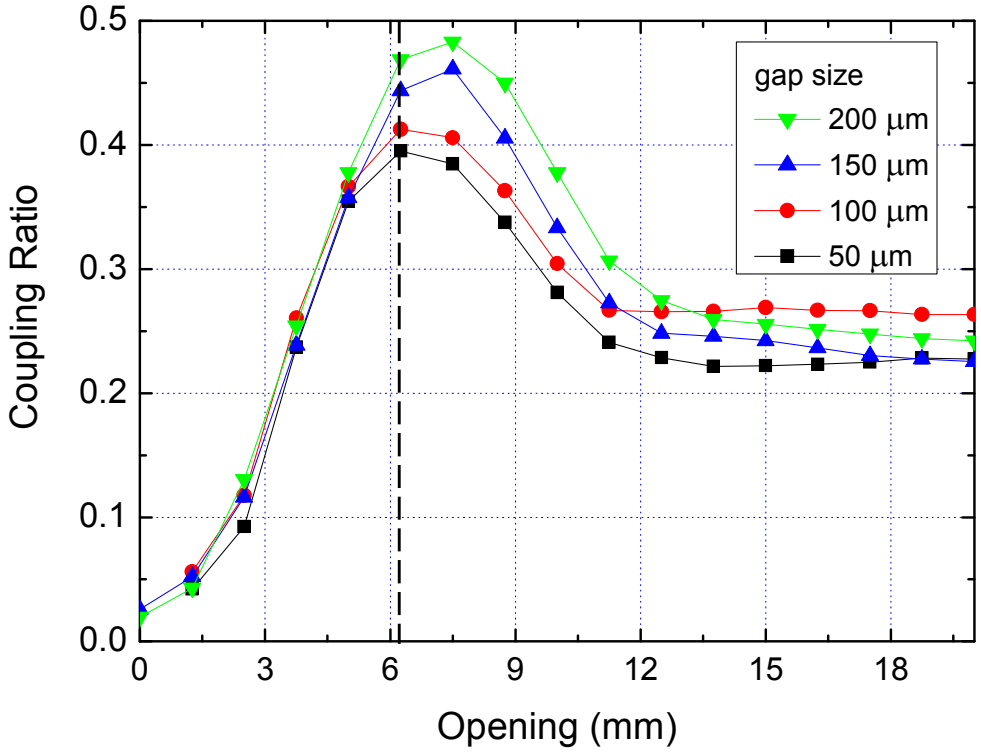

Fig 6.6 Measured amplitude coupling ratios for a flare of 15cm length with different gap sizes. The transmission can be maximized by adjusting the flare opening for the best adiabatic coupling. [publication P9]

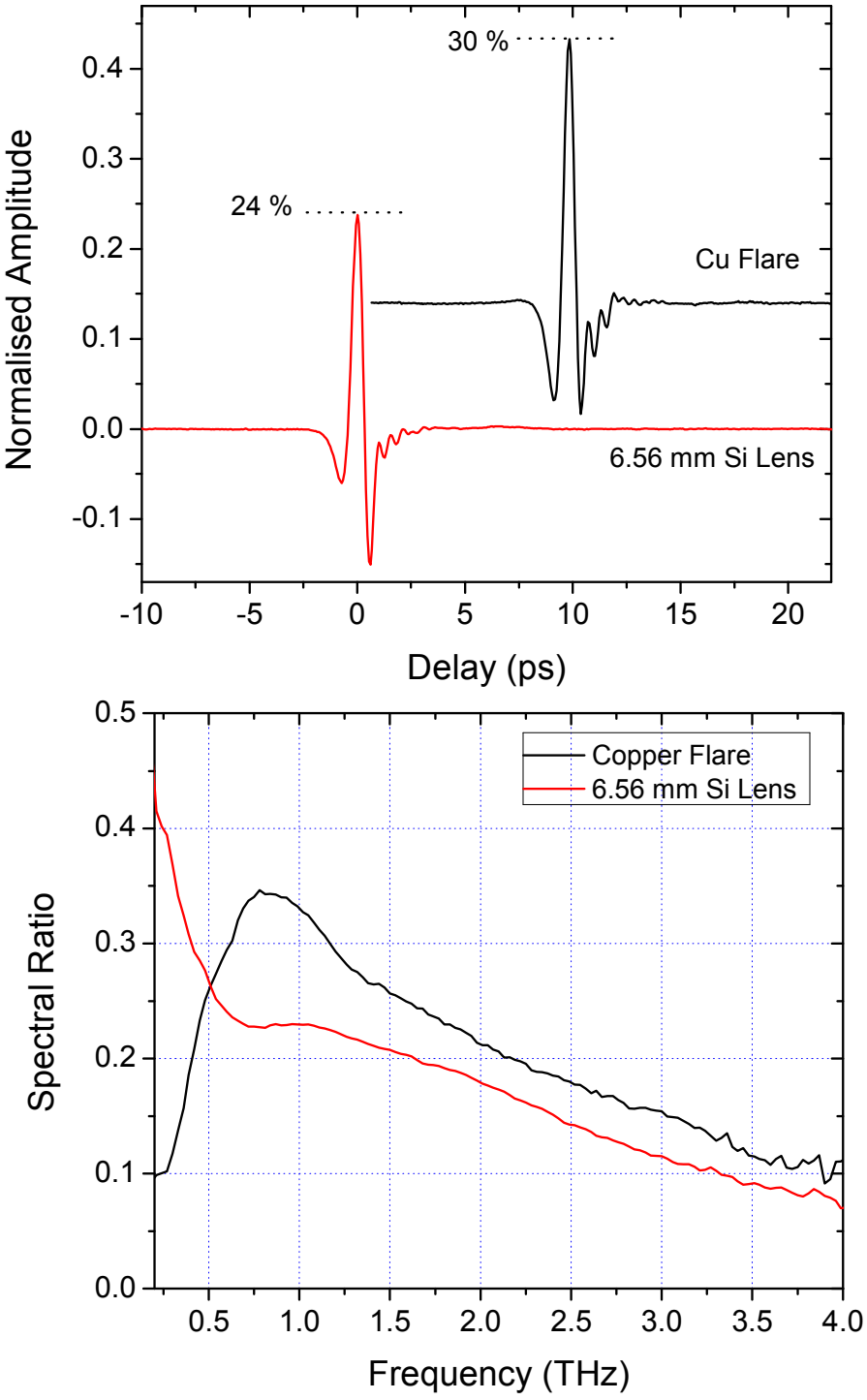

Fig 6.7 Comparison of the coupling characteristics of the 6.56 Si lens and the Cu Flare

[publication P9]

obtained were for the TEM mode operation. The transmission can be further maximized or the best broadband coupling achieved by adjusting the flare opening for the best adiabatic coupling. (Values above 50% were reached) [92, publication P9].

Encouraged by these results the metal flares were incorporated into a 3cm long metal PPWG as shown in Fig 6.5. This is the same metal PPWG with 50 μm gap used with the Si lens coupling. Unlike in the previous case wherein the flare opening could be controlled using a micrometer, the PPWG arrangement did not have any control surfaces. This was not necessary and not spatially feasible as we intended to use the same assembly for cryogenic characterization of samples in the cryostat. Hence the Cu shim was carefully shaped into a funnel shape by hand. It is important to point out that this particular shape wherein the taper starts out parallel and then is sinusoidally and adiabatically tapered to a funnel shape was key to achieve the best coupling. A linearly varying taper and circularly varying tapers did not perform as well as the sinusoidally varying taper. In fact it is found in literature that sinusoidally varying tapers are employed for coupling at microwave frequencies.[96] The spacers are located between the flares but outside of the THz beam. The entire assembly is then screwed together to form a rigid PPWG which could be easy to handle.

Fig 6.7 compares the temporal pulses coupled into the PPWG using a 6.56 mm Si lens and the adiabatic Cu flare. The transmitted THz pulses through the flare coupled PPWG show an increase in amplitude coupling. The amplitude coupling is 30 % compared to the 24 % achieved for the Si lens system. Even though this increase is moderate, the technique's power is demonstrated in the frequency domain wherein at 1 THz the coupling efficiency for the flare is about 35 % compared to the 22 % achieved

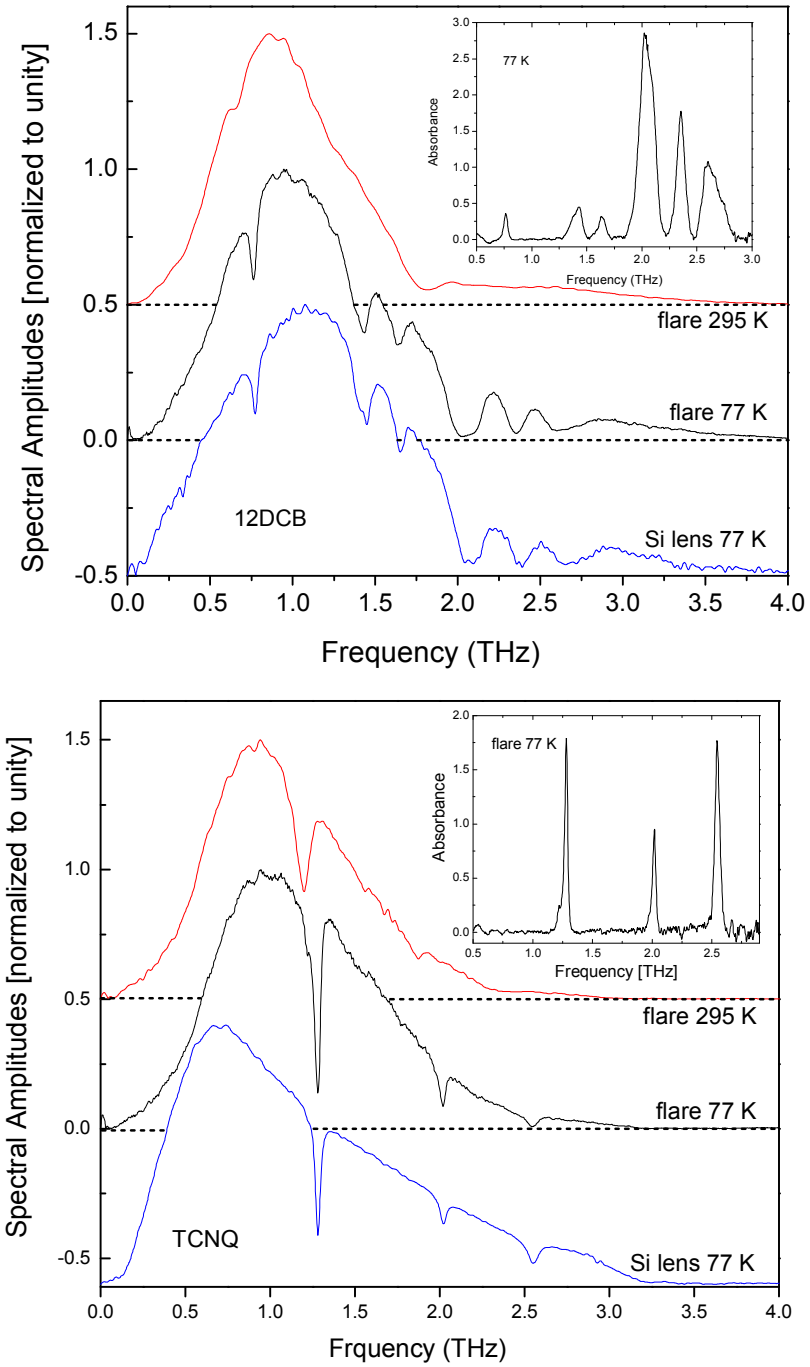

Fig 6.8 Spectral amplitudes for dropcast samples of 1,2-dicyanobenzene **(top)** and TCNQ **(bottom)** in the flare coupled WG at temperatures of at 295 K and 77 K compared to the results for the Si lens coupling. Insets: absorbance at 77 K using the flare coupled PPWG [publicationP9]

for the Si lens system. Moreover, the coupling remains higher than the Si lens system throughout the spectral bandwidth having a coupling ratio of 10 % even at 4 THz. The decrease in coupling ratio towards the high frequencies could be attributed to the increased ohmic losses arising from more metal-THz interaction occurring due to the flares. Ohmic losses are known to increase as the square root of the frequency with increase in frequency (Equations 2.7 – 2.9).

Another important feature observed with the flare coupled PPWG was when the temporal scan was extended beyond 150 ps, the pulse remained distortion free and no reflections were seen despite doing a very long temporal scan. This is an important performance improvement wherein the temporal reflections due to the Si lens were eliminated and simultaneously there was moderate increase in coupling ratios. This increase in signal contributes to enhanced S/N ratios allowing measurements to be performed with better accuracy and as well as having no system limitations being placed on the resolution that could be achieved. Moreover the Cu flares are easy to implement and much more cost effective in comparison to Si lenses.

6.4 Application of Flare coupled PPWG for waveguide THz-TDS

Two molecular samples namely TCNQ and 12DCB, which were earlier characterized by Si lens coupled PPWG were chosen to demonstrate the performance of the flare coupled PPWG for high resolution THz-TDS. Both samples were dropcast from their respective solutions onto the copper shim. The film was swabbed to form a uniform polycrystalline sample layer and this copper shim with the sample was incorporated back

into the PPWG setup as shown in Fig 6.5. Simultaneously a regular Si lens PPWG was also prepared in the same fashion and both the waveguides were characterized at room temperature and at 77 K using the same THz-TDS setup used earlier.

The transmission spectra of both waveguides with the samples incorporated are shown in Fig 6.8. From the figure it is very clear that both the flare coupled PPWG and Si lens coupled PPWG perform similarly. The absorption features show up as small resonance features at room temperature and evolve into narrow features at 77 K. The line centers and linewidths obtained by both the techniques were identical, confirming the fact that both waveguides have similar performance characteristics. One notable difference between the two methods was that the flare coupled PPWG was easy to assemble and had very less alignment time compared to the Si lens coupled PPWG. It was also moderately robust in maintaining its mechanical structure upon cooling and not much degradation in coupling was observed upon cooling due to mechanical stresses on the flare due to cooling. But one noticeable performance issue was with respect to the total bandwidth supported by the 2 waveguides. The flare coupled PPWG, due to larger metal-THz interaction length, had higher ohmic losses towards the high frequencies and as a result the bandwidth transmitted was limited to about 3 THz towards the high frequencies. But other than this the performance of the flares was exceptional and easy to implement.

Chapter 7

Conclusion

This thesis summarizes the successful demonstration of the adaptation of metal parallel plate waveguides for sensitive and high resolution waveguide THz time domain spectroscopy. The technique requires microgram sample quantities in comparison with standard pellet technique which has a milligram sample requirements. The technique is also superior in comparison to the pellet technique in the sense that it has the capability of measuring sub 10 GHz linewidths of absorption resonances with a precision of ±0.5 GHz. Linewidths as narrow as 6 GHz have been measured (lactose). The performance of waveguide THz-TDS approaches the performance of the single crystal technique, in determining the vibrational fingerprint of a molecule with great precision and narrow absorption linewidths.

The validity and generality of the technique is established by applying this technique to measure the high resolution vibrational modes of a wide variety of molecules ranging from organic molecules, inorganic molecules, biological samples, pharmaceutical molecules to threat substances like explosive related solids. The vibrational linewidths obtained for majority of the molecules is the narrowest measured

to date for a sample in solid crystalline state. This demonstration establishes waveguide THz-TDS as a new novel spectroscopic technique capable of extracting high resolution spectral data using microgram sample quantities. This technique when applied in conjunction with the standard THz-TDS or FTIR techniques can lead to an extensive and detailed characterization of the vibrational response of the molecular crystals at THz frequencies.

The thesis also successfully demonstrates the independence of the THz vibrational modes of the sample to the metal used for the parallel plate waveguide. By characterizing a sample with known response at THz frequencies using the pellet as well as waveguide THz-TDS technique 5 substrates namely Al, Cu, Au, mylar coated Al and SAM passivated Au , we have shown the independence the vibrational modes to the substrates used. This establishes the fact that there is minimal metal-analyte interaction limited to the first few crystalline mono layers close to the metal surface. In addition passivated metal surfaces can be incorporated into metal PPWGs and waveguide THz-TDS characterization can be performed on samples with known reactivity to metals.

The ability to incorporate periodic structures within the metal PPWG and the sensitivity of the PPWG to these structures was demonstrated by incorporating symmetric and asymmetric weak Bragg gratings within the PPWG. The ability of this structure to produce very high – Q resonances was demonstrated. Q factors as high as 430 was obtained and is one of the highest Q-factors measured periodic structures at THz frequencies. The sensitivity of the PPWG to such a periodic structure was demonstrated by detecting 50 nm deep structures incorporated within the PPWG. These high - Q

waveguides can be implemented as very sensitive sensors in detecting minute quantities of samples.

The last part of the thesis summarizes the work done in improving the coupling characteristics of the parallel plate waveguide. The performance of the PPWG based applications can be improved by improving the percentage of the THz radiation that can be coupled in to it. The proven microwave technique of horn antennas is applied to the PPWG at THz frequencies by using adiabatically varying metal flares to couple THz radiation in to the PPWG. Greater coupling performance compared to the quasi-optic Si lens coupling, is obtained and the technique is easy to implement.

As with any area of research or set of experiments there is tremendous scope for improvement of the experimental technique or to advance the research field with continued experimentation and exploration. One area which greatly improves the performance of waveguide THz-TDS is by using the adiabatic flare technique to couple the THz radiation into the PPWG. This coupling technique could be greatly improved by using rigid adiabatically varying cylindrical structures which are mechanically robust and easy to assemble. PPWGs with such coupling structures could greatly simplify the coupling technique and also provide better performance. With such cylindrical PPWGs pump - probe characterization experiments on molecules can be performed, wherein you could have an IR/visible pump and THz probe beams. The 2 beams could be co propagated along the PPWG and the pump-probe spectroscopy could be carried out. This capability is not possible with the Si lens coupled PPWG as Si is not transparent in the visible region.

References

1. D. H. Auston, K.P. Cheung, and P.R. Smith, “Picosecond photoconducting Hertzian dipoles”, Appl. Phys. Lett. 45, 284-286 (1984).
2. M. B. Ketchen, D. Grischkowsky, T. C. Chen, C-C. Chi, I. N. Duling, III, N. J. Halas, J-M. Halbout, J. A. Kash, and G. P. Li, “Generation of subpicosecond electrical pulses on coplanar transmission lines”, Appl. Phys. Lett. 48, 751-753 (1986).
3. B. B. Hu, X.-C. Zhang, D. H. Auston and P. R. Smith, “Free-space radiation from electro-optic crystals”, Appl. Phys. Lett. 56, 506-508 (1990).
4. Q. Wu and X.-C. Zhang, “Free-space electro-optic sampling of terahertz beams”, Appl. Phys. Lett. 67, 3523-3525 (1995).
5. Martin van Exter and D. Grischkowsky, "Optical and Electronic Properties of Doped Silicon from 0.1 to 2 THz", Applied Physics Letters, Vol.56, 1694-1696 (1990).
6. Martin van Exter and D. Grischkowsky, "Carrier Dynamics of Electrons and Holes in Moderately-doped Silicon", Phys. Rev. B15, Vol. 41, 12140-9 (1990).
7. D. Grischkowsky, Soeren Keiding, Martin van Exter and Ch. Fattinger, "Far-Infrared Time-Domain Spectroscopy with Terahertz Beams of Dielectrics and Semiconductors", JOSA-B, Vol. 7, 2006-2015 (1990).
8. H. Harde, Soeren Keiding and D. Grischkowsky, "THz Commensurate Echoes: Periodic Rephasing of Molecular Transitions in Free Induction Decay", Phys. Rev. Lett., Vol. 66, 1834-1837 (1991).

9. M. C. Kemp, P. F. Taday, B. E. Cole, J. A. Cluff, A. J. Fitzgerald, and W. R. Tribe, “Security applications of terahertz technology,” Proc. SPIE 5070, 44-52 (2003).

10. K. Yamamoto, M. Yamaguchi, F. Miyamaru, M. Tani, M. Hangyo, T. Ikeda, A. Matsushita, K. Koide, M. Tatsuno, and Y. Minami, “Noninvasive inspection of C-4 explosive in mails by terahertz time-domain spectroscopy,” Jpn. J. Appl. Phys. 43, L414-417 (2004).

11. T. Lo, I. S. Gregory, C. Baker, P. F. Taday, W. R. Tribe, and M. C. Kemp, “The very far-infrared spectra of energetic materials and possible confusion materials using terahertz pulsed spectroscopy,” Vib. Spectrosc. 42, 243-248 (2006).

12. Van Exter, M., and D. Grischkowsky, “Characterization of an optoelectronics terahertz beam system”, IEEE Trans. Microw. Theory Tech. 38, 1684–169 (1990).

13. Gaussian 09, Revision A.1, M. J. Frisch, G. W. Trucks, H. B. Schlegel, G. E. Scuseria, M. A. Robb, J. R. Cheeseman, G. Scalmani, V. Barone, B. Mennucci, G. A. Petersson, H. Nakatsuji, M. Caricato, X. Li, H. P. Hratchian, A. F. Izmaylov, J. Bloino, G. Zheng, J. L. Sonnenberg, M. Hada, M. Ehara, K. Toyota, R. Fukuda, J. Hasegawa, M. Ishida, T. Nakajima, Y. Honda, O. Kitao, H. Nakai, T. Vreven, J. A. Montgomery, Jr., J. E. Peralta, F. Ogliaro, M. Bearpark, J. J. Heyd, E. Brothers, K. N. Kudin, V. N. Staroverov, R. Kobayashi, J. Normand, K. Raghavachari, A. Rendell, J. C. Burant, S. S. Iyengar, J. Tomasi, M. Cossi, N. Rega, J. M. Millam, M. Klene, J. E. Knox, J. B. Cross, V. Bakken, C. Adamo, J. Jaramillo, R. Gomperts, R. E. Stratmann, O. Yazyev, A. J. Austin, R. Cammi, C. Pomelli, J. W. Ochterski, R. L. Martin, K. Morokuma, V. G. Zakrzewski, G. A. Voth, P. Salvador, J. J. Dannenberg, S. Dapprich, A. D. Daniels, Ö. Farkas, J. B. Foresman, J. V. Ortiz, J. Cioslowski, and D. J. Fox, Gaussian, Inc., Wallingford CT, 2009.Berendsen, H. J. C., and S. Hayward, “Collective protein dynamics in relation to function”, Curr. Opin. Struct. Biol. 10,165–169 (2000).

14. P. U. Jepsen, and S. J. Clark, “Precise ab-initio prediction of terahertz vibrational modes in crystalline systems”, Chem. Phys. Lett. 442, 275–280 (2007).

15. R. Sprik, I. N. Duling III, C.-C. Chi, and D. Grischkowsky,“Far infrared spectroscopy with sub-picosecond electrical pulses on transmission lines,” Appl. Phys. Lett. 51, 548–550 (1987).
16. M. Walther, M. R. Freeman, and F. A. Hegmann, “Metal wire terahertz time-domain spectroscopy,” Appl. Phys. Lett. 87, 261107 (2005).
17. M. B. Byrne, J. Cunningham, K. Tych, A. D. Burnett, M. R. Stringer, C. D. Wood, L. Dazhang, M. Lachab, E. H. Lindfield, and A. G. Davies, “Terahertz vibrational absorption spectroscopy using micro-strip-line waveguides,” Appl. Phys. Lett. 93, 182904 (2008).
18. R. W. McGowan, G. Gallot, and D. Grischkowsky, "Propagation of Ultra-Wideband, Short Pulses of THz Radiation through Sub-mm Diameter Circular Waveguides." Optics Letters, Vol 24, 1431-1433 (1999).
19. G. Gallot, S. P. Jamison, R. W. McGowan, and D. Grischkowsky, “Terahertz waveguides,” J. Opt. Soc. Am. B 17, 851–863 (2000).
20. S. P. Jamison, R. W. McGowan, and D. Grischkowsky, "Single-mode waveguide propagation and reshaping of sub-ps terahertz pulses in sapphire fibers", Applied Physics Letters, Vol. 76, 1987- 1989 (2000).
21. R. Mendis and D. Grischkowsky, "Undistorted guided wave propagation of sub-picosecond THz pulses," Optics Letters, Vol. 26, 846-848 (2001).
22. Adam Bingham, Yuguang Zhao and D. Grischkowsky, "THz parallel plate photonic waveguides," Applied Physics Letters, Vol.87, 051101 (2005).
23. Yuguang Zhao and D. Grischkowsky, “Terahertz Demonstrations of Effectively Two Dimensional Photonic Bandgap Structures," Optics Letters, Vol. 31, 1534-1536, (2006).
24. S. Coleman and D. Grischkowsky, “A THz TEM-mode two dimensional interconnect layer incorporating quasi optics," Applied Physics Letters, Vol. 83, 3656-3658 (2003).
25. Jiangquan Zhang and D. Grischkowsky, “Waveguide THz time-domain spectroscopy of nm water layers,” Optics Letters, Vol. 19, 1617-1619 (2004).
26. R. Mendis and D. Grischkowsky, “Plastic Ribbon THz Waveguides,” J.Appl. Phys., 88, 4449-4451 (2000).

27. N. Maruvitz, “Waveguide Handbook”, Peter Peregrinus, London (1993), Chap 2.
28. Rajind Mendis, “First Broadband Experimental study of planar Terahertz Waveguides”, Ph.D thesis, Oklahoma State University, Stillwater, OK, (2001).
29. N. Laman and D. Grischkowsky, “Reduced conductivity in the terahertz skin-depth layer of metal", Applied Physics Letters, 90, 122115 (2007).
30. M. A. Ordal, L. L. Long, R. J. Bell, S. E. Bell, R. R. Bell, R. W. Alexander, Jr., and C. A. Ward, “Optical properties of the metals Al, Co, Cu, Au, Fe, Pb, Ni, Pd, Pt, Ag, Ti, and W in the infrared and far infrared”, Applied Optics, 22, 1099 (1983).
31. CRC Handbook of Chemistry and Physics, 73rd ed. edited by D. R. Lide (CRC, Boca Raton, FL, 1993), pp. 12–34.
32. P. D. Desai, H. M. James, and C. Y. Ho, “Electrical Resistivity of Aluminum and Manganese”, Journal of Physical and Chemical Reference Data, 13, 1131 (1984).
33. M. Cardona, W. Paul, and H. Brooks, “Dielectric constant of germanium and silicon as a function of volume”, Journal of Physics and Chemistry of Solids , 8, 204 (1959).
34. K. G. Lyon, G. L. Salinger, C. A. Swenson, and G. K. White, “Linear thermal expansion measurements on silicon from 6 to 340 K”, Journal of Applied Physics, 48, 865 (1977).
35. O. Esenturk, A. Evans, and E.J. Heilweil, “Terahertz spectroscopy of dicyanobenzenes: Anomalous absorption intensities and spectral calculations”, Chemical Physics Letters, 442, 71-77 (2007).
36. Y. Chen, H. Liu, Y. Deng, D. Schauki, M. J. Fitch, R. Osiander, C. Dodson, J. B. Spicer, M. Shur, and X.-C. Zhang, “THz spectroscopic investigation of 2,4-dinitrotoluene”, Chem. Phys. Lett. 400, 357 (2004).
37. A. M. Stoneham, “Shapes of inhomogeneously broadened resonance lines in solids”, Rev. Mod. Phys., Vol 41(1), 82 (1969).
38. John. Ferraris, D. O. Cowan, V. Walatka, and J. H. Perlstein, “Electron transfer in a new highly conducting donor-acceptor complex”, Journal of American Chemical Society, 95, 948 (1973).

39. P. W. Anderson, P. A. Lee, M. Saitoh, “Remarks on giant conductivity in TTF-TCNQ”, Solid State Communications, 13, 595–598 (1973).
40. R. Long, R. A. Sparks,, K. N. Trueblood, “The crystal and molecular structure of 7,7,8,8-tetracyanoquinodimethane”, Acta Cryst. , 18, 932 (1965).
41. Mercury, version 1.5; Cambridge Crystallographic Data Center, Cambridge, UK.
42. B. Lunelli, C. Pecile, “Polarized Infrared Spectra of TCNQ and TCNQ-d_4 Single Crystals”, J. Chem. Phys., 52, 2375 (1970).
43. C. Carlone, M. A. Lemieux, J. Deslandes, S. Jandl, K. D. Truong, N. K. Hota, Zauhar, J. Can. J. Phys. 1984, 62, 562 (1984).
44. T. Takenaka, “Molecular vibrational spectra of tetracyanoquinodimethane and tetracyanoquinodimethane-d_4 crystals”, Spectrochim. Acta, Part A, 27, 1735 (1971).
45. H.-B. Liu, H. Zhong, N. Karpowicz, Y. Chen, X.-C. Zhang, “Terahertz spectroscopy and imaging for defense and security applications,” Proc. IEEE 95, 1514-1527 (2007).
46. J. Chen, Y. Chen, H. Zhao, G. J. Bastiaans, and X.-C. Zhang, “Absorption coefficients of selected explosives and related compounds in the range of 0.1-2.8 THz,” Opt. Express 15, 12060 (2007).
47. Y. Chen, H. Liu, Y. Deng, D. Schauki, M. J. Fitch, R. Osiander, C. Dodson, J. B. Spicer, M. Shur, and X.- C. Zhang, “THz spectroscopic investigation of 2,4-dinitrotoluene,” Chem. Phys. Lett. 400, 357-361 (2004).
48. Y. Hu, P. Huang, L. Guo, X. Wang, C. Zhang, “Terahertz spectroscopic investigations of explosives,” Phys. Lett. A 359, 728-732 (2006).
49. W. C. McCrone and S.-M. Tsang, “Crystallographic Data. 88. 2,4-Dinitrotoluene,” Anal. Chem. 26, 1848-1849 (1954).
50. D. G. Allis, D. A. Prokhorova, and T. M. Korter, "Solid state modeling of the terahertz spectrum of the high explosive HMX," J. Phys. Chem. A 110, 1951-199 (2006).
51. C.Guadarrama-Prez, J. M. Martnez de La Hoz, P.B. Balbuena, “Theoretical Infrared and Terahertz Spectra of an RDX/Aluminum Complex”, J. Phys. Chem. A, 114 (6), 2284 (2010).

52. N. Bellakhal, K. Draou, B.G. Cheron, J.L. Brisset, "Protective films formed on copper by oxygen plasma treatment", Journal of Electroanalytical Chemistry, 431, 297-299 (1997).

53. W. Cochran, "The Crystal and Molecular Structure of Salicylic Acid", Acta Cryst., 6, 260 (1953).

54. H. Yoneyama, M. Yamashita, S. Kasai, H. Ito and T. Ouchi, "Application of Terahertz Spectrum in the Detection of Harmful Food Additives", Proceedings of IRMMW-THz 2007, 281 (2007).

55. Calum MacLeod, "China admits tainted food link," USA today, April 27 2007; Transcript of FDA press conference on the pet food recall March 30, 2007, http://www.fda.gov/oc/opacom/hottopics/petfood/transcript033007.pdf.

56. Ching-Hui Tseng, Charles K. Mann and Thomas J. Vickers, "FT-Raman Determination of Melamine and Melamine Cyanurate in Nylon", Applied Spectroscopy 48, 535 (1994).

57. http://news.bbc.co.uk/2/hi/asia-pacific/7624498.stm

58. J. R. Schneider and B. Schrader, "Measurement and calculation of the infrared and Raman active molecular and lattice vibrations of the crystalline melamine(1,3,5-triamino-s-triazine)", Journal of Molecular Structure, 29, 1 (1975).

59. G. Gomori, "Buffers in the range of pH 6.5 to 9.6", Proc. Soc. Exptl. Biol. Med., 62, 33–34 (1946).

60. R. G. Bates, R. A. Robinson, "Tris (hydroxymethy1) aminomethane -A useful secondary pH standard", Anal. Chem., , 45, 420 (1973).

61. D. Sirieix, S. Deleyance, M. Paris, S. Massonnet-Castel, A. Carpenter, J. F. Baron, "Tris(hydroxymethyl)aminomethane and sodium bicarbonate to buffer metabolic acidosis in an isolated heart model", Am. J. Respir. Crit. Care Med., 155, 957–963 (1997).

62. R. H. Kallet, R. M. Jasmer, J. M. Luce, L. H. Lin, J. D. Marks, "The treatment of acidosis in acute lung injury with Tris(hydroxymethyl)aminomethane", Am. J. Respir. Crit. Care Med., 161, 1149–1153 (2000).

63. H. E. Swim, “Amine and other nonbicarbonate buffers in cell culture media”, Ann. N.Y. Acad. Sci., 92, 440–446 (1961).

64. R. W. Ramette, C. H. Culberson, R. G. Bates, “Acid-base properties of tris(hydroxymethy1)aminomethane (Tris) buffers in seawater from 5 to 40 °C ”. Anal. Chem., 49, 867 (1977).

65. W. A. Wilson, M. T. Clark, T. C. Pellmar, “Tris buffer attenuates acetylcholine responses in aplysia neurons”, Science, 196, 440–441(1977).

66. H. R. Mauler, “The use of amine buffers in studies with enzymes”, Ann. N.Y. Acad. Sci., 92, 426–440 (1961).

67. R. Rudman, D. Eilerman, “The structure of crystalline Tris: A plastic crystal precursor, buffer, and acetylcholine attenuator”, Science, 200, 531–533 (1978).

68. G. G. Nahas, “The pharmacology of tris(hydroxymethyl)aminomethane (THAM)”, Pharm. Rev., 14, 447–472 (1962).

69. D. Eilerman, R. Rudman, “Polymorphism of crystalline poly (hydroxymethyl) compounds. III. The structures of crystalline and plastic tris(hydroxymethyl)aminomethane”, J. Chem. Phys., 72, 5656 (1980).

70. R, Ouillon, P. Ranson, S. Califano, “Temperature dependence of the bandwidths and frequencies of some anthracene phonons. High resolution Raman measurements”, Chem. Phys., 91, 119–131 (1984).

71. M. Walther, B. M. Fischer, P. U. Jepsen, “Noncovalent intermolecular forces in polycrystalline and amorphous saccharides in the far infrared”, Chem. Phys., 288, 261 (2003).

72. B. M. Fischer, H. Helm, P. U. Jepsen, “Chemical recognition with broadband THz spectroscopy”, Proc. IEEE, 95, 1592–1604 (2007).

73. B. M. Fischer, M. Walther, and P. U. Jepsen, “Far-infrared vibrational modes of DNA components studied by terahertz time domain spectroscopy”, Phys. Med. Biol., 47, 3807–3814, (2002).

74. J. Li, S. A. Lee, A. Anderson, L. Lettress, R. H. Griffey, and V. Mohan., "Temperature-dependent Raman and infrared spectra of nucleosides. III– Deoxycytidine", J. Raman Spectrosc., 34,183–191(2003).

75. P. C. Upadhya, Y. C. Shen, A. G. Davies, and E. H. Linfield, "Terahertz time-domain spectroscopy of glucose and uric acid", J. Biol. Phys., 29, 117–121 (2003).

76. J. I. Nishizawa, K. Suto, T. Sasaki, T. Tanabe, and T. Kimura, "Spectral measurement of terahertz vibrations of biomolecules using a GaP terahertz-wave generator with automatic scanning control", J. Phys. D Appl. Phys., 36, 2958–2961 (2003).

77. M. Walther, B. M. Fischer, and P. U. Jepsen, "Noncovalent intermolecular forces in polycrystalline and amorphous saccharides in the far infrared", Chem. Phys., 288, 261–268 (2003).

78. H. B. Liu, and X.-C. Zhang, "Dehydration kinetics of D-glucose monohydrate studies using THz time-domain spectroscopy", Chem. Phys. Lett., 429, 229–233 (2006).

79. M. Walther, "Modern spectroscopy on biological molecules: structure and bonding investigated by THz time-domain and transient phase-grating spectroscopy", Ph.D. Thesis, Albert-Ludwigs-Universita¨t Freiburg, Freiburg, Germany (2003).

80. C. S. Choi and E. Prince, "The crystal structure of cyclotrimethylenetrinitramine," Acta Crystallogr., Sect. B, B28, 2857–2862 (1972).

81. D. G. Allis, J. A. Zeitler, P. F. Taday, and T. M. Korter, "Theoretical analysis of the solid-state terahertz spectrum of the high explosive RDX," Chem. Phys. Lett. 463, 84–89 (2008).

82. J. Chen, Y. Chen, H. Zhao, G. J. Bastiaans, and X. C. Zhang, "Absorption coefficients of selected explosives and related compounds in the range of 0.1–2.8 THz," Opt. Exp., 15, 12060–12067 (2007).

83. Y. Hu, P. Huang, L. Guo, X. Wang, and C. Zhang, “Terahertz spectroscopic investigations of explosives,” Phys. Lett. A 359, 728–732 (2006).

84. A. Bingham, Y. Zhao, and D. Grischkowsky, “THz parallel plate photonic waveguides”, Appl. Phys. Lett. 87, 051101 (2005).

85. A. L. Bingham and D. Grischkowsky, “High-Q one-dimensional terahertz photonic waveguides”, Appl. Phys. Lett. 90, 091105 (2007).

86. C. R. Giles, “Lightwave applications of fiber Bragg gratings”, J. Lightwave Technol. 15, 1391 (1997).

87. A. D. Kersey, M. A. Davis, H. J. Patrick, M. LeBlac, K. P. Koo, C. G. Askins, M. A. Putnam, and E. J. Friebele, “Fiber Grating Sensors”, J. Lightwave Technol. 15, 1442 (1997).

88. A. Iadicicco, A. Cusano, S. Campopiano, A. Cutolo, and M. Giordano, “Thinned fiber Bragg gratings as refractive index sensors”, IEEE Sens. J., 5, 1288 (2005).

89. C. Wood, J. Cunningham, I. C. Hunter, P. Tosch, E. H. Linfield, and A. G. Davies, “ On-chip pulsed terahertz systems and their applications” Int. J. Infrared Millim. Waves 27, 557 (2006).

90. W. Liang, Y. Huang, Y. Xu, R. K. Lee, and A. Yariv, “Highly sensitive fiber Bragg grating refractive index sensors”, Appl. Phys. Lett. 86, 151122 (2005).

91. D. G. Angeley, Proc. SPIE 4958, 1 2003.

92. M. Theuer, R. Beigang and D. Grischkowsky, “Adiabatic Compression of THz Waves using Metal Flares,” Appl. Phys. Lett. Vol. 96, 191110, (2010).

93. W. Maineult, P. Gellie, A. Andronico, P. Filloux, G. Leo, C. Sirtori, S. Barbieri, E. Peytavit, T. Akalin, J. F. Lampin, H. E. Beere, and D. A. Ritchie, “Metal-metal terahertz quantum cascade laser with micro-transverse electromagnetic- horn antenna,” Appl. Phys. Lett. 93(18), 183508 (2008).

94. S. H. Kim, E. S. Lee, Y. B. Ji, and T.-I. Jeon, “Improvement of THz coupling using a tapered parallel-plate waveguide”, Opt. Exp. 18, 1289 (2010).

95. Jiangquan Zhang and D. Grischkowsky, "Adiabatic Compression of parallel-plate metal waveguides for sensitivity enhancement of waveguide THz time-domain spectroscopy (THz-TDS)," Applied Physics Letters, Vol. 86, 061109 (2005).

96. K. Matsumaru, “Reflection coefficient of E-plane Tapered waveguides”, IRE transactions on Microwave theory and techniques, 143, April (1958).

97. M. A. Ordal, L. L. Long, R. J. Bell, S. E. Bell, R. R. Bell, R. W. Alexander, Jr., and C. A. Ward, “Optical properties of the metals Al, Co, Cu, Au, Fe, Pb, Ni, Pd, Pt, Ag, Ti, and W in the infrared and far infrared”, Applied Optics, 22, 1099 (1983).

98. N. Laman and D. Grischkowsky, “Reduced conductivity in the terahertz skin-depth layer of metal", Applied Physics Letters, 90, 122115 (2007).

The work presented in this thesis is based on the work published in the following papers in refereed journals:

P1. Joseph S. Melinger, N. Laman, **S. Sree Harsha** and D. Grischkowsky, *" Line narrowing of terahertz vibrational modes for organic thin polycrystalline films within a parallel plate waveguide, "* Applied Physics Letters, Vol. 89, 251110 (2006).

P2. Joseph S. Melinger, N. Laman, **S. Sree Harsha**, ShuFan Cheng, and D. Grischkowsky, *"High-Resolution Waveguide Terahertz Spectroscopy of Partially Oriented Organic Polycrystalline Films,"* J. Phys. Chem. A, Vol. 111, 10977 (2007).

P3. N. Laman, **S. Sree Harsha**, D. Grischkowsky, and Joseph S. Melinger, *"High-Resolution Waveguide THz Spectroscopy of Biological Molecules"*, Biophysical Journal, Vol. 94, 1010-1020 (2008).

P4. N. Laman, **S. Sree Harsha**, D. Grischkowsky, *"Narrow-line waveguide Terahertz time-domain spectroscopy of Aspirin and Aspirin precursors,"* Applied Spectroscopy, Vol. 62, 319-326 (2008).

P5. N. Laman, **S. Sree Harsha**, D. Grischkowsky, and Joseph S. Melinger, *"7 GHz resolution waveguide THz spectroscopy of explosives related solids showing new features,"* Optics Express, Vol. 16, 4049-4105 (2008).

P6. Joseph S. Melinger, **S. Sree Harsha**, N. Laman and D. Grischkowsky, *"Guided-wave THz spectroscopy of molecular solids,"* J. Opt. Soc. Am. B., Vol. 26, pp. A79-A89 (2009).

P7. **S. Sree Harsha**, N. Laman, and D. Grischkowsky, *"High Q terahertz Bragg resonances within a metal parallel plate waveguide,"* Applied Physics Letters, Vol. 94, 091118 (2009).

P8. **S. Sree Harsha** and D. Grischkowsky, *"THz (far infrared) characterization of Tris (hydroxymethyl) aminomethane (TRIS) using high resolution waveguide THz-TDS",* Journal of Physical Chemistry A, Vol. 114 (10), 3489, (2010).

P9. Michael Theuer, **S. Sree Harsha** and D. Grischkowsky, *"Flare Coupled Metal Parallel-Plate Waveguides for High Resolution Terahertz Time-Domain Spectroscopy"*, Journal of Applied Physics, Vol. 108, 113105 (2010).

P10. Joseph S. Melinger, **S. Sree Harsha**, N. Laman and D. Grischkowsky, *"Temperature dependent characterization of Terahertz vibrations of explosives and related threat materials"*, Optics Express, Vo1. 8(26), 27238 (2010).

P11. **S. Sree Harsha,** N. Laman and D. Grischkowsky, "High Resolution Waveguide THz-TDS of Melamine" Conference on Lasers and Electro-Optics, 2008 OSA Technical Digest, (Optical Society of America, Washington, D.C., 2008), p.JWA40 (CLEO 2008).

P12. **S. Sree Harsha**, Joseph S. Melinger, and D. Grischkowsky, *"Substrate independence of THz vibrational modes for polycrystalline films of molecular solids in waveguide THz-TDS*", (submitted to Journal of Physical Chemistry A)

VITA

Sree Harsha Srikantaiah

Candidate for the Degree of

Doctor of Philosophy

Thesis: ENGINEERING METAL PARALLEL PLATE WAVEGUIDES AS A 2-D PLANE FOR HIGH RESOLUTION THz TIME DOMAIN SPECTROSCOPY

Major Field: Photonics

Biographical:

Personal Data: Born in Bangalore, Karnataka, India.

Education: BS (Honors) in Physics from Sri Sathya Sai Institute of Higher learning, Prashanthi Nilayam, India 2001. MS in Physics with specialization in Photonics from Sri Sathya Sai Institute of Higher learning, Prashanthi Nilayam, India 2003. Completed the requirements for the Doctor of Philosophy in Photonics at Oklahoma State University, Stillwater, Oklahoma in July, 2011.

Experience: Investigated the propagation of intense ultrafast laser pulses through quadratic nonlinear media and their application in broadband continuum generation; growth and application of polymer embedded metal nanoparticles for optical limiting as Junior Research Fellow at University of Hyderabad, India. Investigated the application of metal parallel plate waveguides for performing high resolution vibrational spectroscopy of molecular solids at THz frequencies as a part of my Ph.D research work at Oklahoma State University, OK.

Professional Memberships: Student member of Optical Society of America (OSA)

Name: Sree Harsha Srikantaiah Date of Degree: July, 2011

Institution: Oklahoma State University Location: Stillwater, Oklahoma

Title of Study: ENGINEERING METAL PARALLEL PLATE WAVEGUIDES AS A 2-D PLANE FOR HIGH RESOLUTION THz TIME DOMAIN SPECTROSCOPY

Pages in Study: 170 Candidate for the Degree of Doctor of Philosophy

Major Field: Photonics

Scope and Method of Study: The research summarized in this dissertation is on the investigation of the application of metal parallel plate waveguides (PPWG) for performing high resolution spectroscopic measurements of molecular solids at THz frequencies. The dissertation also presents results on the incorporation of high Q periodic structures within a metal PPWG and their application in sensitive detection of materials by monitoring change in refractive index. The experimental results were obtained by measuring the transmission of metal PPWG with samples in a standard THz time domain spectroscopy system based on photoconductive switches in 4f geometry.

Findings and Conclusions: The main finding of this endeavor is that waveguide THz time domain spectroscopy using metal PPWGs can be efficiently applied to extract high resolution vibrational resonances associated with molecular solids. This technique discovered as a part of this research is a new and novel method which for the first time facilitates high resolution spectroscopic measurements of solid microcrystalline films which are easy to make in comparison to single crystal samples, but allows us to extract high resolution vibrational modes of the molecules. This technique can be complimentarily applied with the standard THz-TDS and Fourier transform infra-red spectroscopy to resolve the complete vibrational response of any molecular solid. We have also shown that metal PPWG also allows the incorporation of periodic structures like a weak Bragg stack and be applied as a very high - Q frequency filter having application in chemical sensing. The Q factors obtained by us are among the highest obtained for resonant and periodic structures within waveguide structures. We can conclude that the PPWG acts as an efficient 2-D plane which allows for performing high resolution spectroscopy and for incorporating frequency filtering devices with in the sub wavelength gap.

ADVISER'S APPROVAL: Dr. Daniel R. Grischkowsky